Grant Number DAAG55-97-1-0017

A NOVEL MAGNETO-RHEOLOGICAL SHOCK ABSORBER FOR VIBRATION CONTROL

Final Report

Principal Investigator:

Dr. Faramarz Gordaninejad
Professor of Mechanical Engineering
University of Nevada, Reno
Reno, Nevada 89557

Submitted to:

DEPARTMENT OF THE ARMY
ARMY RESEARCH OFFICE

February 2001

REPORT DOCUMENTATION PAGE

Form Approved
OMB NO. 0704-0188

1. AGENCY USE ONLY (Leave Blank)	2. REPORT DATE 2-12-2001	3. REPORT TYPE AND DATES COVERED Final Report 15 Nov 97 - 14 Nov 00

4. TITLE AND SUBTITLE
A Novel Manetorhological Shock Absorber for Vibration Control

5. FUNDING NUMBERS
DAAG55-98-1-0017

6. AUTHOR(S)
Professor Faramarz Gordaninejad

7. PERFORMING ORGANIZATION NAME(S) AND ADDRESS(ES)
University of Nevada, Reno
Office of Sponsored Project Administration/325
Reno, Nevada 89559

8. PERFORMING ORGANIZATION REPORT NUMBER

9. SPONSORING / MONITORING AGENCY NAME(S) AND ADDRESS(ES)
U. S. Army Research Office
P.O. Box 12211
Research Triangle Park, NC 27709-2211

10. SPONSORING / MONITORING AGENCY REPORT NUMBER
Proposal Number: 37747-EG-DPS
•1-

11. SUPPLEMENTARY NOTES
The views, opinions and/or findings contained in this report are those of the author(s) and should not be construed as an official Department of the Army position, policy or decision, unless so designated by other documentation.

12 a. DISTRIBUTION / AVAILABILITY STATEMENT
Approved for public release; distribution unlimited.

12 b. DISTRIBUTION CODE

13. ABSTRACT (Maximum 200 words)

This project focused on the fundamental understanding of behavior and development of novel magneto-rheological fluid (MRF) shock absorbers for mechanical systems. The aim of the study was on the feasibility of integrating controllable, semi-active, MRF shock absorbers in the suspension systems of the U.S. Army's High Mobility, Multi-purpose Wheeled Vehicle (HMMWV).

New MRF damper designs were developed, fabricated and tested to meet and exceed the performance criteria set forth by the original equipment manufacture (OEM) test results. A nonlinear theoretical model was developed which can predict the performance of the MRF dampers. A unique capacity for bypass valving is included in the proposed design. A critical element of vehicle shock absorbers, bypass valving allows the shock absorber to accommodate high-force impulse loading (without failure) typical to off-highway environments. Moreover, a nonlinear fluid-mechanics based theoretical model was developed by employing Bingham plastic and Herschel-Bulkey non-Newtonian fluid models. Three-dimensional electromagnetic finite element analysis was also performed for establishing a base for the MRF damper design. Extensive experiments were conducted to understand the nonlinear behavior of the new MRF dampers.

14. SUBJECT TERMS	15. NUMBER OF PAGES
Magneto-rheological fluid, dampers, semi-active, fail-safe, vibration, damping, HMMWV	72
	16. PRICE CODE

17. SECURITY CLASSIFICATION OR REPORT	18. SECURITY CLASSIFICATION ON THIS PAGE	19. SECURITY CLASSIFICATION OF ABSTRACT	20. LIMITATION OF ABSTRACT
UNCLASSIFIED	UNCLASSIFIED	UNCLASSIFIED	UL

TABLE OF CONTENTS

Section **Page Number**

STATEMENT OF PROBLEM STUDIED

The proposed project was aimed at basic understanding of the nonlinear force-displacement and force-velocity behavior of a new magneto-rheological (MR) fluid damper. The major research issues and the objectives of this project were: a) to develop a theoretical study to predict nonlinear behavior of new MRF dampers; and b) to conduct a comprehensive experimental study on the proposed MRF damper to validate all theoretical findings. Particularly, the focus of the research was on the specifications required for the Army's High Mobility, Multi-purpose Wheeled Vehicle's (HMMWV's) suspension system.

SUMMARY OF IMPORTANT RESULTS

Introduction:

Semi-active vibration control devices are increasingly being investigated and implemented. New advances in high-performance materials have led to the technological growth in the area of semi-active protective devices. The proposed MRF damper system will take advantage of the state-of-the-art in advancement of materials to study and produce a practical, efficient, and inexpensive shock absorber for vibration control of mechanical systems.

A major factor in tactical doctrine for battlefield operation is cross-country mobility for combat vehicles [1]. Advances in technology that allows a significant enhancement in cross-country mobility can affect the battlefield engagement's location and timing. Extensive test results by Army TARDEC have clearly demonstrated that the utilization of semi-active suspension technology in military vehicles can increase the cross-country mobility more than 30% [2]. MR fluid controllable shock absorbers dramatically reduce the mechanical complexity found in current servo-hydraulic controllable shock absorbers. Reservoirs, heat exchangers, pumps and external hydraulic systems are not required when using MR technology. The fast response behavior of MR dampers allow for active control throughout a higher range of frequencies, therefore, increasing active suspension performance. By the utilization of MR fluid dampers, increased reliability, maintainability and performance will result. Development of this new MR technology for vehicle suspension systems can matriculate to commercial vehicles as well.

In order to accurately define the design specifications of the new University of Nevada, Reno (UNR) MR fluid damper, Dr. Francis Hoogterp of the U.S. Army TARDEC was consulted for technical data and performance characteristics of HMMWV suspension components. For proper assessment of shock absorber performance requirements, two original equipment manufacture (OEM), Monroe HMMWV shock absorbers were characterized at the Composite and Intelligent Materials Laboratory (CIML, http://web.me.unr.edu/ciml) for a range of frequencies and displacements. These test results provide a baseline performance standard to be met by the new MR fluid damper design.

The new UNR MR damper design was developed to meet and exceed the performance criteria set forth by the OEM test results. A unique capacity for bypass valving is included in the proposed design. A critical element of vehicle shock absorbers, bypass valving allows the shock absorber to accommodate high-force impulse loading (without failure) typical to off-highway environments. The new MR damper has bypass valving incorporated into the design. The MR damper was tested for the same range of frequencies and displacements as the OEM units. In addition, the same tests were run for a range of electrical current inputs, the means of controlling damping. Moreover, a nonlinear fluid-mechanics based theoretical model was developed by employing Bingham plastic and Herschel-Bulkey non-Newtonian fluid models. Three-dimensional electromagnetic finite element analyses were performed for establishing a base for the MR fluid damper design.

Several prototype UNR MR dampers have been developed and tested which explore the design parameters. These dampers were tested for a range of frequencies, displacements and input currents. Test results show that the new MR fluid shock absorbers can provide three to four times the amount of damping force than provided by the OEM units. In addition, without electrical current applied, the MR fluid shock acts as a passive shock absorber, providing the same performance as the OEM unit.

Because the MR fluid damper uses a built-in electromagnet for controlling fluid viscosity (and ultimately damping), three-dimensional magnetic finite element analysis was performed on the device to determine material types, magnetic wire size, magnetic saturation of fluid, power requirements and optimal geometry for the best MR-effect (the method of changing fluid viscosity). This effort began with development of a three-dimensional solid model, which can be directly ported into different finite element software packages. This new design of damper has also addressed the issue of fluid sealing by adopting a seal pack that does not leak fluid. This prototype MR fluid damper has undergone over more than 1000 different tests without any fluid leakage. Also, experimentally investigated is the use of a satellite accumulator. Because of the nature of the fluid, correct operating pressure for an MR vehicle shock absorber had to be determined experimentally.

This summary is organized in two sections:

1. Nonlinear theoretical modeling of the UNR MRF damper.
2. Experimental studies.

1. THEORETICAL MODELING:

A magneto-rheological fluid consists of micron-sized ferrous particles within a base carrier fluid, such as silicon or mineral oil, and additives. Under the influence of a magnetic field, the ferrous particles polarize and attract each other, resulting in the formation of chains or columns of

particles parallel to the orientation of the magnetic flux lines. This results in a quantifiable change in the "apparent viscosity" of the fluid, which is defined as:

$$\mu_{APP} = \frac{\tau}{\dot{\gamma}} \tag{1}$$

Here, μ_{APP} is the apparent viscosity of fluid, τ represents fluid shear stress at the wall, and $\dot{\gamma}$ is the shear strain rate. The Bingham plastic model is defined as [3]:

$$\tau = \tau_Y + \mu_0 \dot{\gamma} \tag{2}$$

where τ_y is the field-induced shear stress and μ_0 represents plastic viscosity of the fluid. From Equations (1) and (2), one has:

$$\mu_{APP} = \frac{\tau_Y + \mu_0 \dot{\gamma}}{\dot{\gamma}} = \frac{\tau_Y}{\dot{\gamma}} + \mu_0 \tag{3}$$

In the absence of minor head loss terms, as well as fluid inertia, and seal friction, the pressure drop across the piston can be expressed as [4,5]0):

$$\Delta P = \frac{32 \mu_{APP} L_{CH} V_{CH}}{D_{eff}^{\ 2}} \tag{4}$$

where L_{CH} is the length of the channel, V_{CH} is the velocity of the MRF in the channel, D_{eff} is the effective hydraulic diameter ($D_{eff} = [64/(fRe)]D_H$, where fRe is the geometry-specific, laminar friction constant for non-circular flows), and ΔP is the pressure drop. Substitution of Equation (3) into Equation (4) produces:

$$\Delta P = \frac{32 \mu_0 L_{CH} V_{CH}}{D_{eff}^{\ 2}} + \frac{32 K I^{\delta} L_{MR}}{D_{eff}} \tag{5}$$

where KI^{δ} is the shear yield stress of the MRF and L_{MR} is the length of the MR valve. I is the input electric current and K and δ are the constants which are determined by a three-dimensional electro-magnetic finite element analysis.

For different rebound and compression behavior, or to accommodate high-force impact loads, extra passages open as spring-backed valves retract. For this MRF damper design, these passages are in a parallel arrangement. Equating total volumetric flow rate across the piston provides the following relation for the fluid velocity [6]:

$$V_{CH} = \frac{\dot{X}_P A_{PISTON}}{N A_{MR} + \beta M A_{NON-MR} \phi} \tag{6}$$

where $\dot{X}_P$ is the input velocity of piston, A_{PISTON} is the effective area of piston, A_{MR} is the cross-sectional area of MRF channel, A_{NON-MR} is the cross-sectional area of non-MR-effected passages, N is the number of MR channels, M is number of non-MR-effected passages in parallel, β is the contribution (in terms of percent-opening) of the non-MR-effected passages and ϕ is:

$$\phi = \left(\frac{D_B^{\,2}}{D_{eff}^{\,2}}\right)\left[1 + \frac{\tau_Y/\dot{\gamma}}{\mu_0} + \frac{2L_{MR}}{L_P} + \frac{(\tau_Y/\dot{\gamma})2L_{MR}}{\mu_0 L_P}\right] \tag{7}$$

Here D_B is the diameter of return channels, and L_p is the length of the piston. Combining Equations (5)-(7) and multiplying by the area of piston yields the following expression for the damping force, F_{DAMPER}:

$$F_{DAMPER} = \frac{32\mu_0 L_{CH}}{D_{eff}^{\,2}}\left(\frac{(A_{PISTON})^2}{NA_{MR} + \beta MA_{NON-MR}\phi}\right)\underline{\dot{X}}_P + \frac{16KI^{\delta}L_{MR}}{D_{eff}}A_{PISTON}\,\mathrm{sgn}(\underline{\dot{X}}_P) \tag{8}$$

Previous studies had employed the Bingham plastic model. A non-dimensional equation of flow was introduced by Phillips [3] and an approximated form of the Phillips's theory was developed by Gavin, *et al* [7]. Because of its simplicity, the Bingham plastic model has been widely used for field-controllable fluids, however, it can only be used in the limiting case of post-yield phase when the material exhibits Newtonian behavior. ER and MR fluids are generally observed to have a strong field-dependent shear modulus and a yield stress that resists the material's flow until shear stress reaches a critical value. The Bingham plastic model is often used to describe this phenomenon. In the Bingham plastic model, ER and MR fluids are assumed to be Newtonian fluids in post-yield regime, with a constant plastic viscosity assumption. However, for cases where the fluid experiences post-yield shear thinning or shear thickening, the assumption of constant plastic viscosity may not be valid.

In this paper, the previous study is extended to include generalized analyses of ER and MR fluids flowing through pipes and parallel plates using the Herschel-Bulkley model. Non-dimensional equations are derived, and simplified closed-form expressions are presented for determining the pressure drop as a function of material properties, geometry, and volumetric flow rate. The simplified closed-form Herschel-Bulkley model can be reduced to the Bingham plastic model for cases where post-yield shear thinning or thickening are minimal. The theoretical Herschel-Bulkley formulation for flow through pipes is compared with the experimental results using a MR fluid damper which is constructed and tested at UNR. Excellent agreement is obtained.

The Herschel-Bulkley constitutive equation presented in Equation (1) describes the flow of ER and MR fluids through a circular pipe with a constant cross sectional area.

$$\begin{cases} \tau_{rz} = \tau_y + k\left|\dfrac{du}{dr}\right|^n & |\tau_{rz}| \geq \tau_y \\ \dfrac{du}{dr} = 0 & |\tau_{rz}| \leq \tau_y \end{cases} \tag{9}$$

where τ_{rz} is shear stress; $\dfrac{du}{dr}$ is shear strain rate, and k and n are fluid index parameters. τ_y is the fluid yield stress and is a function of the external field. Let us consider a steady, one-

dimensional flow of an incompressible ER or MR fluid through a straight cylindrical pipe of constant cross section. A cylindrical coordinate system, with the notation shown in Figure 1, is assumed. The momentum equation of laminar flow in a pipe can be written as:

$$r\frac{dp}{dz} = -\frac{\partial(r\tau_{rz})}{\partial r} \tag{10}$$

where the pressure gradient, $\frac{dp}{dz}$ is constant along the flow direction. Integrating Equation (10) yields shear stress as a function of radial position:

$$\tau_{rz} = -\frac{1}{2}r\frac{dp}{dz} + \frac{c_0}{r} \tag{11}$$

The axial flow in the pipe requires that c_0 be zero. The flow has a non-yield region, which is signified by the "plug" radius shown in Figure 1. The plug radius, R_p, can be determined by:

$$R_p = \frac{2\tau_y}{dp/dz} \tag{11a}$$

The yield flow region, therefore, is defined when $R_p \le r \le R$. Substitution of Equation (9) into Equation (11) yields:

$$\tau_y + k\left|\frac{du}{dr}\right|^n = -\frac{1}{2}r\frac{dp}{dz} \tag{12}$$

Since $\frac{du}{dr} < 0$, Equation (12) can be written as:

$$\frac{du}{dr} = -\left(-\frac{1}{2}r\frac{dp/dz}{k} - \frac{\tau_y}{k}\right)^{\frac{1}{n}} \tag{13}$$

Solving Equation (13) with boundary condition of $u = 0$ at $r = R$, one obtains the velocity distribution in the yield flow area ($R_p \le r \le R$), as follows:

$$u = \frac{n}{n+1}\frac{2k}{dp/dz}\left[\left(-\frac{dp/dz}{2k}r - \frac{\tau_y}{k}\right)^{\frac{n+1}{n}} - \left(-\frac{dp/dz}{2k}R - \frac{\tau_y}{k}\right)^{\frac{n+1}{n}}\right] \tag{14}$$

In the plug area, $0 \le r \le R_p$, the velocity is constant. By letting $r = R_p$, the plug velocity can be expressed as:

$$u_p = \frac{n}{n+1}\frac{2k}{dp/dz}\left[\left(-\frac{dp/dz}{2k}R_p - \frac{\tau_y}{k}\right)^{\frac{n+1}{n}} - \left(-\frac{dp/dz}{2k}R - \frac{\tau_y}{k}\right)^{\frac{n+1}{n}}\right] \tag{15}$$

The volumetric flow rate can be derived from the following relation:

$$Q = 2\pi\int_{R_p}^{R} urdr + R_p{}^2\pi u_p \tag{16}$$

Substitution of Equations (14) and (15) into Equation (16) yields:

$$Q = \frac{\left(\frac{p'R}{2} - \tau_y\right)^{\frac{n+1}{n}}\pi R^3}{\left(\frac{pR}{2}\right)^3 k^{\frac{1}{n}}}\left[\frac{\left(\frac{p'R}{2} - \tau_y\right)^2}{\frac{3n+1}{n}} + \frac{2\tau_y\left(\frac{p'R}{2} - \tau_y\right)}{\frac{2n+1}{n}} + \frac{\tau_y{}^2}{\frac{n+1}{n}}\right] \tag{17}$$

where $p' = -dp/dz$. Now, let us consider the following dimensionless parameters:

$$X = \frac{4\tau_y}{p'D} = \frac{R_p}{R}; \quad \text{and,} \quad Y = \left(\frac{3n+1}{n}\frac{8Q}{\pi D^3}\right)^n \frac{4k}{p'D} \tag{17a}$$

Where $D=2R$ and X represents the dimensionless plug thickness or dimensionless shear stress. When X=1, the plug radius is the same as the pipe radius and the yield stress of the fluid is equal to its shear stress at the wall which implies that there is no flow in the pipe. Y is the dimensionless volumetric flow rate. By using the above dimensionless variables, Equation (17) can be simplified to [7]:

$$Y = (1-X)\left(1 - aX - bX^2 - cX^3\right)^n \tag{18}$$

Where $a = \frac{1}{2n+1}$; $b = \frac{2n}{(n+1)(2n+1)}$; $c = \frac{2n^2}{(n+1)(2n+1)}$

Expanding the right hand side of Equation (10) by Taylor Series, one has:

$$Y = 1 - (na+1)X + \left(an - bn + \frac{n(n-1)}{2}a^2\right)X^2 + c\left((-nc + bn + n(n-1) - \frac{n(n-1)(n-2)}{6}a^3\right)X^3 + \cdots \tag{19}$$

For $X \le 0.5$, let us assume a linear relationship between X and Y in the form of 1-Y=AX. By linear regression of Equation (19), the coefficient A can be determined as:

$$A=(na+1)-\frac{3}{8}(na-bn+\frac{n(n-1)}{2}a^2) \tag{19a}$$

Therefore, a linear approximation to Equation (18), for all n, when $X<0.5$, can be presented as:

$$Y=1-\left[(na+1)-\frac{3}{8}(na-bn+\frac{n(n-1)}{2}a^2)\right]X \tag{20}$$

Equation (20) represents the Herschel-Bulkley fluid model. If n=1, the Herschel-Bulkley fluid equation is simplified to the Bingham plastic fluid model, as follows:

$$Y=1-\frac{4}{3}X \text{ where } X\le 0.5 \tag{21}$$

Equation (20) can further be simplified to the power law fluid. By setting, $\tau_y=0$ (i.e., X=0), Equation (20) collapses to Y=1, which is the dimensionless form for the power law fluid model. The dimensioned form can be written as:

$$\frac{dp}{dz}=\frac{4k}{D}\left(\frac{8Q}{\pi D^3}\right)^n\left(\frac{3n+1}{n}\right)^n \tag{21a}$$

For a Newtonian fluid, if n is set to 1 in Equation (21a), one has:

$$\frac{dp}{dz}=\frac{128kQ}{\pi D^4} \tag{21b}$$

which is the Hagen-Poiseuille equation.

Returning to the Herschel-Bulkley pipe flow for ER and MR field-controllable fluids, the dimensioned form of Equation (20) provides a closed-form expression for the pressure gradient as follows:

$$\frac{dp}{dz}=A\frac{4\tau_y}{D}+\left(\frac{3n+1}{n}\frac{8Q}{\pi D^3}\right)^n\frac{4k}{D}\ ; \qquad \frac{R_p}{R}\le 0.5 \tag{22}$$

$$\text{where } A=\frac{3n+1}{2n+1}-\frac{3}{16}\frac{(3n+1)(1-n)}{(2n+1)^2(n+1)}$$

Equation (22) describes the pressure loss of a non-Newtonian fluid with yield stress. The pressure loss can be separated in two parts: one is induced by pure viscous flow and the other is caused by yield stress when the non-yield field is not dominant in the entire flow area. When X>0.5, the plug radius reaches half of the pipe radius, the yield stress will play an important role in determining pressure loss. A simplified expression for Equation (18) is obtained by considering the following nonlinear relation between X and Y:

$$Y = A' X(1-X)^{\alpha} \tag{23}$$

Where A' and α are functions of n and their numerical values are presented in Table 1. The dimensioned version of the pressure loss can be derived from Equation (23)

$$\frac{dp}{dz} = \frac{4\tau_y}{D\left[1 - A_0\left(\frac{3n+1}{n}\frac{8Q}{\pi D^3}\right)^{\frac{n}{\alpha}}\left(\frac{k}{\tau_y}\right)^{\frac{1}{\alpha}}\right]}; \quad \text{for } \frac{R_p}{R} > 0.5 \tag{24}$$

where $A_0 = (A')^{\frac{1}{\alpha}}$

The exact, Equation (18), and the simplified, Equations (20) and (23), solutions for the Herschel-Bulkley pipe flow relationships are presented in Figure 2. As shown, the simplified model is an excellent approximation to the exact solution. The relative maximum error between the two models is less than 3%. Therefore, the simplified Herschel-Bulkley relationships presented in Equations (22) and (24) are expected to provide an accurate explicit expression for the pressure loss associated with flow of ER/MR fluid in pipes with circular constant cross sections.

2. EXPERIMENTAL STUDIES:

To establish a foundation for the fail-safe design, first, the characteristics of two OEM HMMWV dampers were studied. The OEM shock absorbers were characterized at 2, 3, 4 and 7Hz frequencies. For each frequency considered, four different peak-to-peak amplitudes of displacement (0.5, 1.0, 1.5 and 2.0cm) were examined. This allowed the design of a passive fail-safe baseline characteristic of the MRF damper.

For the MRF damper, an additional parameter is examined. Increased damping is achieved through applying electrical current to the built-in electromagnet of the device. With no current supplied to the damper (i.e., zero-field, or passive-off), the MRF damper operates in fail-safe mode, emulating OEM shock absorber behavior. As current supplied to the device increases, higher damping forces result. Three different electrical current inputs are investigated.

Experiments performed on a shaking table (Ling Dynamic Systems, model V830-334T). Figure 3 is an illustration of the experimental test setup. A linear motion transducer (LMT) was used to measure displacement and velocity. Electronic signals generated by the load cell and LMT are sent to an external signal processing unit which scales the signal for the data acquisition board, a National Instruments AT-MIO-16X unit. One end of the damper is mounted directly to the shaking table, while the other end is attached to a 13,000N (3,000lb) Eaton Lebow (Model 3132) load cell. A personal computer houses the data acquisition board and the instrumentation

software package, which produce test data. The software used was the National Instruments LabVIEW software package. The shake table is controlled by another computer, which controls power and frequency to the shake table unit. Power, in conjunction with frequency, controls the amplitude of table travel, which is monitored by the LMT. Equipment were calibrated with known masses, frequencies, measured peak-to-peak displacements and metered electrical current values.

Two identical OEM shock absorbers were tested to assure the accuracy of test results. Each test was conducted repetitively for a duration time of no less than ten seconds. Figure 4 shows an illustration of the UNR MRF damper along side (and in the same scale) as the OEM unit. This illustration shows the size comparison of both dampers. The geometric constraints of the shock absorber include length of travel, mounting means and outer diameter (inner diameter of coil suspension spring). The MRF damper was constructed specifically for testing purposes and does not have all of the elements of the commercial unit. For example, elastomer bearings are incorporated into the semi-rigid mount of the OEM damper. This is to accommodate for minor off-axis loading, typical to pivotal loading environments of vehicles. The MRF damper has rigid steel mounts, as its function is to mount only to the testing apparatus. This also eliminates the effects of the spring and damping properties of the elastomer.

Figure 5 is a photograph of the actual MRF damper used for testing. Five different variants of this design were developed and tested to thoroughly explore parameters of design. Figure 6 is a photograph of the satellite accumulator, which is kept separate from the experimental damper to simplify damper assembly and disassembly. The role of the accumulator is to accommodate for the change in available fluid volume as the piston reciprocates inside the cylinder. Most OEM shock absorbers have the accumulator integrated into the unit itself. The MRF damper design presented in this paper also has this capacity, but the accumulator is kept separate for the aforementioned purpose.

Figure 7 presents experimental results for the force-displacement of a HMMWV OEM shock absorber at 2Hz, 1.0cm peak-to-peak amplitude of displacement. Figure 8 illustrates the force-velocity data for the same test. Figures 9 and 10 show results of the same experiment for the UNR HMMWV MRF damper. In comparing Figure 5 and Figure 9, it is apparent that peak-to-peak, passive-off damping force is similar for the MRF damper and the OEM unit. Figure 9 also shows the range of damping that increases as current supplied to the MRF damper increases. The baseline peak-to-peak force at 2Hz for both devices is about 600N (135lbf), while the increase in peak-to-peak force (via current supplied to the MRF damper) is almost 2,200N (500lbf). In comparing the force-velocity data of both units (Figure 6 for the OEM unit and Figure 10 for the MRF damper at zero-field), the offset 'step' in the hysteresis loops at zero velocity is due to the pressure resulting from the accumulator. When current is applied to the MRF damper, damping force increases the height of the offset force step at zero velocity. In Figure 10 the peak velocity increases as damping force increases. This is the result of the experimental setup. The shake table maintains constant frequency, while the peak-to-peak displacement changes, slightly, which results in increased peak velocity.

Figure 11 illustrates another means for evaluating damper performance. Quantifying the area within any given force-displacement hysteresis loop provides an amount of work done by the damper during one complete stroke. For an equivalent linear damper, the damping coefficient can be determined by:

$$C_{eq} = \frac{W}{\pi X^2 \omega} \tag{25}$$

where C_{eq} is the equivalent damping coefficient, W represents the work done by the damper during one cycle, X is the amplitude of displacement, and ω is the frequency in radians per second. As frequency increases and current to the damper increases, the energy absorbed by the damper increases. For the same test data, Figure 12 illustrates the values of peak-to-peak force as a function of input electric current for the MRF damper.

Figure 13 and Figure 14 illustrate the force envelope of the MRF damper as a function of frequency for two different test displacements (1.0 and 1.5cm peak-to-peak, respectively). Also shown for comparison on both graphs are the results of the OEM shock absorber. The benefit of controllable damping presented in this study is made evident by these two graphs; a range of damping force with the MRF damper versus the passive damping force of the OEM shock absorber. As energy inputs vary to the vehicle, the MRF damper has the capability to vary the amount of energy absorption accordingly.

Figure 15 is a comparison of force-displacement experimental and theoretical results for the MRF damper at 2Hz, 1.0cm peak-to-peak displacement. Experiments were performed at passive-off mode (zero input electrical current) and 3.0Amp input electric current. Figure 16 shows the force-velocity results for the same tests. Figures 17 and 18 are theoretical force-displacement results illustrating the effects of the extra by-pass valves mentioned earlier. It is evident that the MRF damper no longer has a symmetrical appearance when the valves are opened.

Conclusions:

New MR fluid dampers were developed, built, tested and proven effective. The accomplishments made by this research have widespread implications. Commercial vehicle suspension systems, including automotive, motorcycle and bicycle applications will benefit from an MR fluid damper design that has incorporated bypass valving into its design. Once established in the Army HMMWV, matriculation of an MR-based suspension system into civilian applications will undoubtedly result.

LIST OF PUBLICATION SUPPORTED UNDER THIS GRANT

Wang, X., and Gordaninejad, F., "Flow Analysis Of Field-Controllable, Electro- and Magneto-Rheological Fluids Using Herschel-Bulkley Model," *Journal of Intelligent Materials, Systems And Structures*, Vol. 10, No. 8, Pp. 601-608, 1999.

Gordaninejad, F. and Kelso, S. P., "Semi-Active Magnetorheoogical Dampers for HMMWV," *Journal of Intelligent Materials, Systems and Structures*, accepted, to appear in 2001.

Ericksen, E. O., and Gordaninejad, F., "A Magneto-Rheological Fluid Shock Absorbers for the Rear Suspension of an Off-Road Motorcycle: A Theoretical Study," *Industrial and Commercial Applications of Smart Structures Technologies, Proceedings of SPIE Conference on Smart Materials and Structures,* Ed. by Jack H. Jacobs, Vol. 3991, pp. 273-282, 2000.

Wang, X., and Gordaninejad, F., "Study of Controllable Fluid Dampers in Flow Mode using Herschel-Bulkley Model," *Damping and Isolation, Proceedings of SPIE Conference on Smart Materials and Structures,* Ed. T. Tupper Hyde, Vol. 3989, pp. 232-243, 2000.

Gordaninejad, F. and Kelso, S. P., "Magneto-Rheological Fluid Shock Absorbers for HMMWV," *Damping and Isolation, Proceedings of SPIE Conference on Smart Materials and Structures,* Ed. T. Tupper Hyde, Vol. 3989, pp. 266-273, 2000.

Ericksen, E. O., and Gordaninejad, F., "A Magneto-Rheological Fluid Shock Absorbers for an Off-Road Motorcycle," *Proceedings of Asia-Pacific Vibration Conference'99*, Ed. By O. J. Huat and L. K. Meow, Vol. 2, pp. 267-271, 1999.

Wang, X., and Gordaninejad, F., "Herschel-Bulkley Analysis of Electro- and Magneto-Rheological Controllable Fluids in Flow Mode," *Proceedings of the 7th International Conference on ER Fluids and MR Suspensions*, pp. 580-591, 1999.

Kelso, S. P. and Gordaninejad, F., "Magneto-Rheological Fluid Shock Absorbers for Off-Highway, High-Payload Vehicles," *Passive Damping and Isolation, Proceedings of the SPIE Conference on smart materials and structures*, Ed. by L. Porter Davis Vol. 3672 pp. 44-54, 1999.

Gordaninejad, F., "A Novel Magneto-Rheological Shock Absorber for Vibration Control," Project Summary for ARO, 1998.

Gordaninejad, F., "A Novel Magneto-Rheological Shock Absorber for Vibration Control," Project Summary for ARO, 1999.

Gordaninejad, F., "A Novel Magneto-Rheological Shock Absorber for Vibration Control," Interim Report for ARO, 2000.

LIST OF PARTICIPANT IN THE PROJECT

Dr. Faramarz Gordaninejad, PI
Mr. Shawn P. Kelso, MS Degree in mechanical engineering, received December 1998.
Mr. Everet O. Ericksen, MS Degree in mechanical engineering, received May 1999.
Mr. Xiaojie Wang, Ph.D. in mechanical engineering, 1998-present.
Mr. Marc Karamanogian, Undergraduate Student in mechanical engineering, 1999-2000
Mr. Anthony Vassar, Undergraduate Student in mechanical engineering, 1998-2000

REPORT OF INVENTIONS

1. Gordaninejad, F. and Kelso, S. P., "Magneto-Rheological Fluid Shock Absorbers," Patent, accepted, pending publication, 2001.

2. Gordaninejad, F. and Ericksen, E. O., "Magneto-Rheological Fluid Devices," Patent, pending.

BIBLIOGRAPHY

1. Larminie, J. C. (1992). "The Value of Cross-Country Mobility," Proceedings of I.S.T.V.S. Conference on Off-Road Vehicles, London, UK.

2. Hoogterp, F. B., Saxon, N. L., and Schihl, P. J., 1993, "Semiactive Suspension for military Vehicles," SAE Technical Paper No. 930847.

3. Phillips, R. W., 1969, "Engineering applications of fluids with a variable yield stress," Ph.D. Dissertation, University of California.

4. Gordaninejad, F. and Kelso, S. P., "Magneto-Rheological Fluid Shock Absorbers for HMMWV," *Damping and Isolation, Proceedings of SPIE Conference on Smart Materials and Structures,* Ed. T. Tupper Hyde, Vol. 3989, pp. 266-273, 2000.

5. Kelso, S. P. and Gordaninejad, F., "Magneto-Rheological Fluid Shock Absorbers for Off-Highway, High-Payload Vehicles," *Passive Damping and Isolation, Proceedings of the SPIE Conference on smart materials and structures*, Ed. by L. Porter Davis Vol. 3672 pp. 44-54, 1999.

6. Kelso, S. P., 1998, "Development and Investigation of Magneto-Rheological Fluid (MRF) Dampers for Off-Highway, High-payload Vehicles," Master Thesis, University of Nevada, Reno.

7. Gavin, H. P. ,Hanson, R. D., and Filisko, F. E., 1996, "Electrorheological dampers, part I: analysis and design," *Journal of Applied Mechanics*, Vol. 63, pp669-675.

8. Chilton, R. A., and Stainsby, R., 1998, "Pressure loss equations for laminar and turbulent Non-Newtonian pipe flow," Journal *of Hydraulic Engineering,* Vol. 124, No.5, pp522-529.

Table 1. Values of A', α and A_0 for Different n.

n	α	A'	$A_0 = (A')^{-\frac{1}{\alpha}}$
1	2.260	3.289	0.590
0.8	2.105	3.031	0.591
0.4	1.784	2.700	0.573

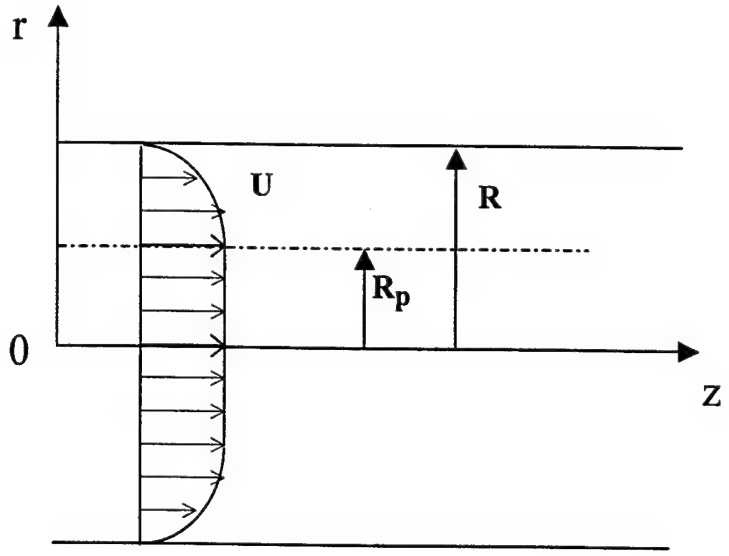

Figure 1. ER or MR fluid low profile in a pipe with a circular constant cross section.

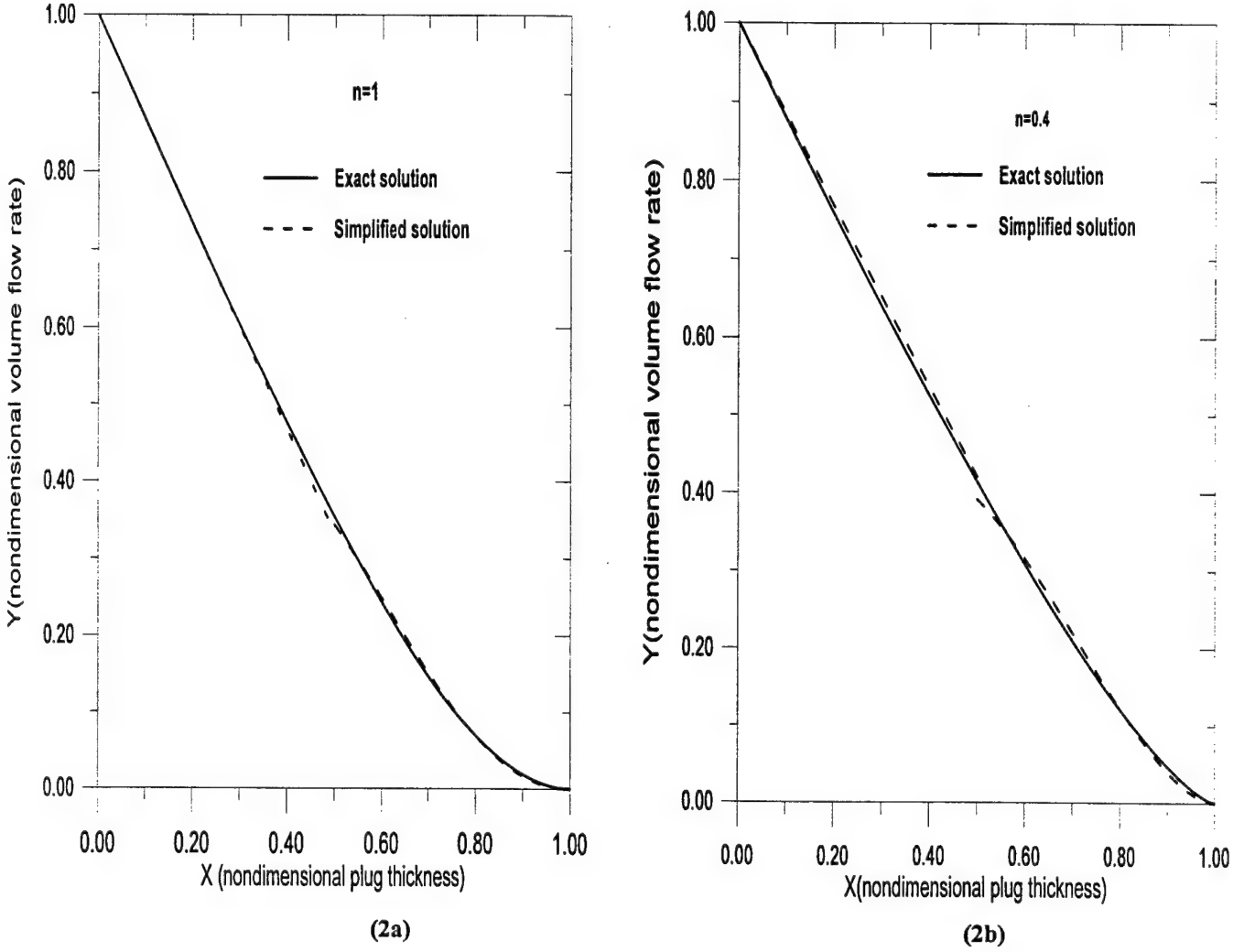

Figure 2. Comparison between the exact and simplified versions of Herschel-Bulkley pipe flow formulation for two different flow indices, n=1 and n=0.4.

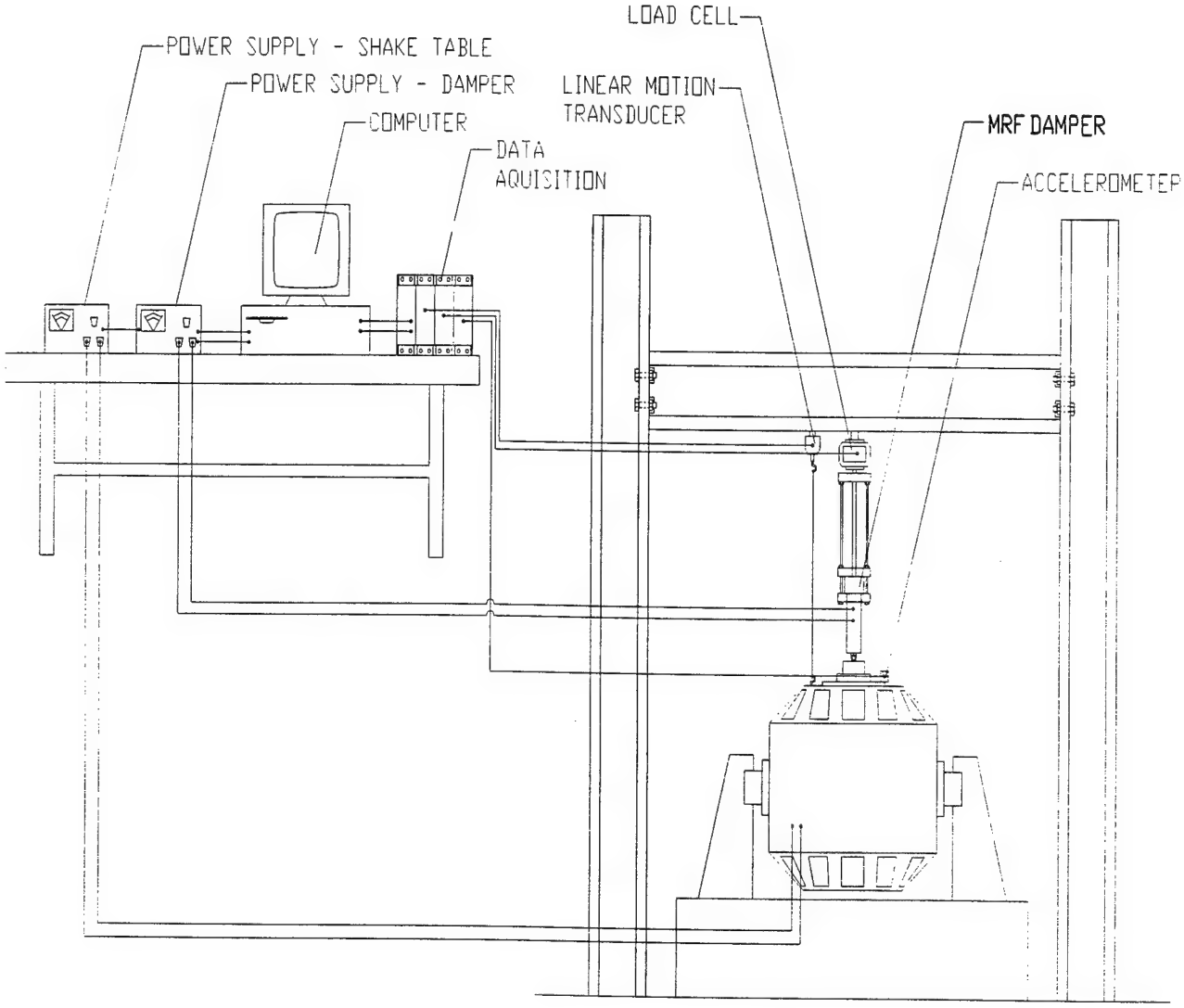

Figure 3. Schematic of the experimental setup.

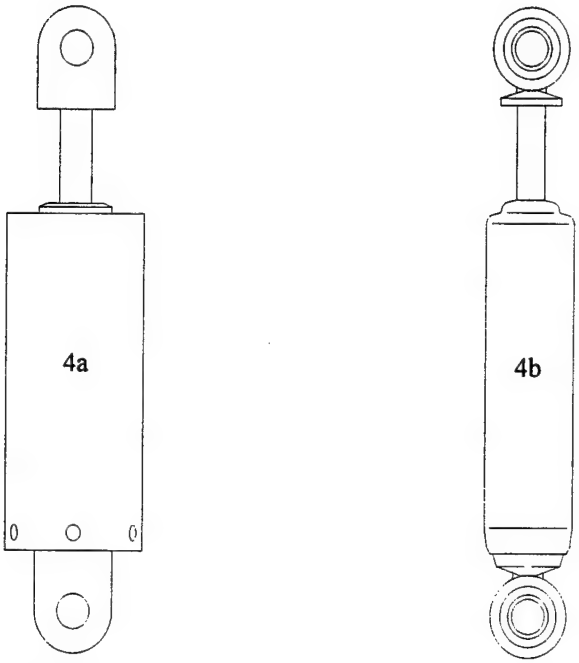

Figures 4. MRF (4a) and OEM (4b) dampers at the same scale.

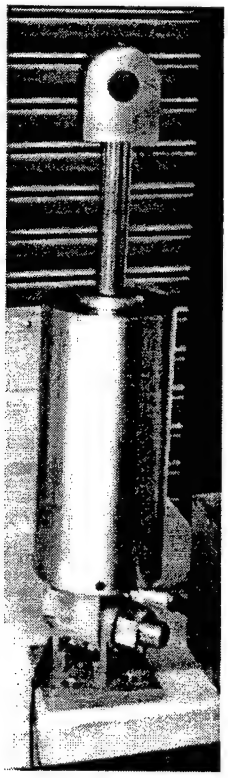

Figure 5. Photograph of the UNR MRF HMMWV damper.

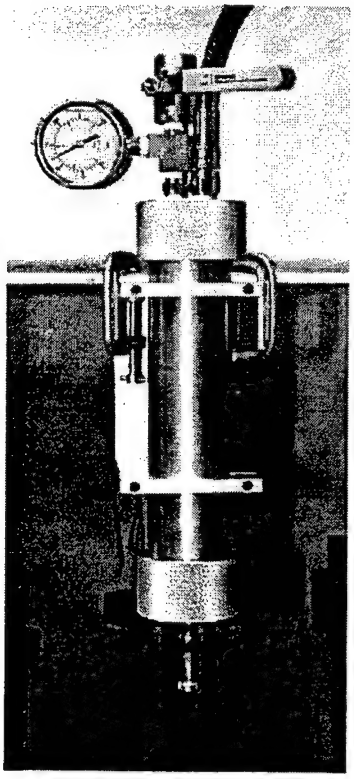

Figure 6. Photograph of the satellite accumulator.

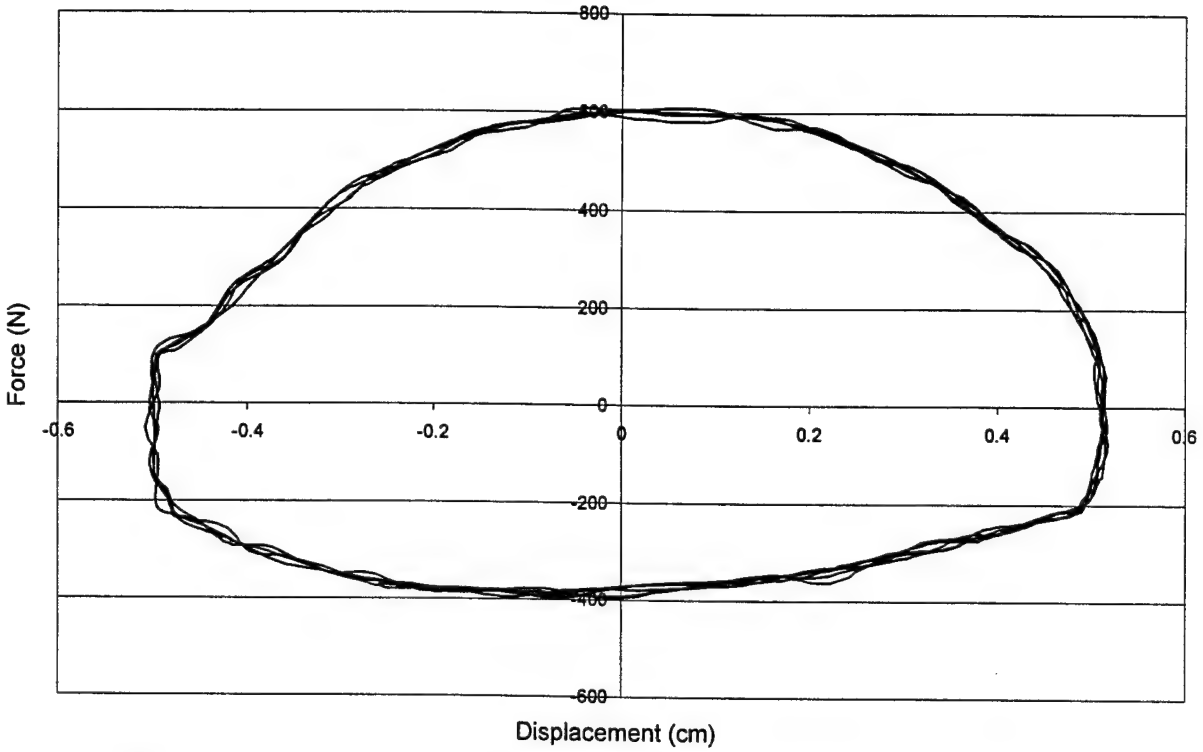

Figure 7. Force-displacement loop for OEM shock absorber at 2Hz, 1.0cm p-t-p.

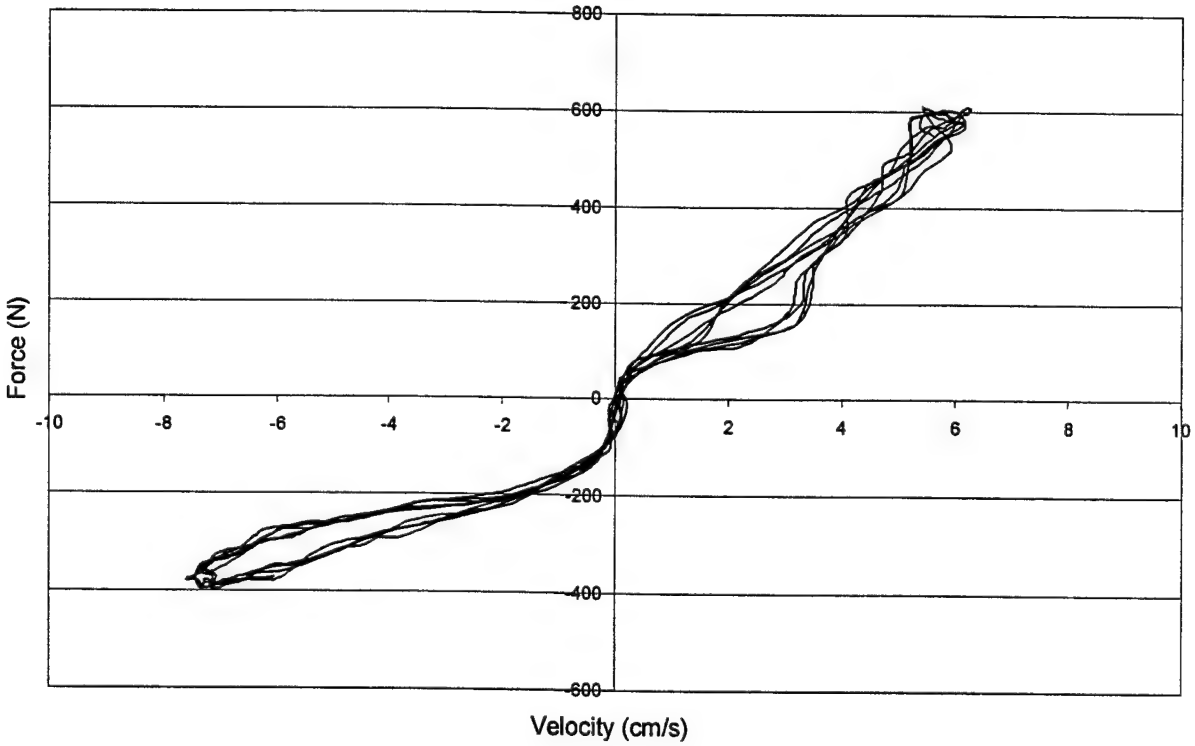

Figure 8. Force-velocity loop for the OEM shock absorber at 2Hz, 1.0cm p-t-p displacement.

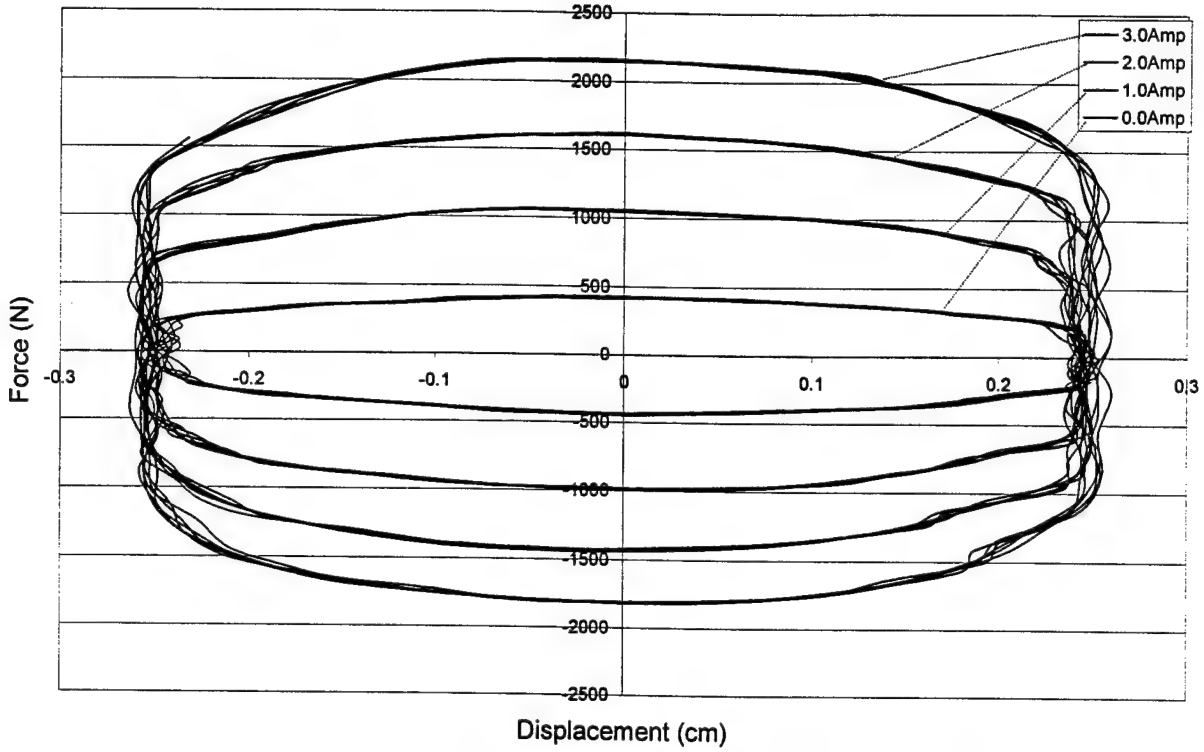

Figure 9. Force-displacement loops for the MRF damper at 2Hz, 1.0cm p-t-p displacement for different electrical current inputs.

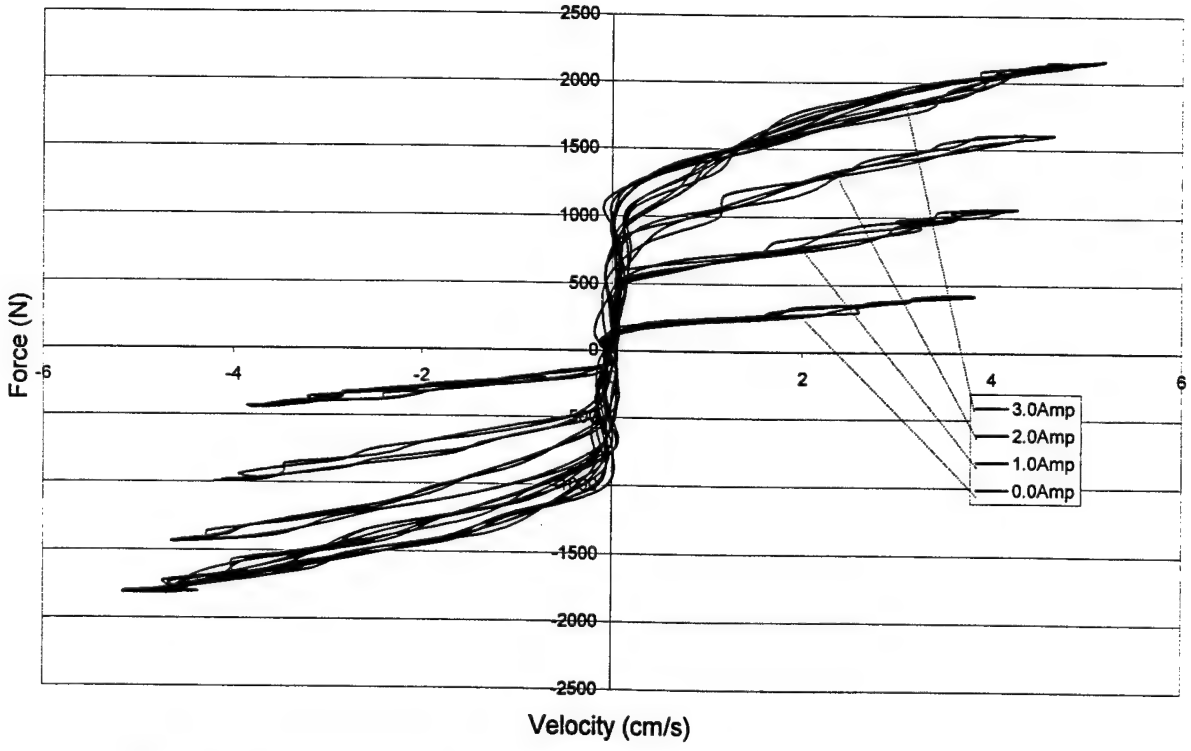

Figure 10. Force-velocity loops for MRF damper at 2Hz, 1.0cm p-t-p displacement for different electrical current inputs.

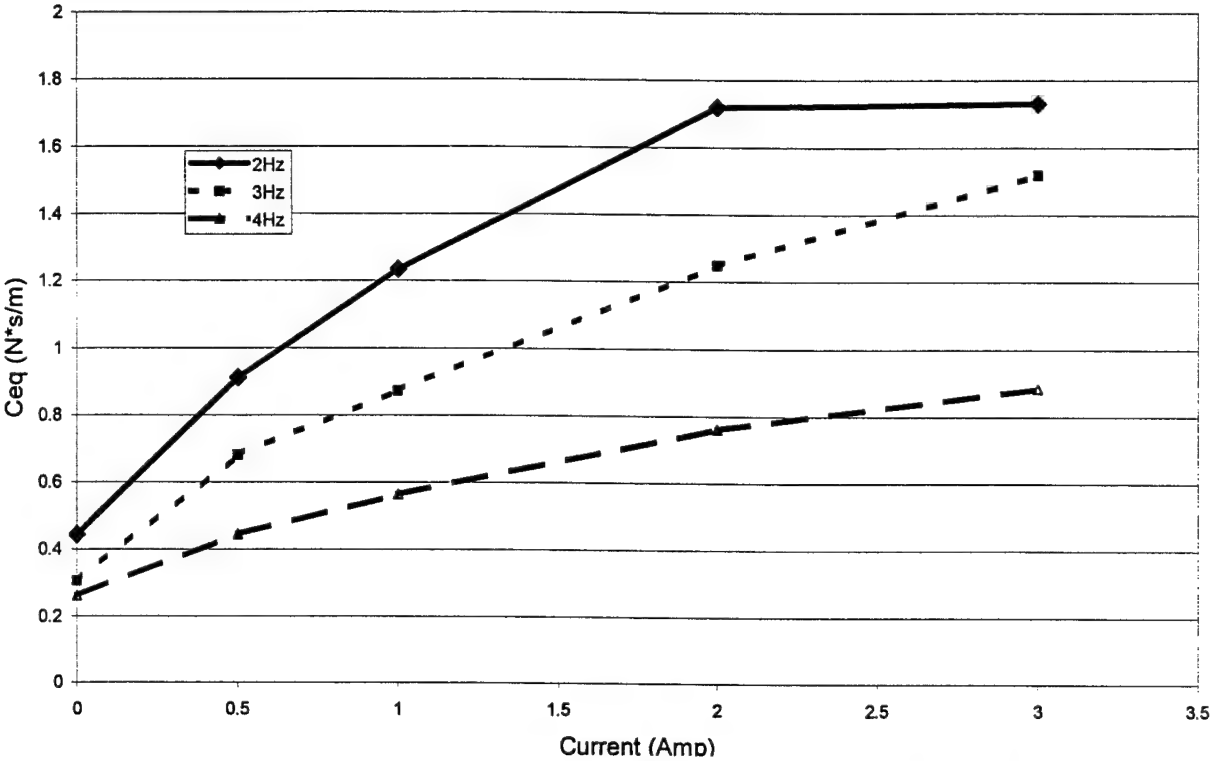

Figure 11. Experimental results for equivalent damping coefficient (C_{eq}) versus current for different frequencies for the MRF damper tested at 1.0cm peak-to-peak displacement.

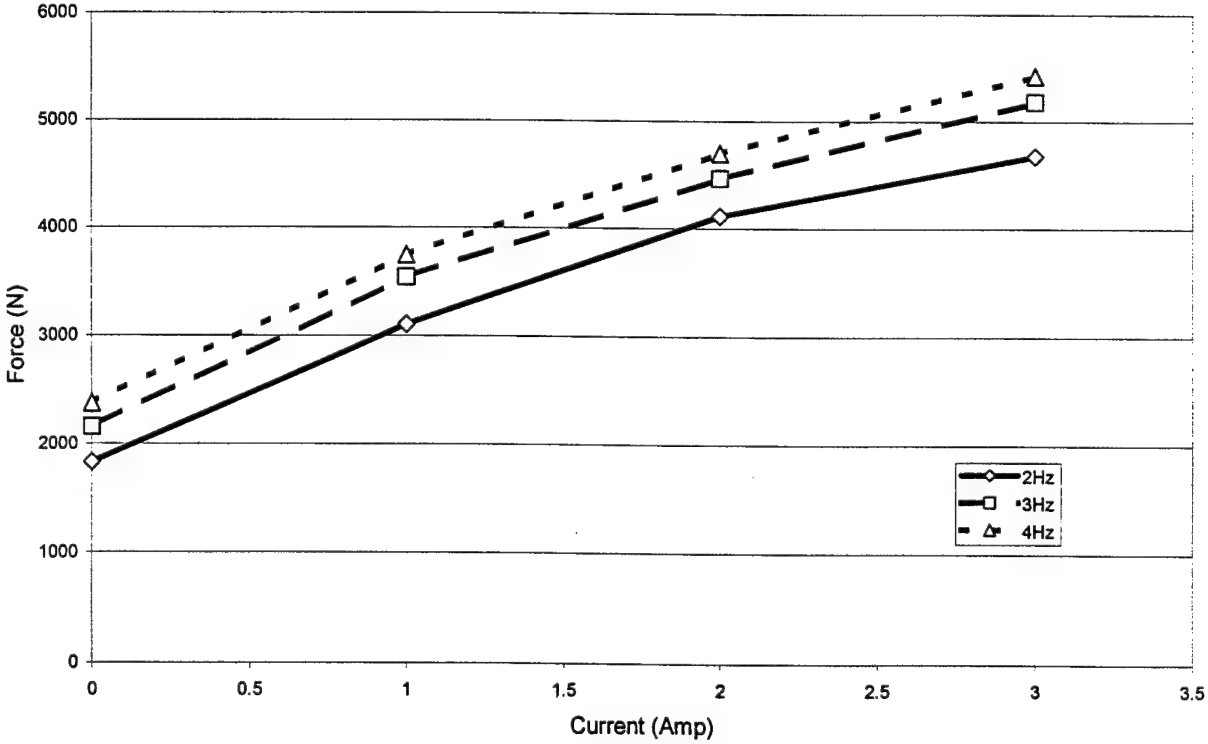

Figure 12. Experimental results for peak-to-peak force as a function of input electric current for the MRF damper at different frequencies (1.0cm peak-to-peak displacement).

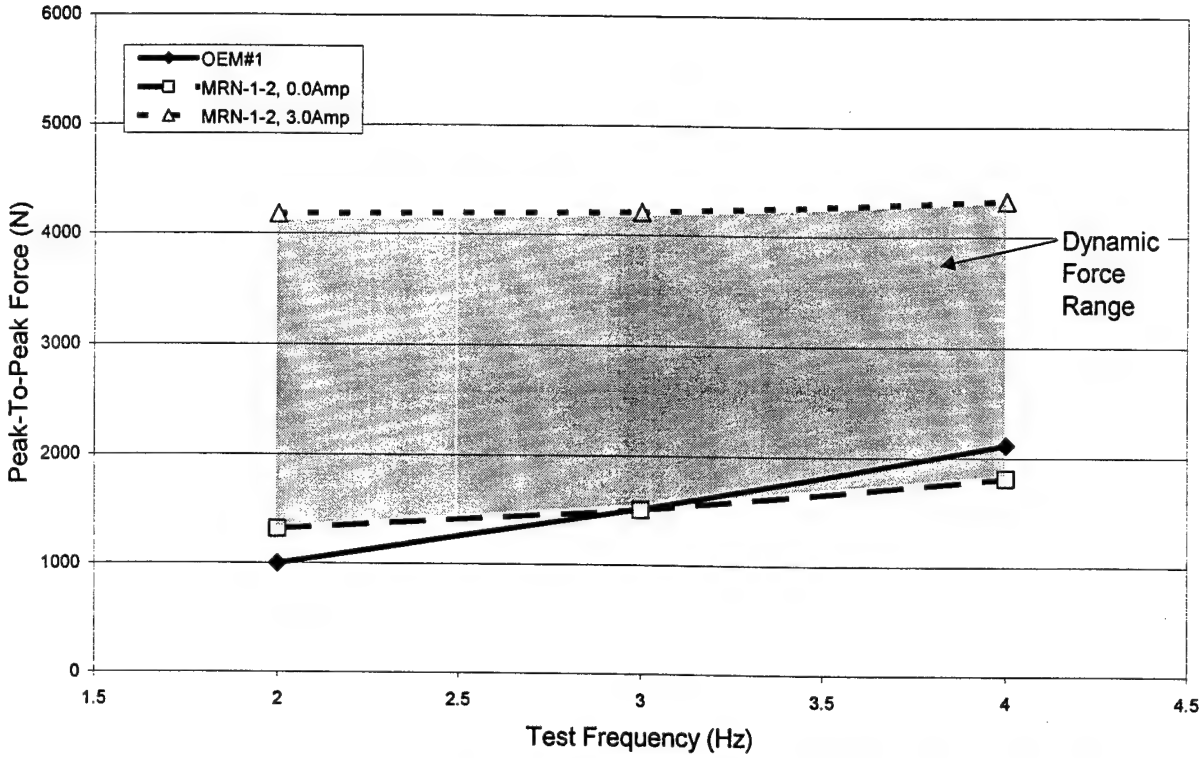

Figure 13. Comparison of peak-to-peak force as a function of frequency for the OEM unit and the MR fluid damper at 1.0cm peak-to-peak displacement.

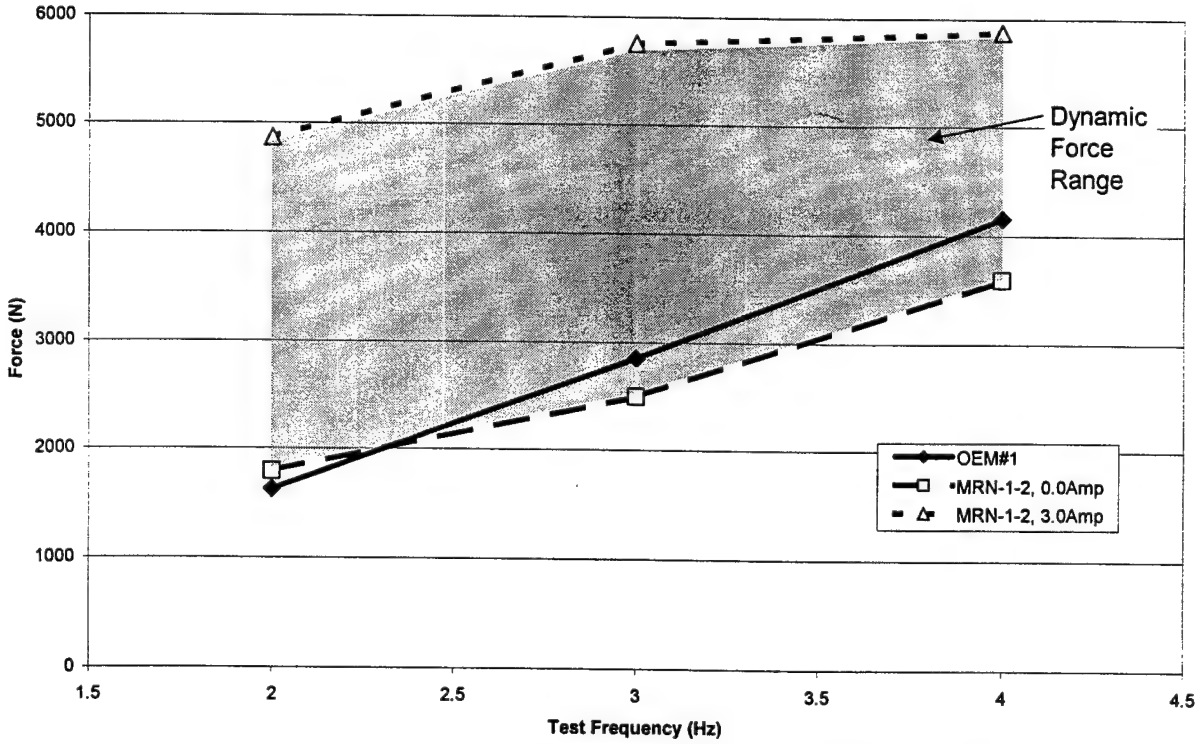

Figure 14. Comparison of peak-to-peak force as a function of frequency for the OEM unit and the MR fluid damper at 1.5cm peak-to-peak displacement.

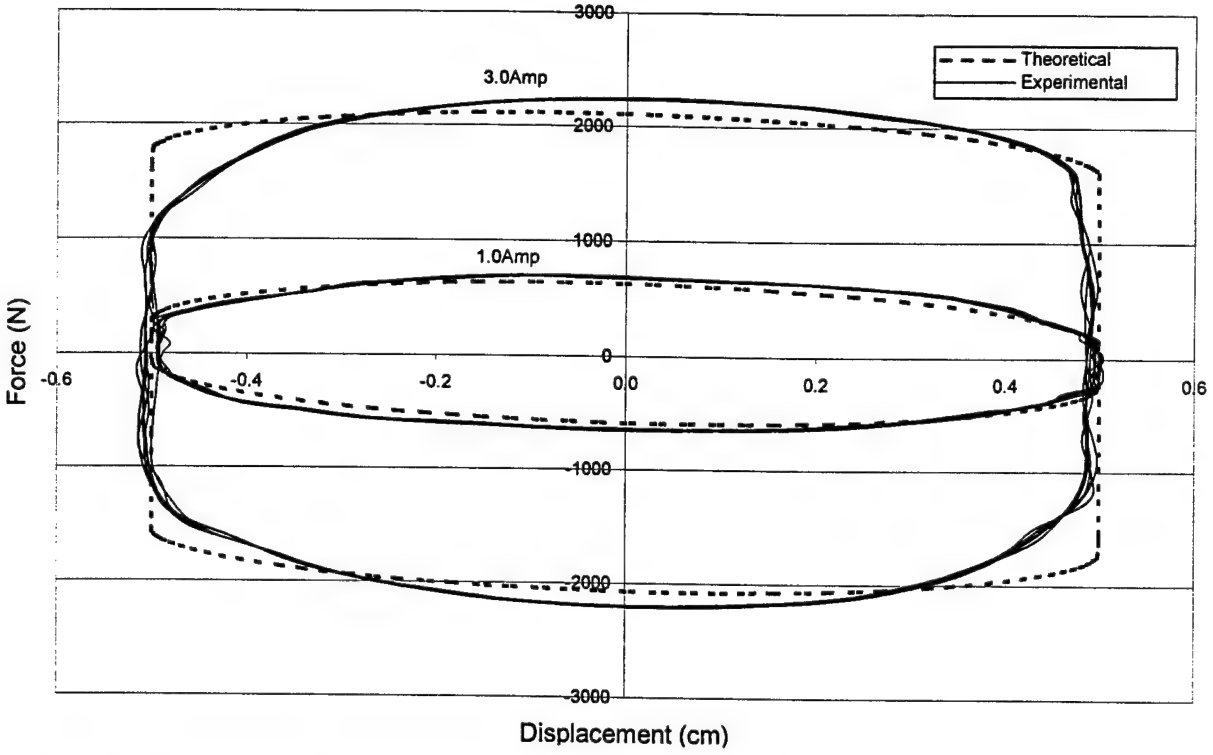

Figure 15. Comparison between theoretical and experimental force versus displacement of the MRF damper for passive-off and 3.0Amp input electric current.

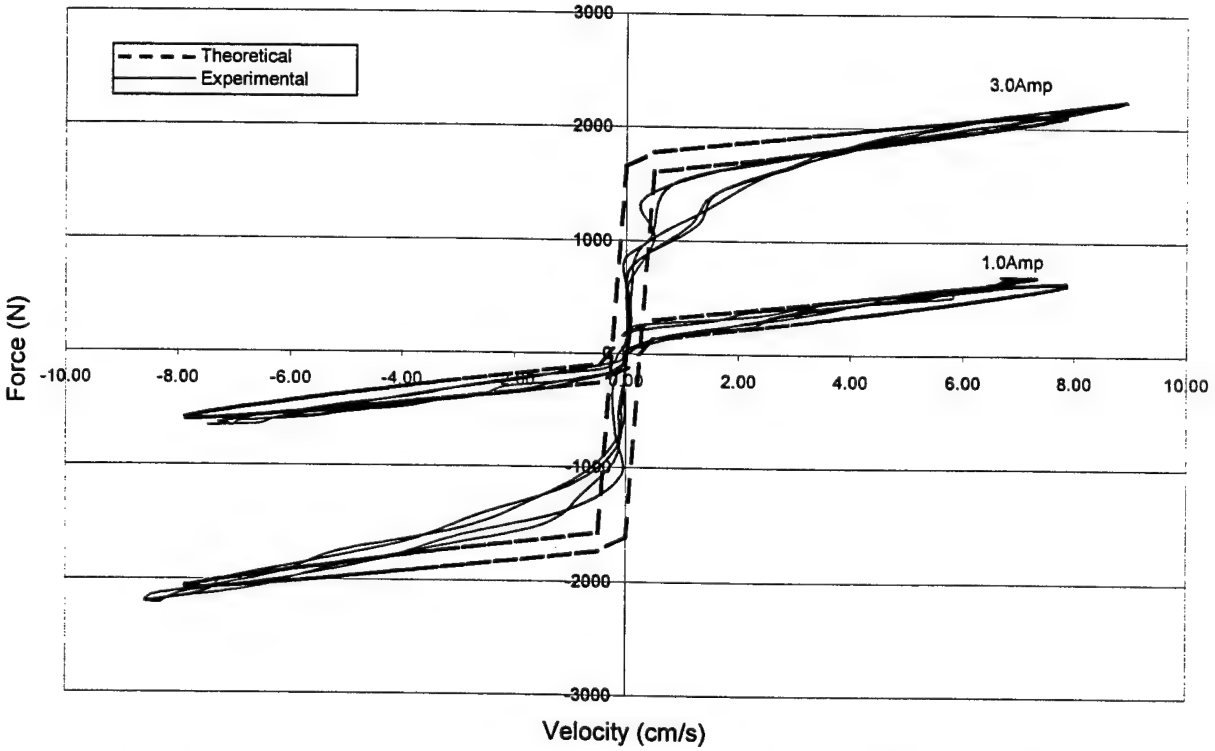

Figure 16. Comparison between theoretical and experimental force versus velocity of the MRF damper for passive-off and 3.0Amp input current.

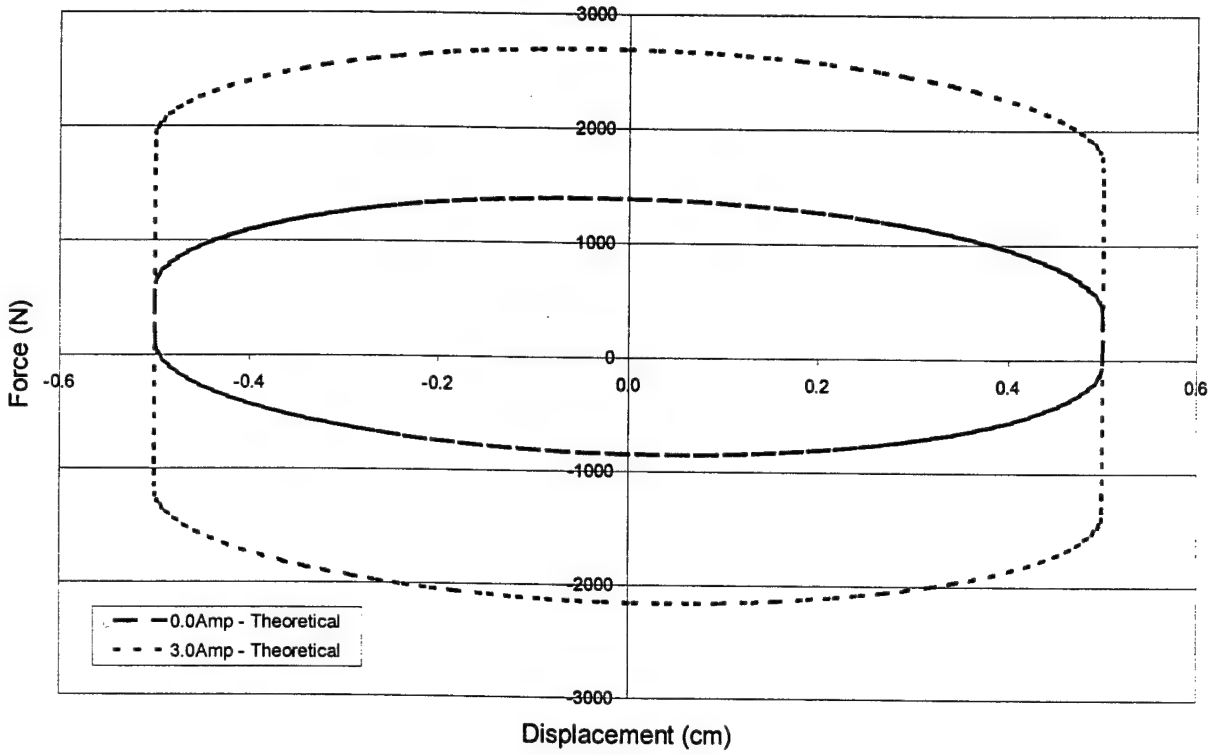

Figure 17. Theoretical force-displacement results for the MRF damper with return valves opened 0.0% on the compression stroke at 3Hz, 1.0cm p-t-p, for passive-off and 3.0Amp electric current.

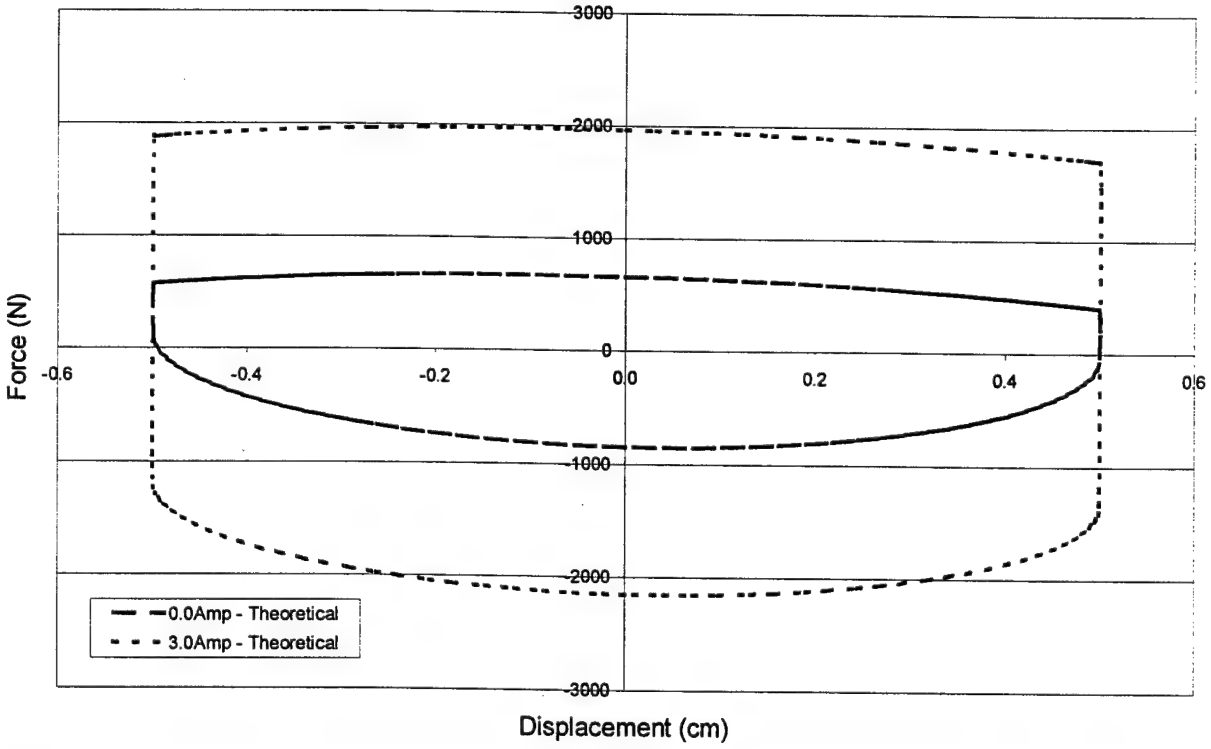

Figure 18. Theoretical force-displacement results for the MRF damper with return valves opened 25% on the compression stroke at 3Hz, 1.0cm p-t-p, for passive-off and 3.0Amp electric current.

APPENDIX A

Gordaninejad, F. and Kelso, S. P., "Semi-Active Magnetorheoogical Dampers for HMMWV," *Journal of Intelligent Materials, Systems and Structures*, accepted, to appear in 2001.

FAIL-SAFE MAGNETO-RHEOLOGICAL FLUID DAMPERS FOR OFF-HIGHWAY, HIGH-PAYLOAD VEHICLES

Faramarz Gordaninejad[1] and Shawn P. Kelso[2]

Department of Mechanical Engineering
Composite and Intelligent Materials Laboratory
University of Nevada, Reno, Nevada 89557, USA
Phone: 775-784-6990, Fax: 775-784-1701, E-mail: faramarz@unr.edu

ABSTRACT

This paper presents the study of a field-controllable, semi-active magneto-rheological fluid (MRF) shock absorber for high-payload, off-highway vehicles. A MRF damper is developed that is tailored for ground vehicles which undergo a wide range of dynamic loading. The MRF damper also has the capability for different rebound and compression characteristics. The new MRF shock absorber emulates the original equipment manufacture shock absorber behavior in its passive-off mode. Theoretical and experimental studies are performed to examine this MRF damper. The Bingham Plastic theory is employed to model the nonlinear behavior of the MRF. A fluid-mechanics-based theoretical model along with a three-dimensional finite element electromagnetic analysis is utilized to predict the MRF damper performance. The theoretical and experimental results are demonstrated to be in good agreements.

Keywords: Fail-safe, Field-controllable, Semi-active, Magneto-rheological fluid damper, Off-highway, Ground vehicle, HMMWV.

[1] Professor, the author to whom correspondence should be addressed
[2] Graduate Research Assistant

1. INTRODUCTION

Advances in technology that allow a significant enhancement in cross-country mobility of combat vehicles, such as high mobility multi-purpose wheeled vehicles (HMMWVs), can affect the battlefield engagement's location and timing (Larminie, 1992). Experiments have demonstrated that the utilization of semi-active suspension technology in military vehicles can substantially increase the cross-country mobility (Hoogterp *et al.*, 1993). The present study provides an innovative, fail-safe, semi-active, magneto-rheological fluid (MRF) damper for the suspension system of HMMWVs.

To achieve HMMWV's high performance in demanding cross-country terrain, the value of a properly designed and reliable suspension system cannot be over estimated. Conventional suspension system design has reached its practical limits towards significantly increasing cross-country performance (Hoogterp *et al.*, 1993). A semi-active suspension system, which consists of a conventional spring and a controllable damper, has shown to be a practical solution for enhancing the performance of suspension systems. The variable damper provides a controllable damping force. It has also been demonstrated that semi-active suspensions can provide the same performance as active suspensions (which includes power actuators) without high power consumption and with very small design variations from conventional passive systems (Ivers, and Miller, 1991, and Barak, 1989).

As a component of a semi-active suspension system, the role of the MRF shock absorber is to have the capacity to produce variable damping reactive to the input motion. The ability to vary damping for a wide range of input motion is the main feature of semi-active suspension systems.

Other features include control of body roll during turning, control of vehicle pitch during braking and acceleration, and accommodation for a variable vehicle mass (i.e., empty or full payloads). In comparison to typical passive suspension systems, semi-active shock absorbers allow for softer damping when needed, in addition to harder damping for situations that demand it. The main benefits of this technology for ground vehicles are: faster operational speeds over similar terrain and improved vibration isolation for sensitive payloads.

MRF dampers are semi-active devices that contain magneto-rheological fluids (Carlson, *et al.*, 1995). The activation of MRF damper's built-in magnetic field causes a fast change in the shear yield stress and the viscosity of a MR fluid. The fluid changes state from liquid to semi-solid in milliseconds. The result is an infinitely variable, controllable damper capable of large damping forces. MRF dampers offer an attractive solution to energy absorption in mechanical systems and structures. This is because they can be battery operated, require minimal power for operation, and have additional benefits, such as, the absence of mechanical valving (for flow control) in the damper, insensitivity to impurities penetration, fluid stability, and long operational life. Most importantly, MRF dampers can be considered as "fail-safe" devices.

This study presents a fail-safe MRF damper. In the absence of an electric input current to the damper or in the case of a malfunction in the control hardware, the new MRF damper provides the same damping force that is produced by an original equipment manufacture (OEM) passive viscous damper. A new generation of MRF dampers has been developed at the University of Nevada, Reno (UNR) that provide a fail-safe and robust vibration damping solution (Gordaninejad and Kelso, 1999, and Gordaninejad and Breese, 2000). Several innovative prototypes MRF dampers have been developed and studied in recent years for different

applications, such as mountain bicycles, motorcycles, vehicles, and seismic applications (Breese and Gordaninejad, 1999, Breese and Gordaninejad, 2000, Breese, et al., 2000, Dogruoz, et al. 2000, Ericksen, and Gordaninejad, 1999, Ericksen, and Gordaninejad, 2000, Gordaninejad and Breese, 2000, Gordaninejad and Ericksen, 2000, Gordaninejad, and Kelso, 2000, Gordaninejad, et al 1998 (a), and 1998 (b), Liu, Y., et al., Kelso and Gordaninejad, 1999, Wang and Gordaninejad, 2000 (a), and 2000 (b)). The main advantage of UNR MRF dampers is that they can produce a damping force nearly the same as an OEM passive viscous damper at their passive-off state (zero electric input current) while providing a sizable dynamic force range to allow controllability. This is schematically demonstrated in Figure 5, where the OEM viscous passive damper has a linear response and the MRF damper at passive-off state is designed so that it is slightly softer than the OEM damper. At maximum power input, the damper can provide sufficient dynamic force range for the application.

The fail-safe design of MRF dampers requires that the device must have a certain viscous damping capability. The viscous damping force in a damper is a function of material properties as well as geometric dimensions within the damper. This requires a combined investigation of the damper and the fluid.

In this work, theoretical and experimental studies of a new MRF damper are presented (Gordaninejad and Kelso, 1999). The MRF damper can provide a controllable range of damping force that can utilize the on-board power supply of the HMMWV. A new method for achieving controllable damping via manipulation of MR passage geometry allows for fine-tuning of passive and semi-active damping behavior. The UNR damper design also has the capacity to effectively utilize existing ground vehicle shock absorber technology in the arenas of by-pass

valves and over-travel protection. A theoretical model is developed that has the capability of predicting the behavior of the MRF damper. Utilizing a fluid-mechanics based model and the Bingham plastic theory, the theoretical model accommodates for the geometric parameters as well as material and input motion characteristics. In addition, the theoretical model includes the effects of bypass-valves.

2. THEORETICAL MODELING OF THE MRF DAMPER

A magneto-rheological fluid consists of micron-sized ferrous particles within a base carrier fluid, such as silicon or mineral oil, and additives. Under the influence of a magnetic field, the ferrous particles polarize and attract each other, resulting in the formation of chains or columns of particles parallel to the orientation of the magnetic flux lines. This results in a quantifiable change in the "apparent viscosity" of the fluid, which is defined as:

$$\mu_{APP} = \frac{\tau}{\dot{\gamma}} \tag{1}$$

Here, μ_{APP} is the apparent viscosity of fluid, τ represents fluid shear stress at the wall, and $\dot{\gamma}$ is the shear strain rate. The Bingham plastic model is defined as (Phillips, 1969):

$$\tau = \tau_Y + \mu_0 \dot{\gamma} \tag{2}$$

where τ_y is the field-induced shear stress and μ_0 represents plastic viscosity of the fluid. From Equations (1) and (2), one has:

$$\mu_{APP} = \frac{\tau_Y + \mu_0 \dot{\gamma}}{\dot{\gamma}} = \frac{\tau_Y}{\dot{\gamma}} + \mu_0 \tag{3}$$

In the absence of minor head loss terms, as well as fluid inertia, and seal friction, the pressure drop across the piston can be expressed as (Kelso, 1998, Kelso and Gordaninejad, 1999, Gordaninejad and Kelso, 2000):

$$\Delta P = \frac{32\mu_{APP} L_{CH} V_{CH}}{D_{eff}^{\ 2}} \tag{4}$$

where L_{CH} is the length of the channel, V_{CH} is the velocity of the MRF in the channel, D_{eff} is the effective hydraulic diameter ($D_{eff} = [64/(fRe)]D_H$, where fRe is the geometry-specific, laminar friction constant for non-circular flows), and ΔP is the pressure drop. Substitution of Equation (3) into Equation (4) produces:

$$\Delta P = \frac{32\mu_0 L_{CH} V_{CH}}{D_{eff}^{\ 2}} + \frac{32KI^{\delta} L_{MR}}{D_{eff}} \tag{5}$$

where KI^{δ} is the shear yield stress of the MRF and L_{MR} is the length of the MR valve. I is the input electric current and K and δ are the constants which are determined by a three-dimensional electro-magnetic finite element analysis.

For different rebound and compression behavior, or to accommodate high-force impact loads, extra passages open as spring-backed valves retract. For this MRF damper design, these passages are in a parallel arrangement. Equating total volumetric flow rate across the piston provides the following relation for the fluid velocity (Kelso, 1998):

$$V_{CH} = \frac{\dot{X}_P A_{PISTON}}{NA_{MR} + \beta M A_{NON-MR}\phi} \tag{6}$$

where $\underline{\dot{X}}_P$ is the input velocity of piston, A_{PISTON} is the effective area of piston, A_{MR} is the cross-sectional area of MRF channel, $A_{NON\text{-}MR}$ is the cross-sectional area of non-MR-effected passages, N is the number of MR channels, M is number of non-MR-effected passages in parallel, β is the contribution (in terms of percent-opening) of the non-MR-effected passages and ϕ is:

$$\phi = \left(\frac{D_B^{\,2}}{D_{eff}^{\,2}}\right)\left[1 + \frac{\tau_Y / \dot{\gamma}}{\mu_0} + \frac{2L_{MR}}{L_P} + \frac{(\tau_Y / \dot{\gamma})2L_{MR}}{\mu_0 L_P}\right] \tag{7}$$

Here D_B is the diameter of return channels, and L_p is the length of the piston. Combining Equations (5)-(7) and multiplying by the area of piston yields the following expression for the damping force, F_{DAMPER}:

$$F_{DAMPER} = \frac{32\mu_0 L_{CH}}{D_{eff}^{\,2}}\left(\frac{(A_{PISTON})^2}{NA_{MR} + \beta M A_{NON-MR}\phi}\right)\underline{\dot{X}}_P + \frac{16KI^{\delta}L_{MR}}{D_{eff}} A_{PISTON}\,\mathrm{sgn}(\underline{\dot{X}}_P) \tag{8}$$

3. EXPERIMENTAL STUDY

To establish a foundation for the fail-safe design, first, the characteristics of two OEM HMMWV dampers were studied. The OEM shock absorbers were characterized at 2, 3, 4 and 7Hz frequencies. For each frequency considered, four different peak-to-peak amplitudes of displacement (0.5, 1.0, 1.5 and 2.0cm) were examined. This allowed the design of a passive fail-safe baseline characteristic of the MRF damper.

For the MRF damper, an additional parameter is examined. Increased damping is achieved through applying electrical current to the built-in electromagnet of the device. With no current

not have all of the elements of the commercial unit. For example, elastomer bearings are incorporated into the semi-rigid mount of the OEM damper. This is to accommodate for minor off-axis loading, typical to pivotal loading environments of vehicles. The MRF damper has rigid steel mounts, as its function is to mount only to the testing apparatus. This also eliminates the effects of the spring and damping properties of the elastomer.

Figure 3 is a photograph of the actual MRF damper used for testing. Five different variants of this design were developed and tested to thoroughly explore parameters of design. Figure 4 is a photograph of the satellite accumulator, which is kept separate from the experimental damper to simplify damper assembly and disassembly. The role of the accumulator is to accommodate for the change in available fluid volume as the piston reciprocates inside the cylinder. Most OEM shock absorbers have the accumulator integrated into the unit itself. The MRF damper design presented in this paper also has this capacity, but the accumulator is kept separate for the aforementioned purpose.

4. EXPERIMENTAL AND THEORETICAL RESULTS

Figure 5 presents experimental results for the force-displacement of a HMMWV OEM shock absorber at 2Hz, 1.0cm peak-to-peak amplitude of displacement. Figure 6 illustrates the force-velocity data for the same test. Figures 7 and 8 show results of the same experiment for the UNR HMMWV MRF damper. In comparing Figure 5 and Figure 7, it is apparent that peak-to-peak, passive-off damping force is similar for the MRF damper and the OEM unit. Figure 7 also shows the range of damping that increases as current supplied to the MRF damper increases. The baseline peak-to-peak force at 2Hz for both devices is about 600N (135lbf), while the

increase in peak-to-peak force (via current supplied to the MRF damper) is almost 2,200N (500lbf). In comparing the force-velocity data of both units (Figure 6 for the OEM unit and Figure 8 for the MRF damper at zero-field), the offset 'step' in the hysteresis loops at zero velocity is due to the pressure resulting from the accumulator. When current is applied to the MRF damper, damping force increases the height of the offset force step at zero velocity. In Figure 8 the peak velocity increases as damping force increases. This is the result of the experimental setup. The shake table maintains constant frequency, while the peak-to-peak displacement changes, slightly, which results in increased peak velocity.

Figure 9 illustrates another means for evaluating damper performance. Quantifying the area within any given force-displacement hysteresis loop provides an amount of work done by the damper during one complete stroke. For an equivalent linear damper, the damping coefficient can be determined by:

$$C_{eq} = \frac{W}{\pi X^2 \omega} \tag{9}$$

where C_{eq} is the equivalent damping coefficient, W represents the work done by the damper during one cycle, X is the amplitude of displacement, and ω is the frequency in radians per second. As frequency increases and current to the damper increases, the energy absorbed by the damper increases. For the same test data, Figure 10 illustrates the values of peak-to-peak force as a function of input electric current for the MRF damper.

Figure 11 and Figure 12 illustrate the force envelope of the MRF damper as a function of frequency for two different test displacements (1.0 and 1.5cm peak-to-peak, respectively). Also

shown for comparison on both graphs are the results of the OEM shock absorber. The benefit of controllable damping presented in this study is made evident by these two graphs; a range of damping force with the MRF damper versus the passive damping force of the OEM shock absorber. As energy inputs vary to the vehicle, the MRF damper has the capability to vary the amount of energy absorption accordingly.

Figure 13 is a comparison of force-displacement experimental and theoretical results for the MRF damper at 2Hz, 1.0cm peak-to-peak displacement. Experiments were performed at passive-off mode (zero input electrical current) and 3.0Amp input electric current. Figure 14 shows the force-velocity results for the same tests. Figures 15 and 16 are theoretical force-displacement results illustrating the effects of the extra by-pass valves mentioned earlier. It is evident that the MRF damper no longer has a symmetrical appearance when the valves are opened.

5. CONCLUSIONS

A new, fail-safe, controllable, semi-active MRF fluid damper was developed and studied to determine the viability of implementation of this technology into ground vehicles. It has been demonstrated that the MRF damper has a broad dynamic force range and can emulate OEM damper behavior at its passive-off fail-safe mode. The new design also allows for integration of current hydraulic automotive shock absorber technology, such as by-pass valves and over-travel protection. In conjunction with a semi-active control system, this technology has shown promise for implementation into ground vehicles.

6. ACKNOWLEDGEMENTS

This study is funded by the U. S. Army Research Office Grant Number DAAG55-98-10017. The authors are thankful for the encouragement by Dr. Gary Anderson, the Program Director. Helpful comments of Mr. Hitchcock are also appreciated.

7. REFERENCES

Barak, P., 1989, "Design and Evaluation of an Adjustable Automatic Suspensions," SAE Paper No. 890089.

Breese, D. G. and Gordaninejad, F., 1999, "Heating of Magneto-Rheological Fluid Dampers: A Theoretical Study," *Smart Systems for Bridges, Structures, and Highways, Proceedings of the 1999 SPIE Conference on smart materials and structures*, Vol. 3671, pp. 2-10.

Breese, D. G., and Gordaninejad, F., 2000, "Semi-Active Controllable Magneto-Rheological Fluid Dampers for A Mountain Bicycle," *Proceedings of SPIE Conference on Smart Materials and Structures,* Newport Beach, California, March, in press.

Breese, D. G., Gordaninejad, F., and Ericksen, E. O., 2000, "Heat Generation of Magneto-Rheological Fluid Dampers: A Theoretical Study Utilizing Fluid Dynamics Approach," *Proceedings of SPIE Conference on Smart Materials and Structures,* Newport Beach, California, March, in press.

Carlson, J. D., Catanzarite, D. M. and St. Clair, K. A., 1995, "Commercial Magneto-Rheological Fluid Devices," *Proceedings of the 5th International Conference on ER Fluids, MR Fluids and Associated Technology*, U. Sheffield, UK, pp. 20-28.

Dogruoz, M. B., Gordaninejad, F., Wang, L. C., and Stipanovic, A., 2000, "Heat Transfer of Magneto-Rheological Dampers," *Proceedings of SPIE Conference on Smart Materials and Structures,* Newport Beach, California, March, in press.

Ericksen, E. O., and Gordaninejad, F., 1999, "A Magneto-Rheological Fluid Shock Absorbers for an Off-Road Motorcycle," *Proceedings of Asia-Pacific Vibration Conference'99*, Ed. By O. J. Huat and L. K. Meow, Vol. 2, pp. 267-271.

Ericksen, E. O., and Gordaninejad, F., 2000, "A Magneto-Rheological Fluid Shock Absorbers for the Rear Suspension of an Off-Road Motorcycle: A Theoretical Study, *Proceedings of SPIE Conference on Smart Materials and Structures,* Newport Beach, California, March, in press.

Gordaninejad, F. and Breese, D. G., 2000, "Magneto-Rheological Fluid Dampers," U. S. Patent No. 6,019,201.

Gordaninejad, F. and Kelso, S., 1999, "Controllable Magneto-Rheological Fluid Shock Absorbers," patent pending.

Gordaninejad, F., and Breese, D. G., 2000, "Heating of Magnetorheological Fluid Dampers," *Journal of Intelligent Materials, Systems and Structures*, accepted, in press.

Gordaninejad, F., and Ericksen, E. O., 2000, "A Magneto-Rheological Fluid Shock Absorbers for the Rear Suspension of an Off-Road Motorcycle: A Theoretical Study," *Proceedings of SPIE Conference on Smart Materials and Structures,* Newport Beach, California, March, in press.

Gordaninejad, F. and Kelso, S. P., 2000, "Magneto-Rheological Fluid Shock Absorbers for HMMWV," *Proceedings of SPIE Conference on Smart Materials and Structures,* Newport Beach, California, March, in press.

Gordaninejad, F., Saiidi, M., Hansen, B. C., and Chang, F-K, 1998 (a), "Magneto-Rheological Fluid Dampers for Control of Bridges," *Proceedings of the Second World Conference on Structural Control,* Ed. By Kobori et al, Wiley, pp. 991-1000, *Kyoto*, Japan.

Gordaninejad, F., Saiidi, M., Hansen, B. C., and Chang, F-K, 1998 (b), "Control of Bridges Using Magneto-Rheological Fluid Dampers and Fiber-Reinforced, Composite-Material Column," *Smart Systems for Bridges, Structures, and Highways, Proceedings of the 1998 SPIE Conference on smart materials and structures*, Vol. 3325, pp. 2-11.

Hoogterp, F. B., Saxon, N. L., and Schihl, P. J., 1993, "Semiactive Suspension for military Vehicles," SAE Technical Paper No. 930847.

Ivers, D. E., and Miller, L. R., 1991, "Semi-Active Suspension Technology: An Evolutionary View," DE-Vol. 40, Advanced Automotive Technologies, ASME.

Kelso, S. P., 1998, "Development and Investigation of Magneto-Rheological Fluid (MRF) Dampers for Off-Highway, High-payload Vehicles," Master Thesis, University of Nevada, Reno.

Kelso, S. P. and Gordaninejad, F., 1999, "Magneto-Rheological Fluid Shock Absorbers for Off-Highway, High-Payload Vehicles," *Passive Damping and Isolation, Proceedings of the 1998 SPIE Conference on smart materials and structures*, Ed. by L. Porter Davis Vol. 3672 pp. 44-54.

Larminie, J. C., 1992, "The Value of Cross-Country Mobility," *Proceedings of I.S.T.V.S. Conference on Off-Road Vehicles*, London, UK.

Liu, Y., Gordaninejad, F., Evrensel, C. A., Wang, X., and Hitchcok, 2000, "Semi-active Control of a Bridge Using Controllable Magneto-Rheological Dampers," *Proceedings of SPIE Conference on Smart Materials and Structures,* Newport Beach, California, March, in press.

Phillips, R. W., 1969, "Engineering applications of fluids with a variable yield stress," Ph.D. Dissertation, University of California.

Wang, X., and Gordaninejad, F., 1999, "Herschel-Bulkley Analysis of Electro- and Magneto-Rheological Controllable Fluids in Flow Mode," *Proceedings of the 7th International Conference on ER Fluids and MR Suspensions*, pp. 580-591.

Wang, X., and Gordaninejad, F., 2000 (a), "Study of Controllable Fluid Dampers in Flow Mode using Herschel-Bulkley Model," *Proceedings of SPIE Conference on Smart Materials and Structures,* Newport Beach, California, March, in press.

Wang, X., and Gordaninejad, F., 2000 (b), "Flow Analysis of Field-Controllable, Electro- And Magneto-Rheological Fluids Using Herschel-Bulkley Model," *Journal of Intelligent Materials, Systems and Structures*, accepted, in press.

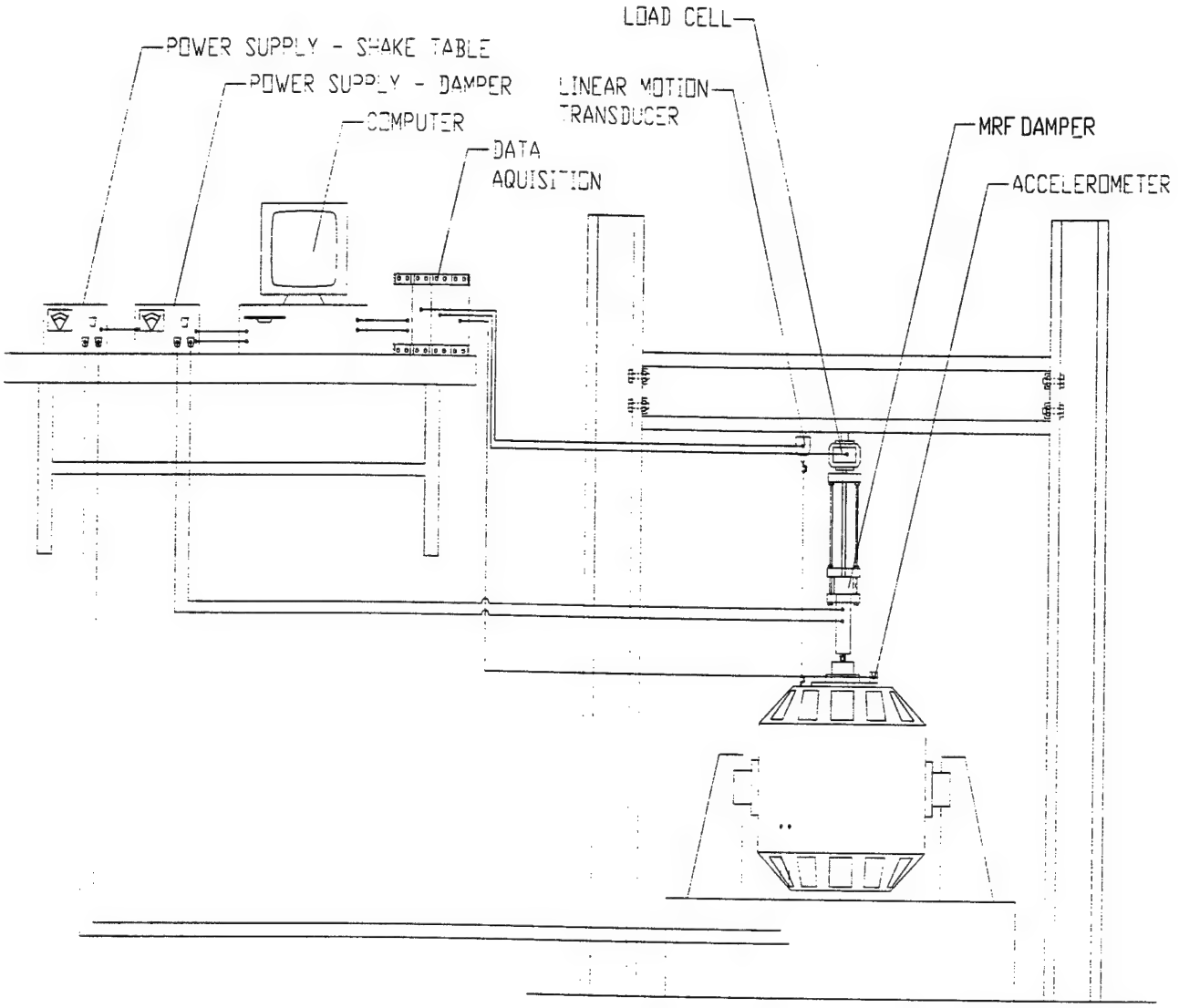

Figure 1. Schematic of the experimental setup.

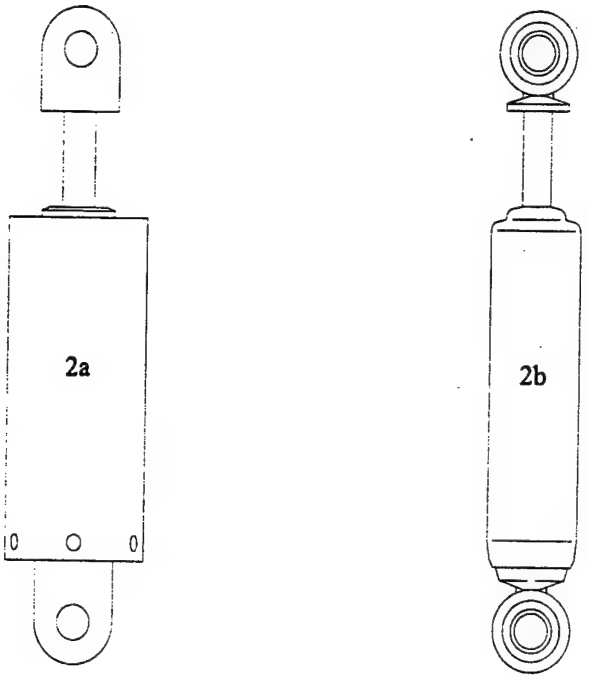

Figures 2. MRF (2a) and OEM (2b) dampers at the same scale.

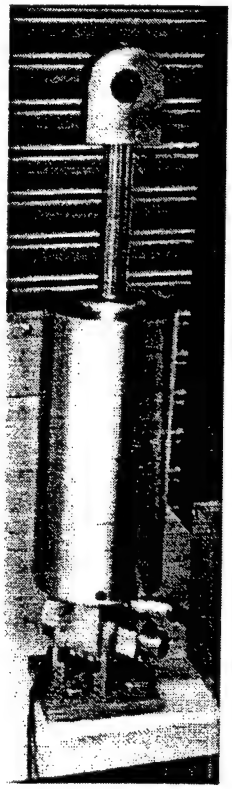

Figure 3. Photograph of the UNR MRF HMMWV damper.

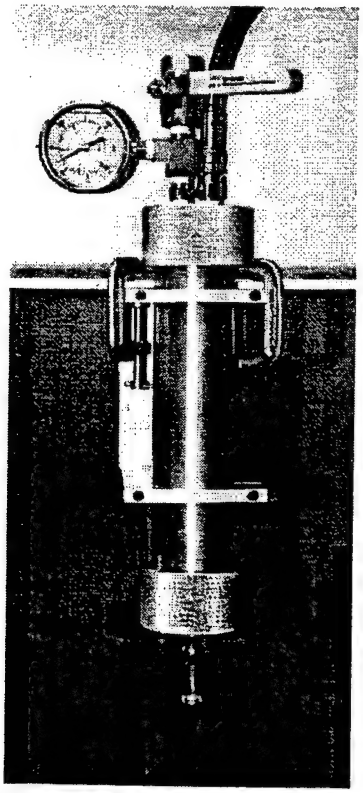

Figure 4. Photograph of the satellite accumulator.

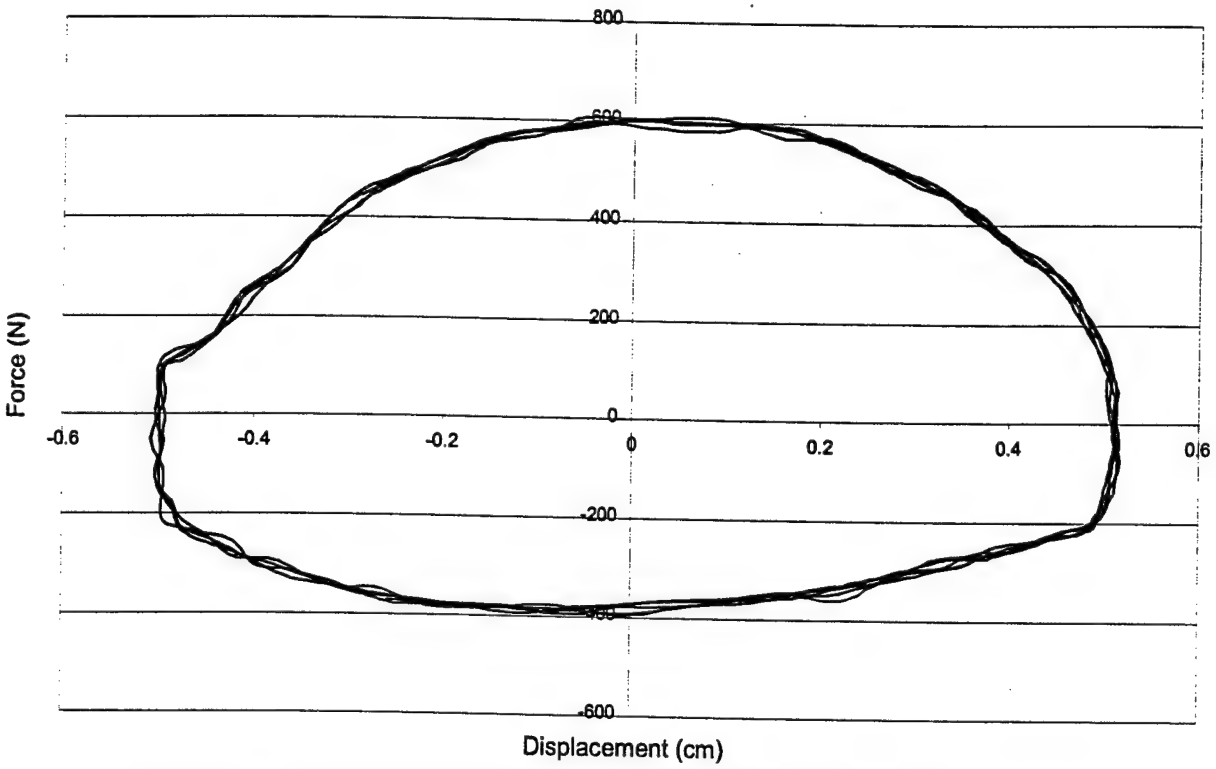

Figure 5. Force-displacement loop for OEM shock absorber at 2Hz, 1.0cm p-t-p.

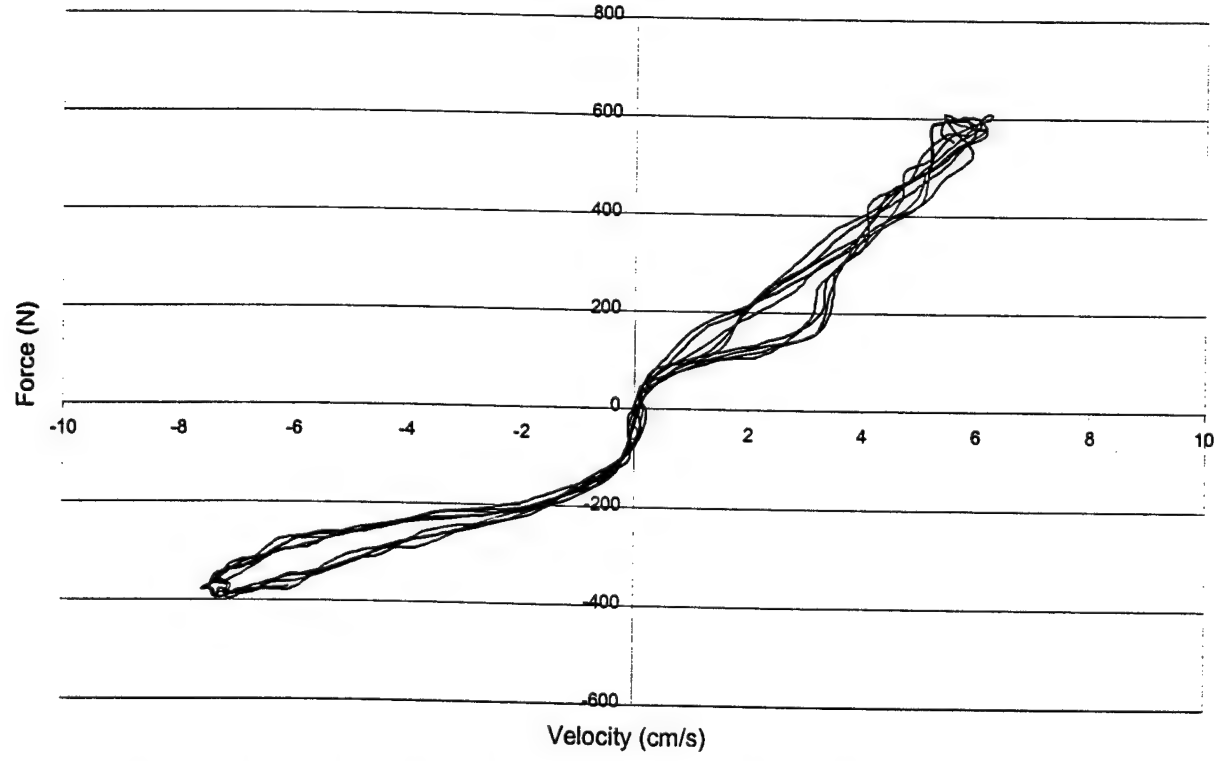

Figure 6. Force-velocity loop for the OEM shock absorber at 2Hz, 1.0cm p-t-p displacement.

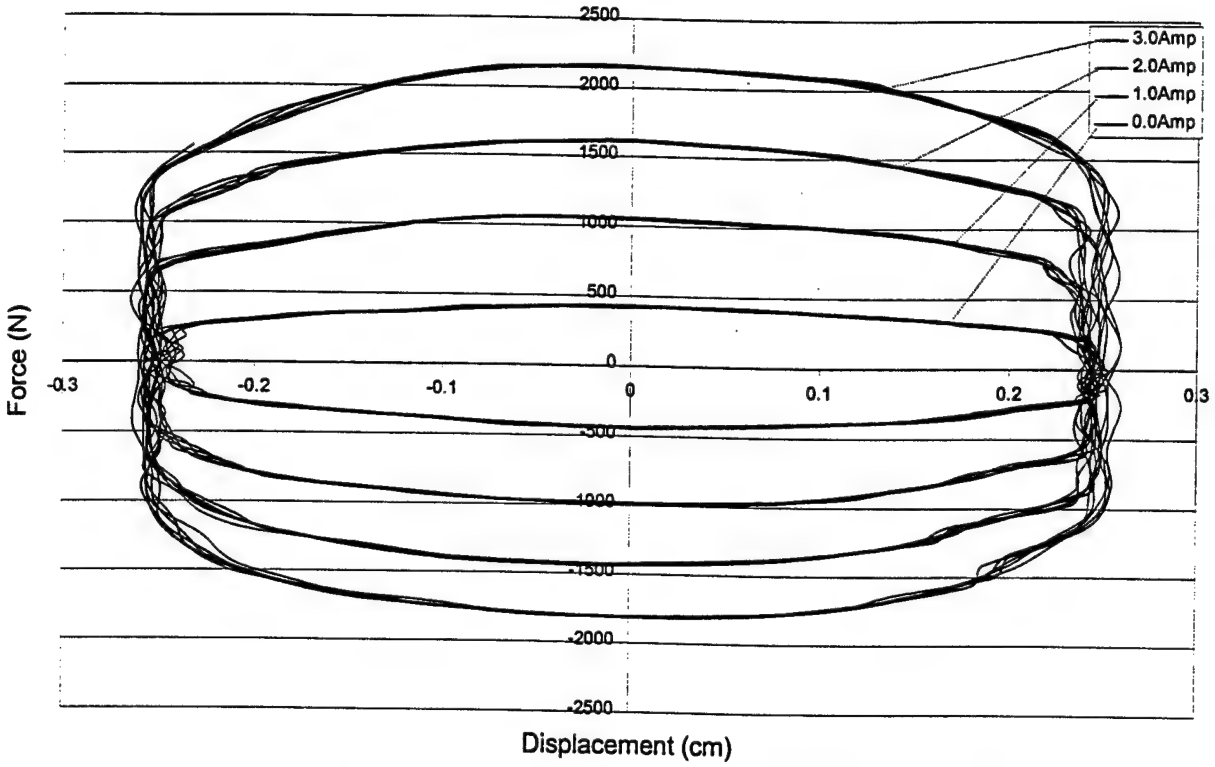

Figure 7. Force-displacement loops for the MRF damper at 2Hz, 1.0cm p-t-p displacement for different electrical current inputs.

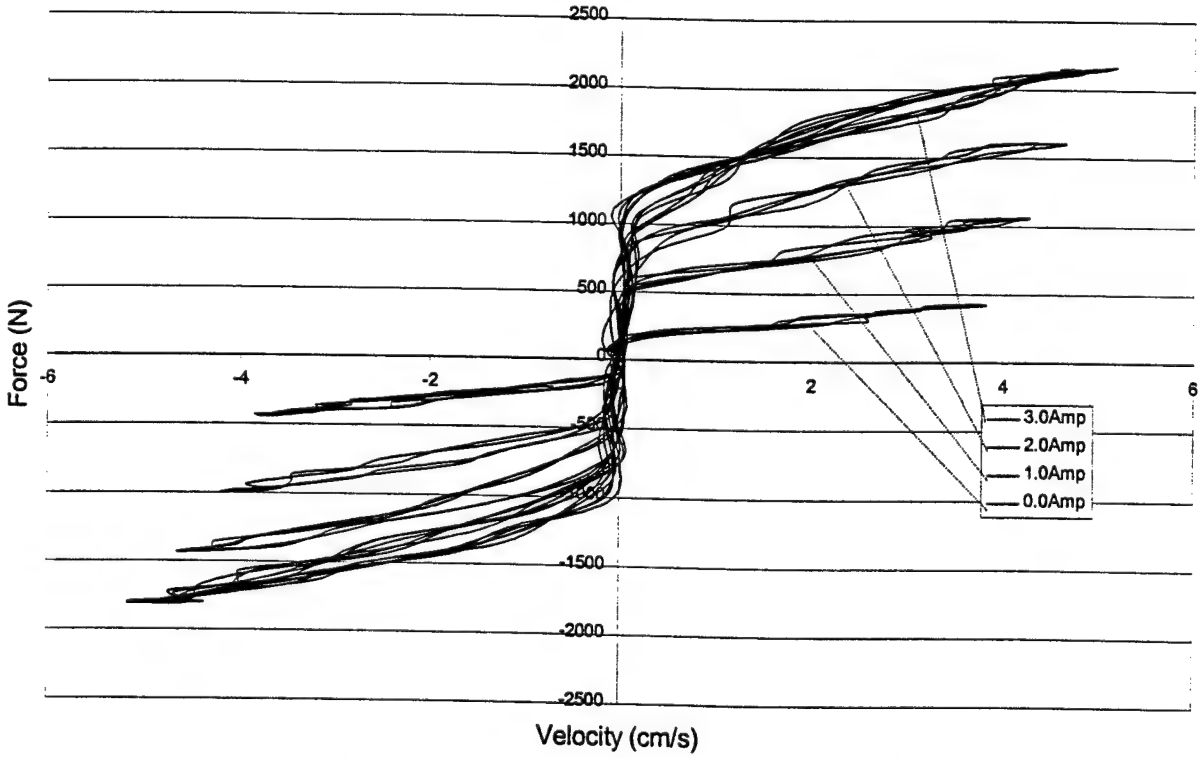

Figure 8. Force-velocity loops for MRF damper at 2Hz, 1.0cm p-t-p displacement for different electrical current inputs.

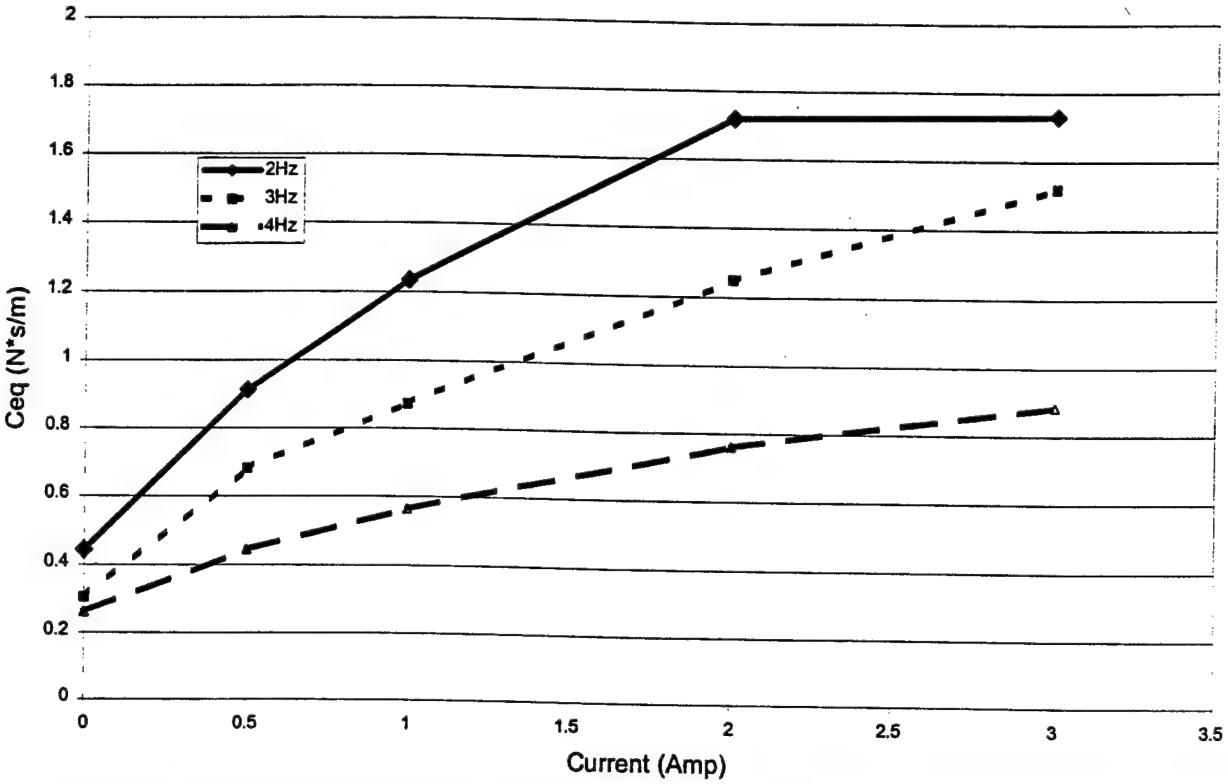

Figure 9. Experimental results for equivalent damping coefficient (C_{eq}) versus current for different frequencies for the MRF damper tested at 1.0cm peak-to-peak displacement.

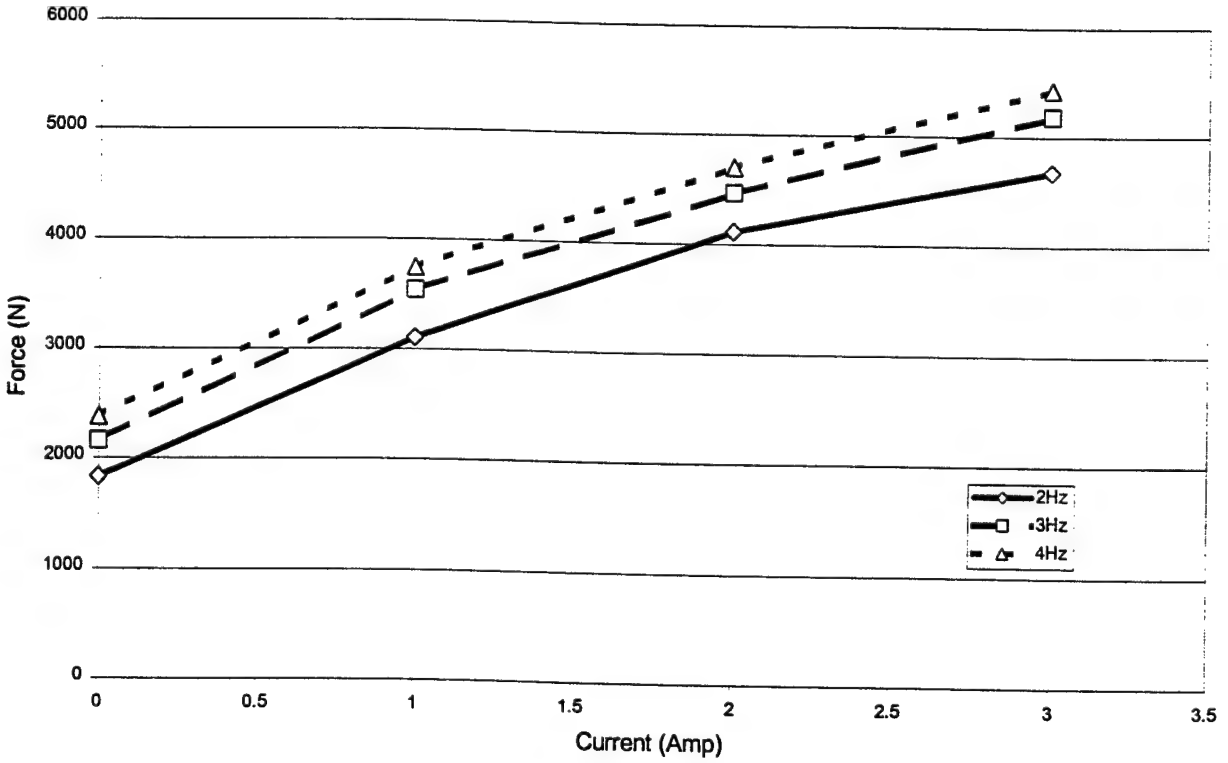

Figure 10. Experimental results for peak-to-peak force as a function of input electric current for the MRF damper at different frequencies (1.0cm peak-to-peak displacement).

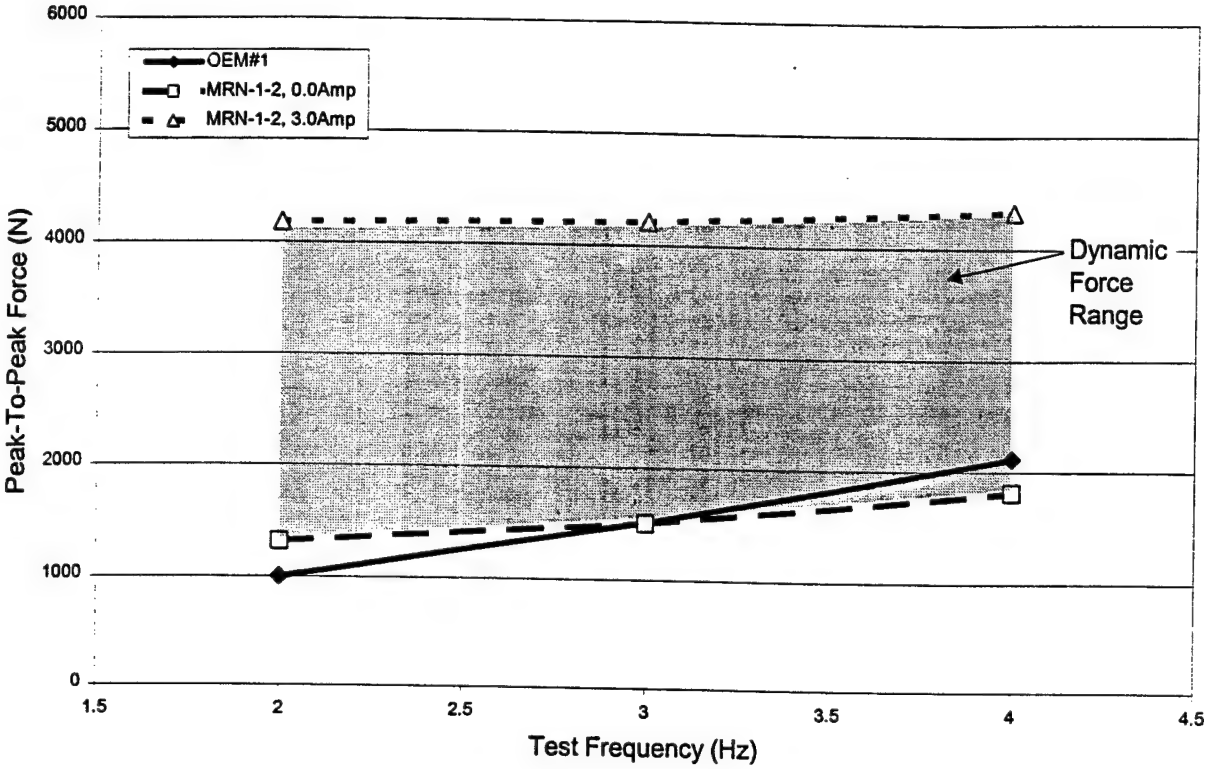

Figure 11. Comparison of peak-to-peak force as a function of frequency for the OEM unit and the MR fluid damper at 1.0cm peak-to-peak displacement.

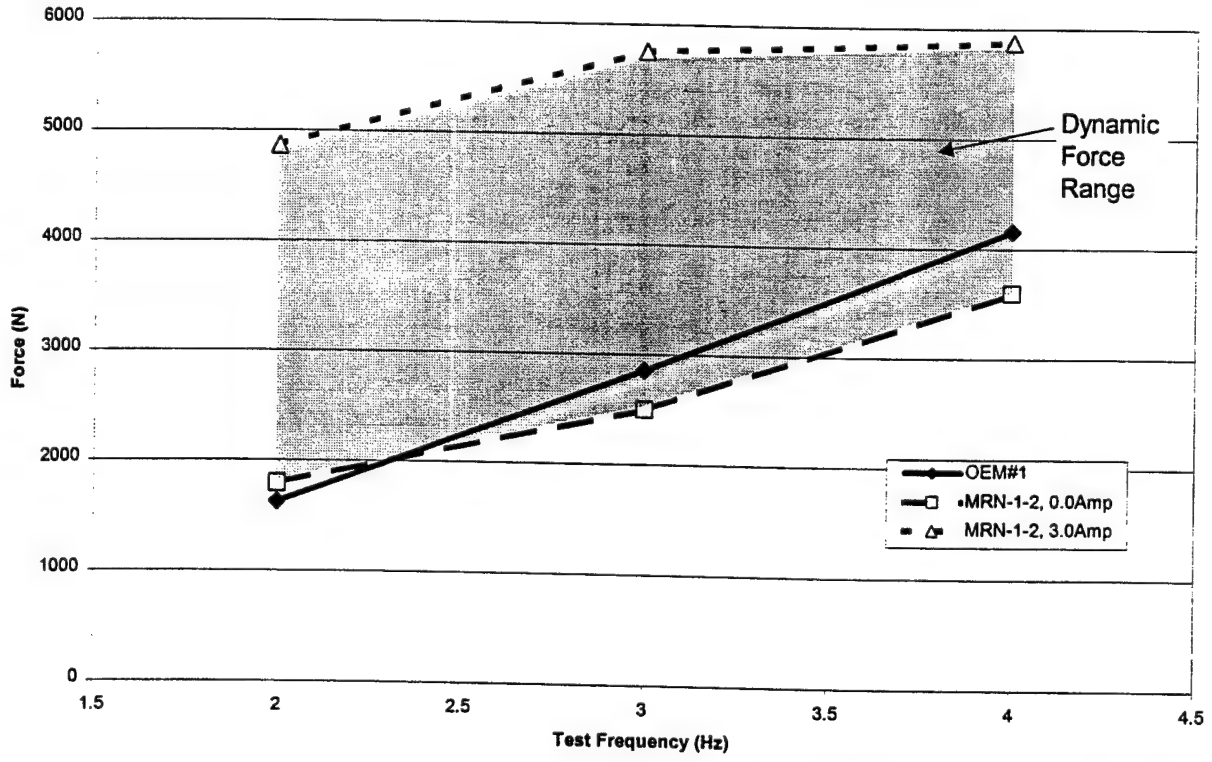

Figure 12. Comparison of peak-to-peak force as a function of frequency for the OEM unit and the MR fluid damper at 1.5cm peak-to-peak displacement.

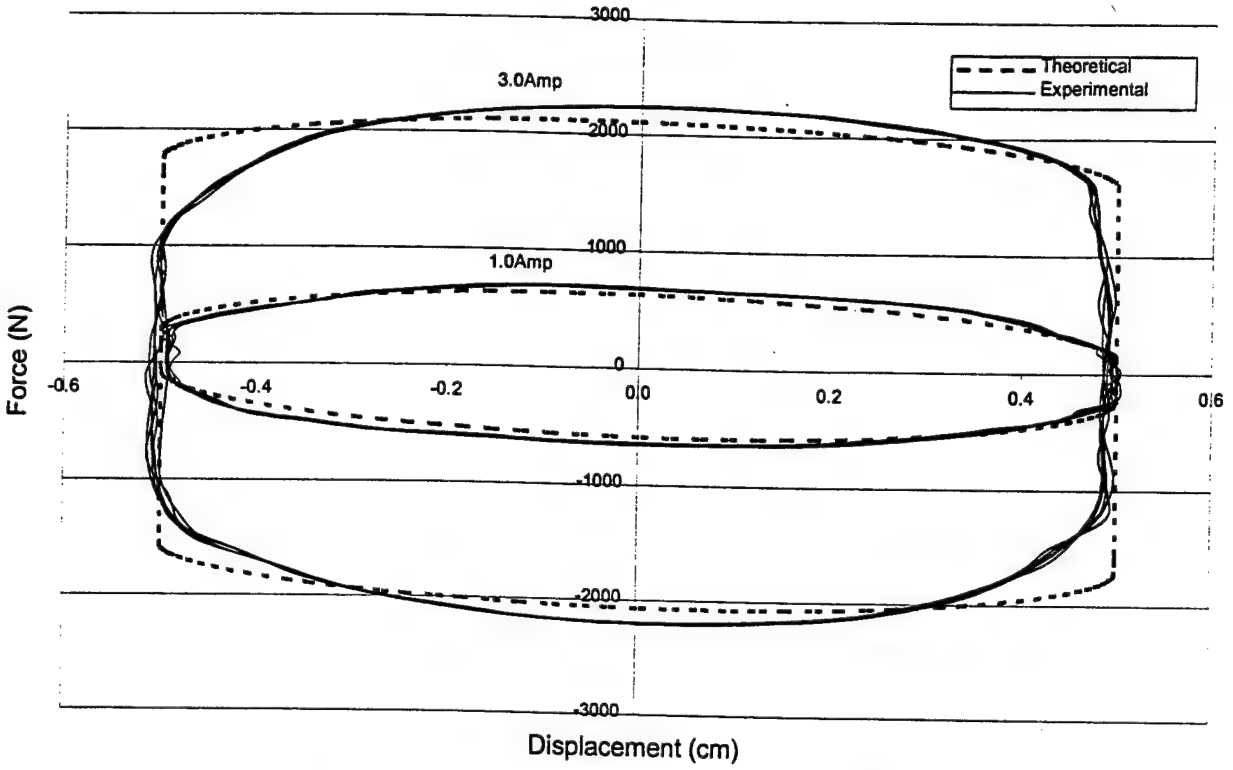

Figure 13. Comparison between theoretical and experimental force versus displacement of the MRF damper for passive-off and 3.0Amp input electric current.

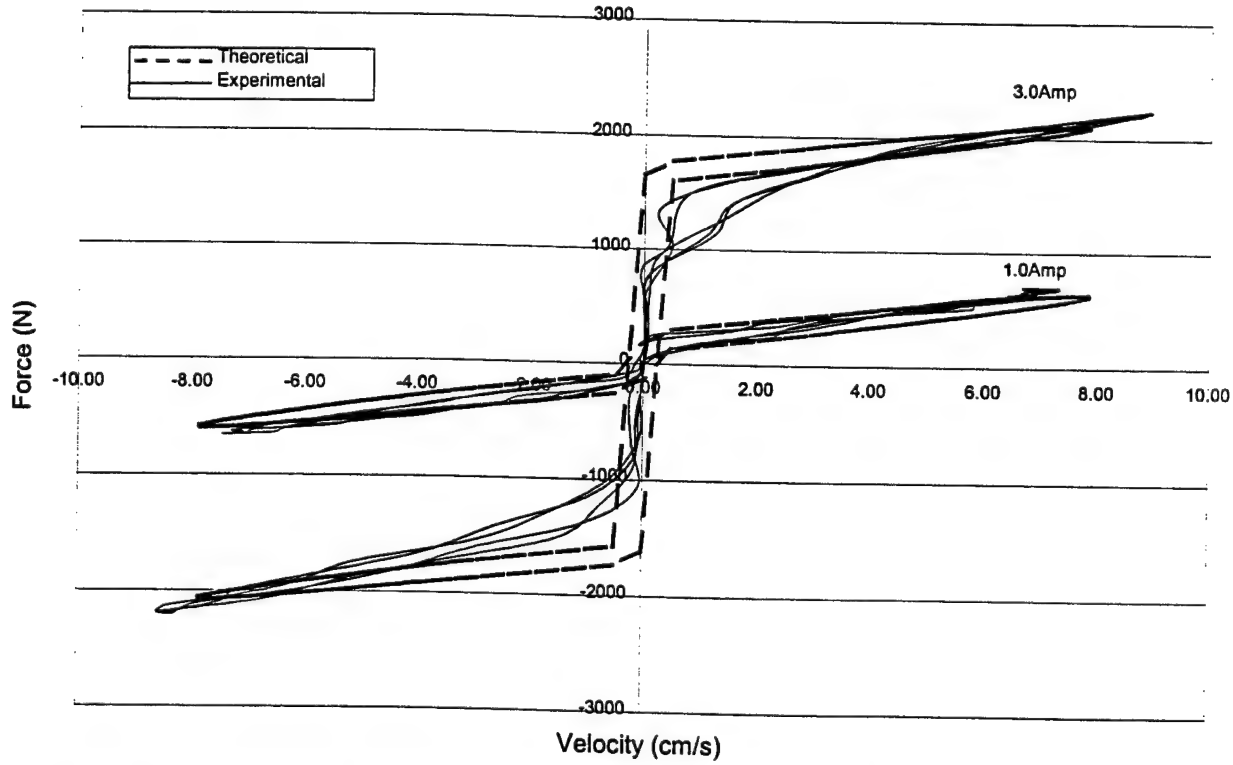

Figure 14. Comparison between theoretical and experimental force versus velocity of the MRF damper for passive-off and 3.0Amp input current.

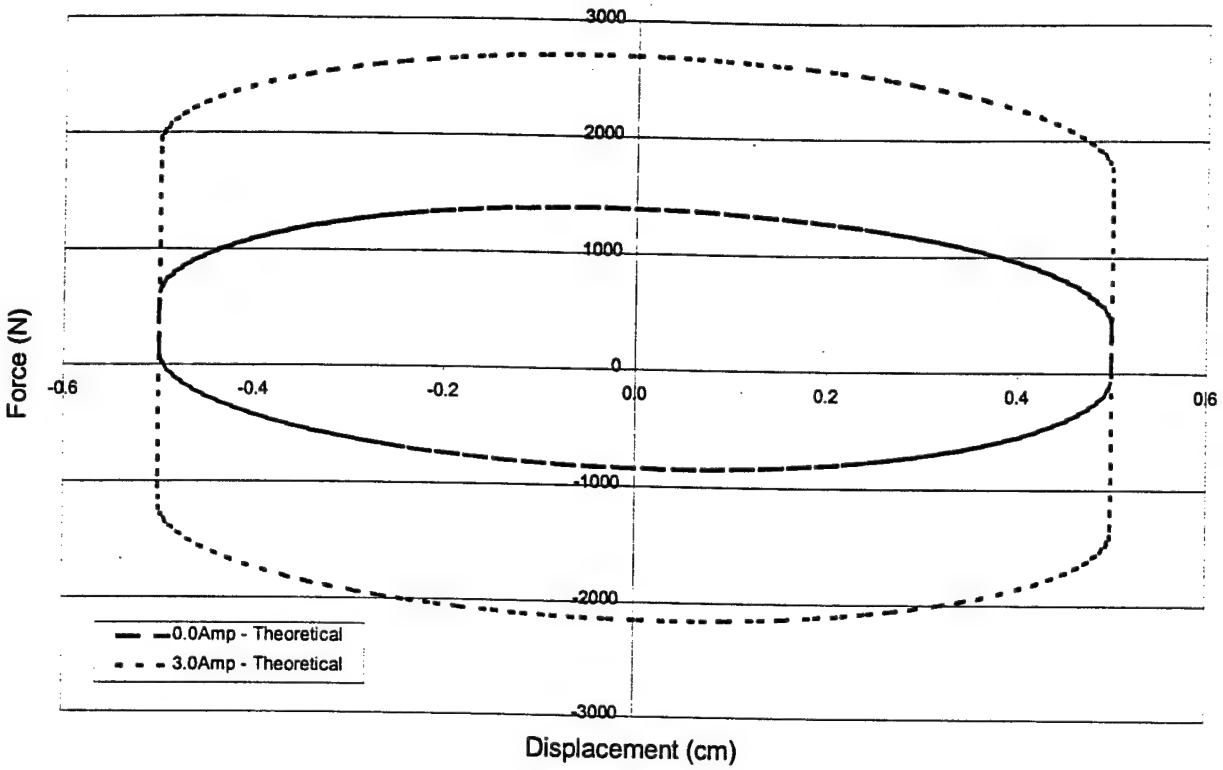

Figure 15. Theoretical force-displacement results for the MRF damper with return valves opened 0.0% on the compression stroke at 3Hz, 1.0cm p-t-p, for passive-off and 3.0Amp electric current.

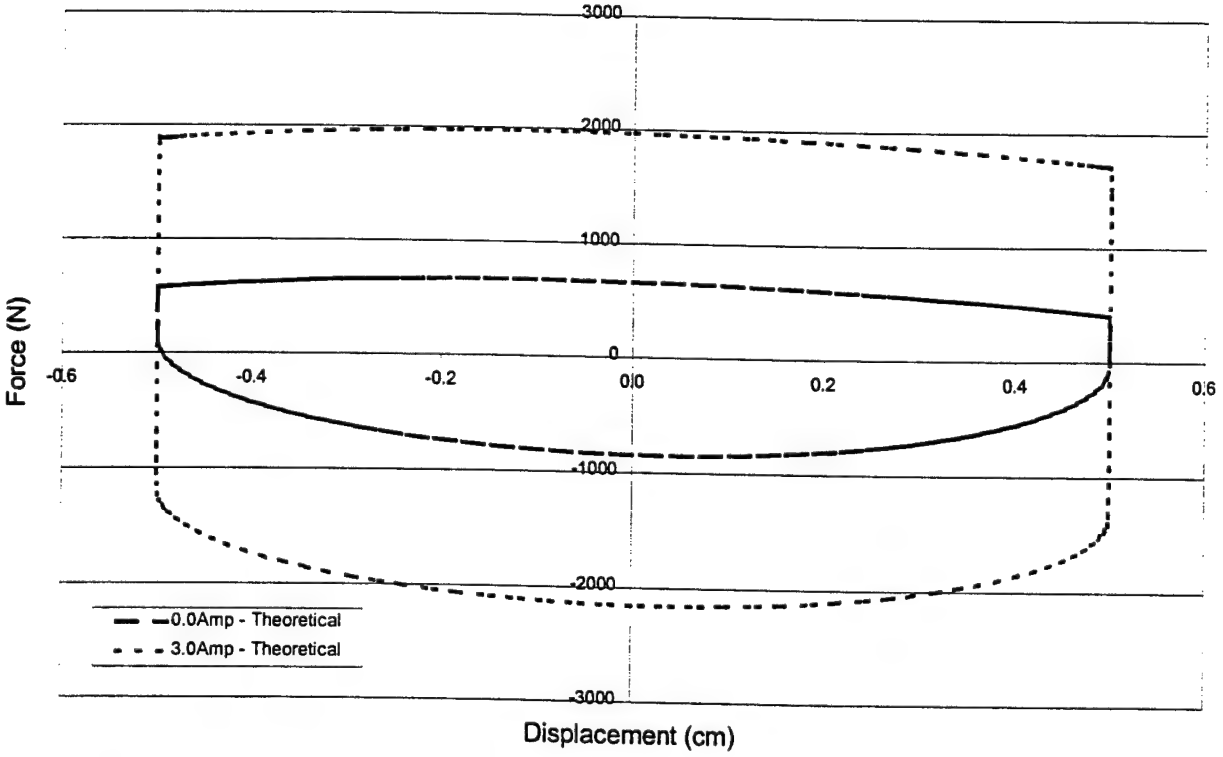

Figure 16. Theoretical force-displacement results for the MRF damper with return valves opened 25% on the compression stroke at 3Hz, 1.0cm p-t-p, for passive-off and 3.0Amp electric current.

APPENDIX B

Wang, X., and Gordaninejad, F., "Flow Analysis Of Field-Controllable, Electro- and Magneto-Rheological Fluids Using Herschel-Bulkley Model," *Journal of Intelligent Materials, Systems And Structures*, Vol. 10, No. 8, Pp. 601-608, 1999.

Flow Analysis of Field-Controllable, Electro- and Magneto-Rheological Fluids Using Herschel-Bulkley Model

XIAOJIE WANG AND FARAMARZ GORDANINEJAD*

Department of Mechanical Engineering, Composite and Intelligent Materials Laboratory, University of Nevada, Reno, Nevada 89557

ABSTRACT: The Bingham plastic constitutive model has been widely used to predict the post-yield behavior of electro- and magneto-rheological fluids (ER and MR fluids). However, if these fluids experience shear thinning or shear thickening, the Bingham plastic model may not be an accurate predictor of behavior, since the post-yield plastic viscosity is assumed to be constant. In a recent study, it was theoretically and experimentally demonstrated that the Herschel-Bulkley fluid model can be successfully employed when evaluating non-Newtonian post-yield behavior of ER and MR fluids. In this paper, we extend our previous work and adopt the Herschel-Bulkley model to include a detailed analysis of ER and MR fluid dynamics through pipes and parallel plates. Simplified explicit expressions for the exact formulation are also developed. It is shown that the proposed simplified model of the Herschel-Bulkley steady flow equations for pipes and parallel plates can be used as an accurate design tool while providing a convenient and generalized mathematical form for modeling ER and MR fluids. Theoretical and experimental analyses are presented for a MR fluid damper, which is designed, developed, and tested at the University of Nevada, Reno (UNR).

INTRODUCTION

ELECTRO- and magneto-rheological (ER and MR) fluids demonstrate non-linear material behavior when subjected to an external electric or magnetic field, respectively. The rheological behavior of these materials can be separated into two distinct pre- and post-yield regimes. In most devices, such as, dampers, valves, and clutches, the post-yield behavior of ER and MR fluids is the dominant mode of operation. When the fluid undergoes a shear thinning or thickening, its post-yield behavior is non-linear. This effect requires a fluid model to account for the non-Newtonian behavior of ER and MR fluids in the post-yield regime.

Previous studies have employed the Bingham plastic model. A non-dimensional equation of flow was introduced by Phillips (1969) and an approximated form of the Phillips's theory was developed by Gavin, et al. (1996). Because of its simplicity, the Bingham plastic model has been widely used for field-controllable fluids, however, it can only be used in the limiting case of post-yield phase when the material exhibits Newtonian behavior. ER and MR fluids are generally observed to have a strong field-dependent shear modulus and a yield stress that resists the material's flow until shear stress reaches a critical value. The Bingham plastic model is often used to describe this phenomenon (Stanway et al., 1996). In the Bingham plastic model, ER and MR fluids are assumed to be Newtonian fluids in post-yield regime, with a constant plastic viscosity assumption. However, for cases where the fluid experiences post-yield shear thinning or shear thickening, the assumption of constant plastic viscosity may not be valid.

Goodwin et al. (1997) reported that the ER fluids prepared with particles of low conductivity showed pseudo-plastic behavior with the power law index that was a function of conductivity. Mokeev et al. (1992) employed the continuous inhomogeneous dielectric medium approximation to model Couette shear in high-concentration ER fluid under electric field. They obtained an exponential dependence of the effective viscosity on the electric intensity and shear rate, which in the limiting case is reduced into the Bingham plastic model. Shulman and Korobko (1978) considered refining the Bingham plastic model into a four-parametric Casson-type model with coefficients depending on electric intensity. Stanway et al. (1989) proposed a model to describe controllable fluid damper behavior. An experimental technique of nonlinear sequential filtering was used to estimate the parameters associated with an nth-power velocity model for the damping mechanism.

In a recent work by Marksmeier et al. (1998), a new ER grease material was evaluated at UNR. A prototype ER grease damper was developed and tested. The shear thinning effect of ER grease was more pronounced than that of regular ER fluid. In order to accurately model the damper behavior, the Herschel-Bulkley model was used. This model allows for a non-linear post-yield behavior. Subsequently, by using a lumped parameter model for the damper, the force-displacement and force-velocity relations were established. The comparisons between experimental results and theoretical analyses utilizing both the Herschel-Bulkley and the Bingham plastic models confirmed that the

*Author to whom correspondence should be addressed.

1045-389X/99/08 0601-08 $10.00/0 DOI: 10.1106/P4FL-L1EL-YFLJ-BTRE

Herschel-Bulkley model predictions are more accurate than the Bingham plastic model. It was also concluded that the Herschel-Bulkley fluid model is a generalized model for viscoplastic flow with yield stress and can be a valuable tool in the analysis and design of controllable fluid dampers.

In this paper, the previous study is extended to include generalized analyses of ER and MR fluids flowing through pipes and parallel plates using the Herschel-Bulkley model. Non-dimensional equations are derived, and simplified closed-form expressions are presented for determining the pressure drop as a function of material properties, geometry, and volumetric flow rate. The simplified closed-form Herschel-Bulkley model can be reduced to the Bingham plastic model for cases where post-yield shear thinning or thickening are minimal. The theoretical Herschel-Bulkley formulation for flow through pipes is compared with the experimental results using a MR fluid damper which is constructed and tested at UNR. Excellent agreement is obtained.

MODELING OF ER AND MR FLUID FLOW USING THE HERSCHEL-BULKLEY MODEL

In this section, formulations for pipes and parallel plates are presented. In addition, a simplified model is developed for each case. It is demonstrated that the Herschel-Bulkley formulation can collapse to the Bingham plastic model for fluid index number of $n = 1$.

Flow Through a Circular Pipe with a Constant Cross Section

The Herschel-Bulkley constitutive equation presented in Equation (1) describes the flow of ER and MR fluids through a circular pipe with a constant cross sectional area.

$$\begin{cases} \tau_{rz} = \tau_y + k\left|\dfrac{du}{dr}\right|^n & |\tau_{rz}| \geq \tau_y \\ \dfrac{du}{dr} = 0 & |\tau_{rz}| \leq \tau_y \end{cases} \tag{1}$$

where τ_{rz} is shear stress; du/dr is shear strain rate, and k and n are fluid index parameters. τ_y is the fluid yield stress and is a function of the external field. Let us consider a steady, one-dimensional flow of an incompressible ER or MR fluid through a straight cylindrical pipe of constant cross section. A cylindrical coordinate system, with the notation shown in Figure 1, is assumed. The momentum equation of laminar flow in a pipe can be written as:

$$r\frac{dp}{dz} = -\frac{\partial(r\tau_{rz})}{\partial r} \tag{2}$$

where the pressure gradient, dp/dz is constant along the flow direction. Integrating Equation (2) yields shear stress as a function of radial position:

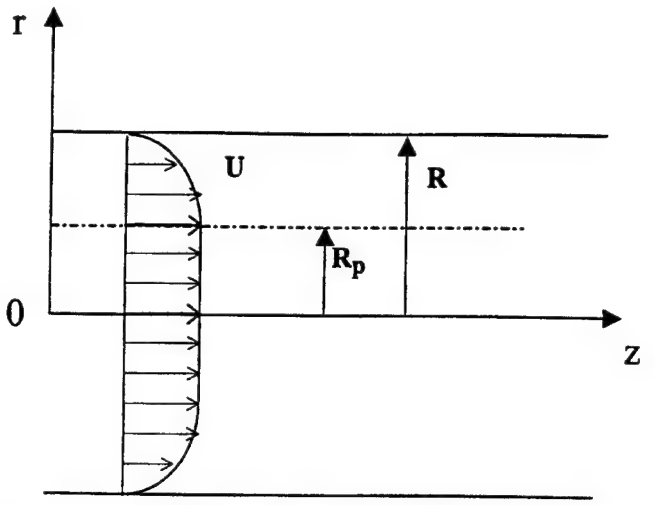

Figure 1. *ER or MR fluid flow profile in a pipe with a circular constant cross section.*

$$\tau_{rz} = -\frac{1}{2}r\frac{dp}{dz} + \frac{c_0}{r} \tag{3}$$

The axial flow in the pipe requires that c_0 be zero. The flow has a non-yield region, which is signified by the "plug" radius shown in Figure 1. The plug radius, R_p, can be determined by:

$$R_p = \frac{-2\tau_y}{dp/dz} \tag{3a}$$

The yield flow region, therefore, is defined when $R_p \leq r \leq R$. Substitution of Equation (1) into Equation (3) yields:

$$\tau_y + k\left|\frac{du}{dr}\right|^n = -\frac{1}{2}r\frac{dp}{dz} \tag{4}$$

Since $du/dr < 0$, Equation (4) can be written as:

$$\frac{du}{dr} = -\left(-\frac{1}{2}r\frac{dp/dz}{k} - \frac{\tau_y}{k}\right)^{\frac{1}{n}} \tag{5}$$

Solving Equation (5) with boundary condition of $u = 0$ at $r = R$, one obtains the velocity distribution in the yield flow area ($R_p \leq r \leq R$), as follows:

$$u = \frac{n}{n+1}\frac{2k}{dp/dz}\left[\left(-\frac{dp/dz}{2k}r - \frac{\tau_y}{k}\right)^{\frac{n+1}{n}} - \left(-\frac{dp/dz}{2k}R - \frac{\tau_y}{k}\right)^{\frac{n+1}{n}}\right] \tag{6}$$

In the plug area, $0 \leq r \leq R_p$, the velocity is constant. By letting $r = R_p$, the plug velocity can be expressed as:

$$u_p = \frac{n}{n+1}\frac{2k}{dp/dz}\left[\left(-\frac{dp/dz}{2k}R_p - \frac{\tau_y}{k}\right)^{\frac{n+1}{n}} - \left(-\frac{dp/dz}{2k}R - \frac{\tau_y}{k}\right)^{\frac{n+1}{n}}\right] \quad (7)$$

The volumetric flow rate can be derived from the following relation:

$$Q = 2\pi\int_{R_p}^{R} urdr + R_p^2\pi u_p \quad (8)$$

Substitution of Equations (6) and (7) into Equation (8) yields:

$$Q = \frac{\left(\frac{p'R}{2}-\tau_y\right)^{\frac{n+1}{n}}\pi R^3}{\left(\frac{pR}{2}\right)^3 k^{\frac{1}{n}}}\left[\frac{\left(\frac{p'R}{2}-\tau_y\right)^2}{\frac{3n+1}{n}} + \frac{2\tau_y\left(\frac{p'R}{2}-\tau_y\right)}{\frac{2n+1}{n}} + \frac{\tau_y^2}{\frac{n+1}{n}}\right] \quad (9)$$

where $p' = -dp/dz$. Now, let us consider the following dimensionless parameters:

$$X = \frac{4\tau_y}{p'D} = \frac{R_p}{R}; \quad \text{and} \quad Y = \left(\frac{3n+1}{n}\frac{8Q}{\pi D^3}\right)^n \frac{4k}{p'D} \quad (9a)$$

where $D = 2R$ and X represents the dimensionless plug thickness or dimensionless shear stress. When $X = 1$, the plug radius is the same as the pipe radius and the yield stress of the fluid is equal to its shear stress at the wall which implies that there is no flow in the pipe. Y is the dimensionless volumetric flow rate. By using the above dimensionless variables, Equation (9) can be simplified to (Chilton and Stainsby, 1998):

$$Y = (1-X)(1-aX-bX^2-cX^3)^n \quad (10)$$

where

$$a = \frac{1}{2n+1}; \quad b = \frac{2n}{(n+1)(2n+1)}; \quad c = \frac{2n^2}{(n+1)(2n+1)}$$

Expanding the right hand side of Equation (10) by Taylor Series, one has:

$$Y = 1-(na+1)X + \left(an - bn + \frac{n(n-1)}{2}a^2\right)X^2 + c\left(-nc + bn + n(n-1) - \frac{n(n-1)(n-2)}{6}a^3\right)X^3 + \cdots \quad (11)$$

For $X \le 0.5$, let us assume a linear relationship between X and Y in the form of $1 - Y = AX$. By linear regression of Equation (11), the coefficient A can be determined as:

$$A = (na+1) - \frac{3}{8}\left(na - bn + \frac{n(n-1)}{2}a^2\right) \quad (11a)$$

Therefore, a linear approximation to Equation (10), for all n, when $X < 0.5$, can be presented as:

$$Y = 1 - \left[(na+1) - \frac{3}{8}\left(na - bn + \frac{n(n-1)}{2}a^2\right)\right]X \quad (12)$$

Equation (12) represents the Herschel-Bulkley fluid model. If $n = 1$, the Herschel-Bulkley fluid equation is simplified to the Bingham plastic fluid model, as follows:

$$Y = 1 - \frac{4}{3}X \quad \text{where} \quad X \le 0.5 \quad (13)$$

Equation (12) can further be simplified to the power law fluid. By setting, $\tau_y = 0$ (i.e., $X = 0$), Equation (12) collapses to $Y = 1$, which is the dimensionless form for the power law fluid model. The dimensioned form can be written as:

$$\frac{dp}{dz} = \frac{4k}{D}\left(\frac{8Q}{\pi D^3}\right)^n\left(\frac{3n+1}{n}\right)^n \quad (13a)$$

For a Newtonian fluid, if n is set to 1 in Equation (13a), one has:

$$\frac{dp}{dz} = \frac{128kQ}{\pi D^4} \quad (13b)$$

which is the Hagen-Poiseuille equation.

Returning to the Herschel-Bulkley pipe flow for ER and MR field-controllable fluids, the dimensioned form of Equation (12) provides a closed-form expression for the pressure gradient as follows:

$$\frac{dp}{dz} = A\frac{4\tau_y}{D} + \left(\frac{3n+1}{n}\frac{8Q}{\pi D^3}\right)^n\frac{4k}{D}; \quad \frac{R_p}{R} \le 0.5 \quad (14)$$

where

$$A = \frac{3n+1}{2n+1} - \frac{3}{16}\frac{(3n+1)(1-n)}{(2n+1)^2(n+1)}$$

Equation (14) describes the pressure loss of a non-Newtonian fluid with yield stress. The pressure loss can be separated in two parts: one is induced by pure viscous flow and the other is caused by yield stress when the non-yield field is not dominant in the entire flow area. When $X > 0.5$, the plug radius reaches half of the pipe radius, the yield stress will

play an important role in determining pressure loss. A simplified expression for Equation (10) is obtained by considering the following nonlinear relation between X and Y:

$$Y = A'X(1-X)^{\alpha} \tag{15}$$

where A' and α are functions of n and their numerical values are presented in Table 1. The dimensioned version of the pressure loss can be derived from Equation (15)

$$\frac{dp}{dz} = \frac{4\tau_y}{D\left[1 - A_0\left(\frac{3n+1}{n}\frac{8Q}{\pi D^3}\right)^{\frac{n}{\alpha}}\left(\frac{k}{\tau_y}\right)^{\frac{1}{\alpha}}\right]}; \quad \text{for} \quad \frac{R_p}{R} > 0.5 \tag{16}$$

where

$$A_0 = (A')^{-\frac{1}{\alpha}}$$

The exact, Equation (10), and the simplified, Equations (12) and (15), solutions for the Herschel-Bulkley pipe flow relationships are presented in Figure 2. As shown, the simplified model is an excellent approximation to the exact solution. The relative maximum error between the two models is less than 3%. Therefore, the simplified Herschel-Bulkley relationships presented in Equations (14) and (16) are expected to provide an accurate explicit expression for the pressure loss associated with the flow of ER/MR fluid in pipes with circular constant cross sections.

Flow through Parallel Plates

A similar approach used for pipes with circular cross sections can be employed to develop relations for Herschel-Bulkley flow between two parallel plates. Let us assume that the parallel plates are fixed and a constant pressure gradient p' provides the fluid flow between the plates. The Herschel-Bulkley solution for steady, one-dimensional flow with no-slip boundary condition yields the following volumetric flow rate:

$$\frac{4Q}{wh^2}\left(\frac{2k}{p'h}\right)^{\frac{1}{n}} = (1-z_p)^{\frac{n+1}{n}}\left[\frac{(1-z_p)^2}{\frac{3n+1}{n}} + \frac{2z_p(1-z_p)}{\frac{2n+1}{n}} + \frac{z_p^2}{\frac{n+1}{n}}\right] \tag{17}$$

where w is the width of parallel plates and z_p is the dimensionless plug thickness defined as:

$$z_p = \frac{2\tau_y}{p'h} = \frac{h_p}{h} \tag{17a}$$

Here, h is the distance between the two parallel plates, and h_p is the plug thickness. Let us define the following dimensionless variable:

$$V = \left(\frac{2n+1}{2n}\right)^n \left(\frac{4Q}{wh^2}\right)^n \frac{2k}{p'h} \tag{17b}$$

Using Equation (17b), Equation (17) can be rewritten as:

$$V = (1-z_p)^{n+1}\left(\frac{n}{n+1}z_p + 1\right)^n \tag{18}$$

Expanding Equation (18), one has:

$$V = 1 + c_1 z_p + c_2 z_p^2 + c_3 z_p^3 \cdots \tag{19}$$

where

$$c_1 = -\frac{2n+1}{n+1}; \quad c_2 = \frac{n(1+2n)(1-n)}{2(n+1)^2}; \quad c_3 = \frac{n(n^2+1)}{2(n+1)}$$

For $z_p \le 0.5$, using the same method as described in the previous section, the linear approximation of Equation (19) can be expressed as:

$$V = 1 + \left(c_1 + \frac{3}{8}c_2 + \frac{3}{20}c_3\right)z_p; \quad z_p \le 0.5 \tag{20}$$

For $z_p > 0.5$, a similar expression to the one given in Equation (15) can be obtained, as follows:

$$V = B' z_p (1-z_p)^{\beta}; \quad z_p > 0.5 \tag{21}$$

where B' and β are functions of power index, n, that are obtained by curve fitting to analytical solutions of Equation (18), and are presented in Table 2. Again, similar to the pipe flow case, Figure 3 demonstrates the simplified Herschel-Bulkley model for laminar flow between the parallel plates. Equations (20) and (21) show an excellent approximation to the exact formulation presented in Equation (18). The dimensioned forms of Equations (20) and (21) are:

Table 1. Values of A′, α and A_0 for different n.

n	α	A'	$A_0 = (A')^{-1/\alpha}$
1	2.260	3.289	0.590
0.8	2.105	3.031	0.591
0.4	1.784	2.700	0.573

Table 2. Values of B′, β and B_0 for different n.

n	β	B'	$B_0 = (B')^{-1/\beta}$
1	2.629	3.952	0.593
0.8	2.475	3.810	0.583
0.4	1.816	2.727	0.575

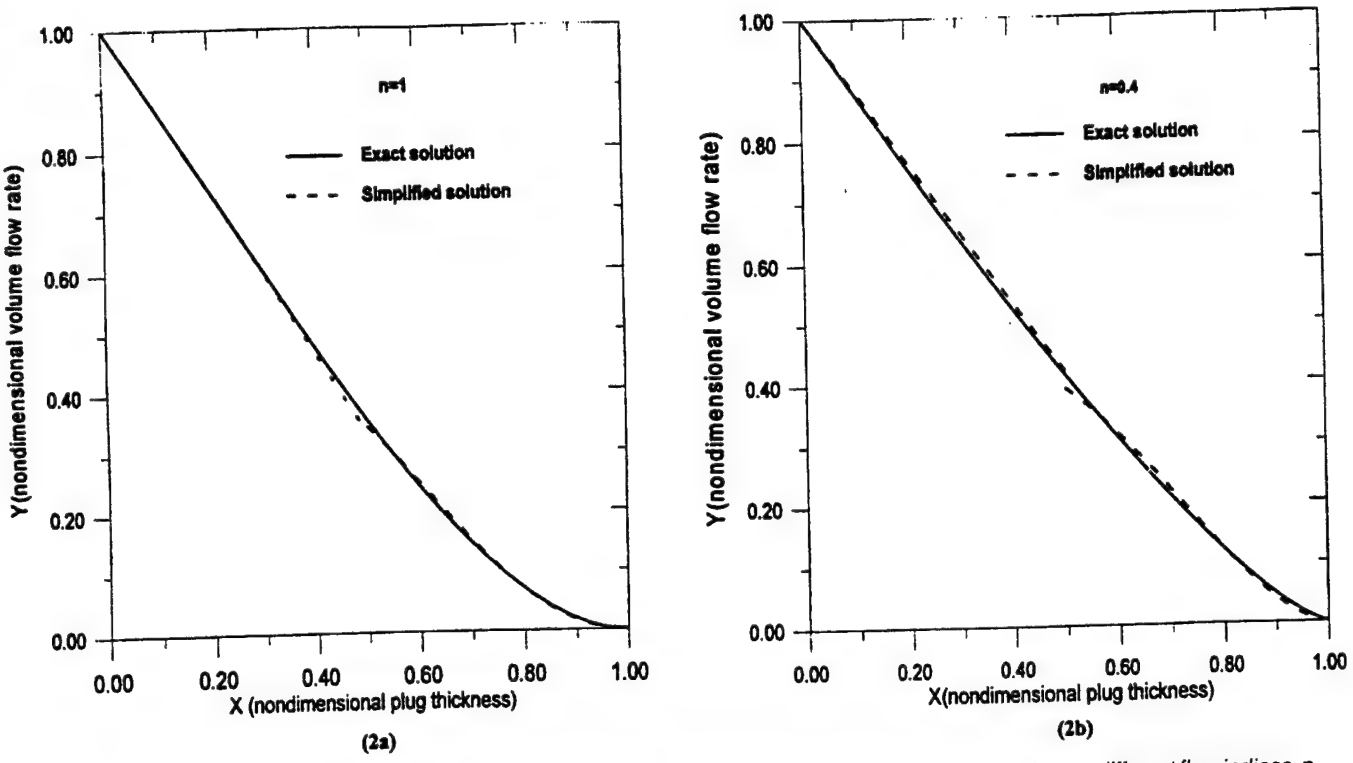

Figure 2. *Comparison between the exact and simplified versions of Herschel-Bulkley pipe flow formulation for two different flow indices,* n = *1 and* n = *0.4.*

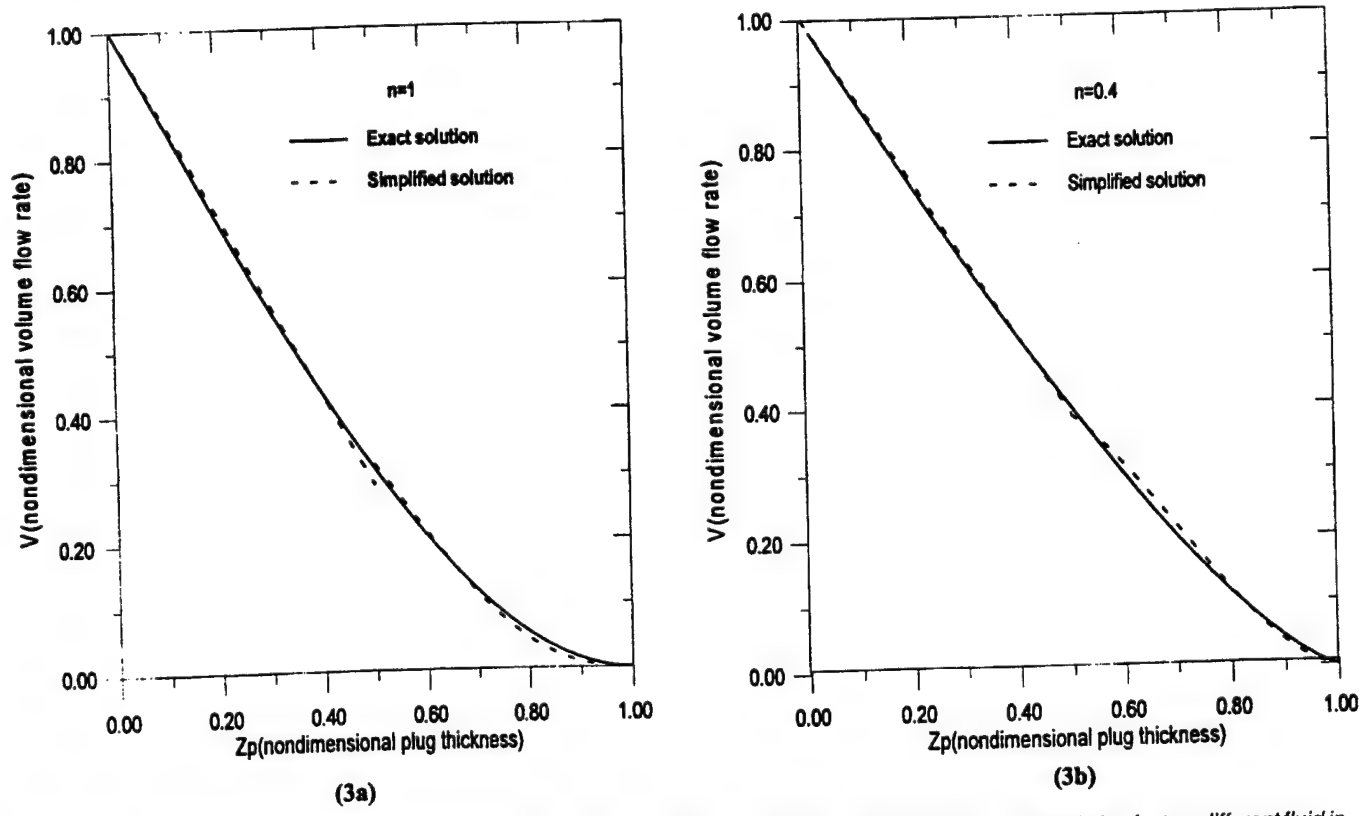

Figure 3. *Comparison between the exact and simplified versions of Herschel-Bulkley parallel plates flow formulation for two different fluid indices,* n = *1 and* n = *0.4.*

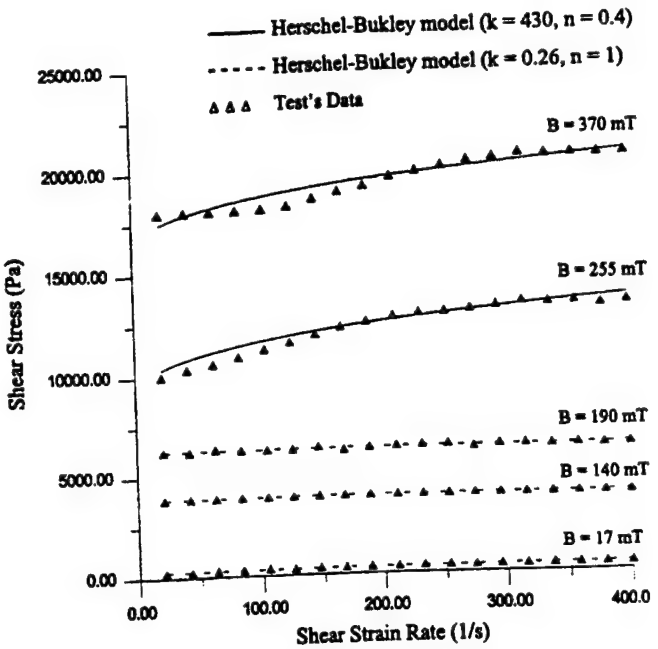

Figure 6. *Shear stress versus shear strain rate at various magnetic field strengths.*

of low magnetic field strength, MR fluids exhibit Bingham plastic behavior with a constant plastic viscosity being equal to the zero-field viscosity of Newtonian fluids. However, at higher magnetic field strengths, the MR fluid exhibits pseudo-plastic behavior with a field-dependent yield stress. Considering the shear thinning effect, the Herschel-Bulkley model is adapted (where $k = 430$ and $n = 0.4$) to represent the measured shear stress versus shear strain rate data (see Figure 6). The yield stress τ_y is a function of the applied magnetic field strength. For this UNR MR fluid damper the relationship between the yield stress τ_y and the input current I is:

$$\tau_y = 2.7 \times 10^4 I^{1.5} \tag{26}$$

where the units for τ_y and I are Pa and amp, respectively. Equation (26) is conformed with both the experimental and theoretical results that the yield stress τ_y is a power-law function of the flux density, $\tau_y \propto B^{1.5}$ (Ginder, 1998).

The overall pressure drop ΔP across the piston is mainly contributed by two parts, one is the pressure drop ΔP_{vis} which is due to the fluid viscosity, and the other is the pressure drop ΔP_{mr} across the MR valve normal to the axis of the shaft. The total pressure drop across the piston head can be written as following:

$$\Delta P = \Delta P_{vis} + 2\Delta P_{mr} \tag{27}$$

For a Newtonian Poiseuille flow in a pipe, the pressure drop ΔP_{vis} is expressed as:

$$\Delta P_{vis} = \frac{128 \mu Q L_2}{\pi D_2^4} \tag{28}$$

The MR valve pressure drop ΔP_{mr} can be calculated by Equations (14) or (16), which depends on the value of nondimensional parameter X. Here, a new dimensionless parameter is introduced:

$$T^* = \frac{\tau_y}{k\left(\frac{(3n+1)}{n}\frac{8Q}{\pi D^3}\right)^n} \tag{29a}$$

Since $T^* = X/Y$, then, from Equation (10) one can obtain T^* in term of X.

$$T^* = \frac{X}{(1-X)(1-aX-bX^2-cX^3)^n} \tag{29b}$$

Now, let us define

$$T^*_{crit} = T^*_{X=0.5} = \frac{1}{(1-0.5a-0.25b-0.125c)^n} \tag{29c}$$

Then, if $T^* \le T^*_{crit}$, Equation (14) is used to determine the pressure loss, otherwise Equation (16) is employed.

For this MR fluid damper's geometry, the volume flow rate can be expressed as:

$$Q = NQ_m = \frac{\pi}{4} V (D_p^2 - D_s^2) \tag{30}$$

where N is the number of the MR valves, and Q_m is the volume flow rate through each MR valve. Using Equations (14) and (16), the pressure drop across one MR valve can be written as:

$$\Delta P_{mr} = A\frac{4\tau_y L_1}{D_1} + \left(\frac{3n+1}{n}\frac{8Q_m}{\pi D_1^3}\right)^n \frac{4kL_1}{D_1} \quad \text{for} \quad T^* \le T^*_{crit} \tag{31}$$

$$\Delta P_{mr} = \frac{4\tau_y L_1}{D_1\left[1 - A_0\left(\frac{3n+1}{n}\frac{8Q_m}{\pi D_1^3}\right)^{\frac{n}{\alpha}}\left(\frac{k}{\tau_y}\right)^{\frac{1}{\alpha}}\right]} \quad \text{for} \quad T^* > T^*_{crit} \tag{32}$$

The force output is a result of a pressure drop across the piston and can be written as

$$F = \Delta P \frac{\pi}{4}(D_p^2 - D_s^2) + F_f \,\mathrm{sgn}(V) \tag{33}$$

where F_f is the damper seal friction force (nearly 50 N).

A comparison of experimental and analytical results is presented in Figure 7, for a sinusoidal motion with a frequency of 0.5 Hz and amplitude of 1 cm. The analytical results are obtained directly from Equations (27), (28), (31) or (32) and (33). Table 3 lists the material and geometric prop-

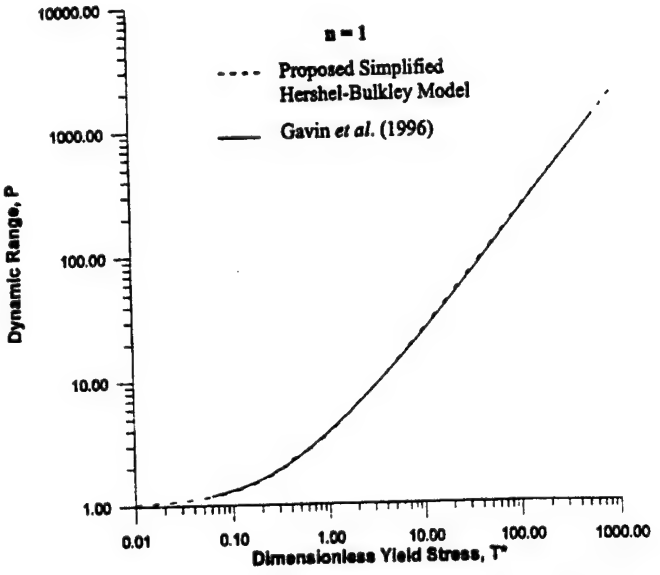

Figure 4. Comparison between the proposed model and Gavin's (1996) approximated solution of Philips (1969) Bingham Plastic model, n = 1.

$$\frac{dp}{dz} = B\frac{2\tau_y}{h} + \left(\frac{2n+1}{n}\frac{2Q}{wh^2}\right)^n \frac{2k}{h}; \quad \text{for} \quad \frac{h_p}{h} \le 0.5 \quad (22)$$

$$\frac{dp}{dz} = \frac{2\tau_y}{h\left[1 - B_0\left(\frac{2n+1}{n}\frac{2Q}{wh^2}\right)^{\frac{n}{\beta}}\left(\frac{k}{\tau_y}\right)^{\frac{1}{\beta}}\right]}; \quad \text{for} \quad \frac{h_p}{h} > 0.5 \quad (23)$$

where,

$$B = \frac{2n+1}{n+1} - \frac{3n(1+2n)(1-n)}{16(n+1)^2} - \frac{3n(n^2+1)}{40(n+1)} \quad \text{and} \quad B_0 = (B')^{-\frac{1}{\beta}}$$

The simplified model presented in Equations (22) and (23) provides a general expression for the analysis of flow between parallel plates that can be employed as a useful tool in the design of ER and MR devices. The Herschel-Bulkley model developed in this study can be reduced to the Bingham plastic model by setting $n = 1$. Using the values of Table 2, $\beta = 2.629$ and $B' = 3.952$, and, Equation (22) and (23), can be respectively reduced to:

$$\frac{dp}{dz} = \frac{12kQ}{wh^3} + 2.85\frac{\tau_y}{h}; \quad \text{for} \quad \frac{h_p}{h} \le 0.5 \quad (24)$$

$$\frac{dp}{dz} = \frac{2\tau_y}{h\left[1 - 0.593\left(\frac{6Qk}{wh^2\tau_y}\right)^{0.380}\right]}; \quad \text{for} \quad \frac{h_p}{h} > 0.5 \quad (25)$$

Gavin et al. (1996) presented an approximate formula to the exact solution of the cubic Bingham flow equation, with a relative error of ±2% for the range $0 < T^* < 1000$. Here, Equations (24) and (25) are compared to those of Gavin et al. (1996). For comparison purposes, the results from Equations (24) and (25) are converted to the same dimensionless variables $P = (wh^3p')/(12Qk)$ and $T^* = (wh^2\tau_y)/(12Qk)$ adopted by Gavin et al. (1996). Figure 4 shows excellent agreement between the proposed simplified Herschel-Bulkley model presented in this study and those of Gavin et al. (1996). It should be noted that the working range of proposed Equations (24) and (25) is not limited to $0 < T^* < 1000$.

EXPERIMENTAL VERIFICATION OF THE HERSCHEL-BULKLEY MODEL

The theoretical Herschel-Bulkley model presented in this study is verified by a comparison between the theoretical and experimental results. The experimental results are obtained using a new MR fluid damper developed at UNR (Gordaninejad and Breese, 1998). A cross-sectional view of the UNR MR fluid damper's piston is shown in Figure 5. This figure shows the fluid flow path through the piston as well as the geometric dimensions.

The rheological property of MR fluid (LORD 132LD) is measured by a universal dynamic spectrometer (Li et al., 1999). Figure 6 shows the shear stress versus shear strain rate at various magnetic field strengths. It is found that at a range

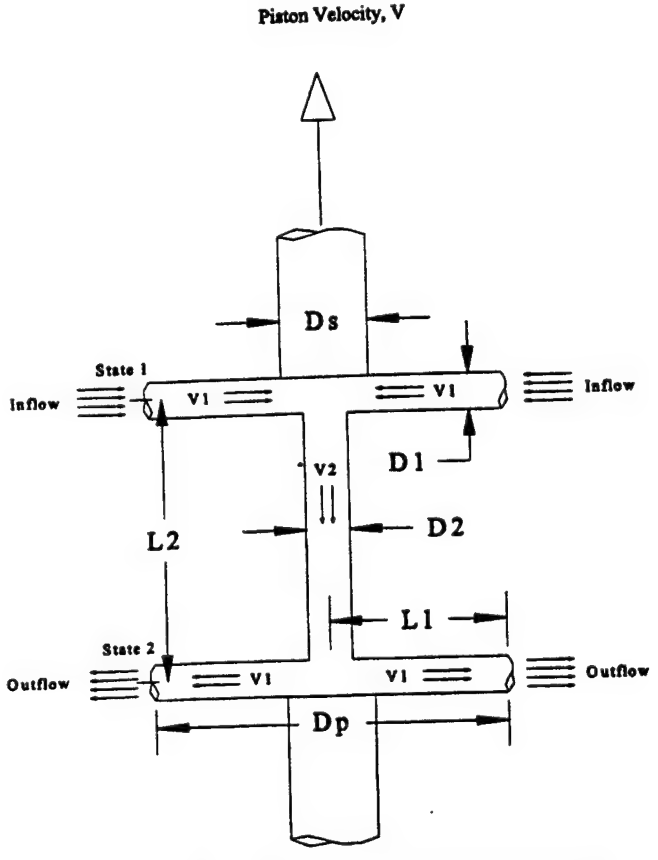

Figure 5. Schematic of flow path for a UNR MR fluid damper.

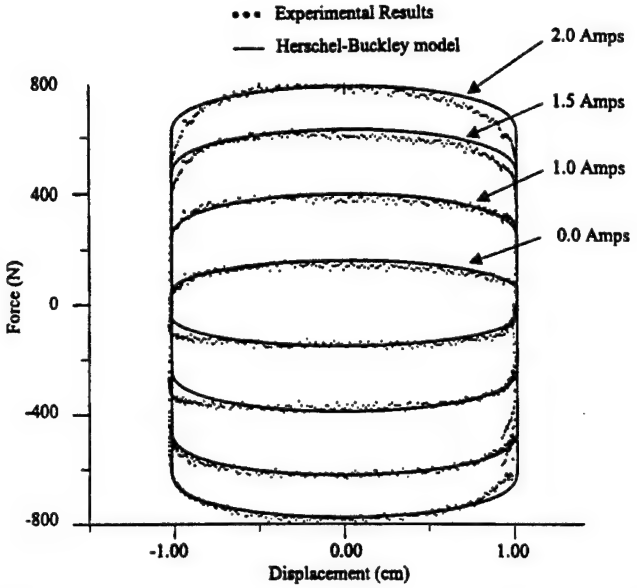

Figure 7. *Comparison between theoretical and experimental results for a sinusoidal motion at 0.5 Hz frequency and 1.0 cm (0.4 in.) amplitude for different input electric current 0.0, 1.0, 1.5 and 2.0 amps.*

erties used in the theoretical analysis. As demonstrated in Figure 7, the Herschel-Bulkley fluid model can accurately predict the damping force of the MR damper for different levels of input current.

SUMMARY AND CONCLUSIONS

The rheological behavior of ER and MR fluids can be identified as two distinct pre- and post-yield regimes. In most ER and MR devices such as dampers the dominant fluid behavior occurs in the post-yield regime. ER and MR materials under shear thinning or shear thickening effects exhibit a non-linear behavior in the post-yield regime. To predict the flow rate of these fluids, an accurate constitutive model is needed in which the behavior of the fluid under shear thinning or shear thickening is taken into consideration.

In this study, a detailed analysis of ER and MR field-controllable fluid flow through pipes and parallel plates was presented using the Herschel-Bulkley model. A steady, one-dimensional laminar flow was assumed. Dimensionless variables were used to simplify the continuity and momentum equations. The non-dimensional plug thickness was determined to be a crucial parameter in developing the simplified expressions for the analytical solution. When the non-dimensional plug thickness is less than 0.5, linear asymptotical forms of non-dimensional equations were developed. When the non-dimensional plug thickness is more than 0.5, smaller volumetric flow rates can be expected. In this case, a simplified exponential form was derived.

It was demonstrated that the Herschel-Bulkley model in this study can be reduced to Bingham plastic, power law, and Newtonian fluid models, by setting yield stress, τ_y, and index, n, to certain specific-case values. In addition, the proposed simplified Herschel-Bulkley model for steady flow in pipes and parallel plates can provide a convenient and generalized mathematical form for analysis and design of ER and MR devices.

Table 3. Material and geometric properties used in the Herschel-Bulkley theoretical analysis.

k	430 Pa·s^n
n	0.4
N	4
μ	0.4 Pa·s
D_p	0.0508 m
D_s	0.0127 m
D_1	0.00635 m
D_2	0.00635 m
L_1	0.00292 m
L_2	0.0939 m

ACKNOWLEDGEMENTS

This study is funded by the U. S. Army Research Office Grant Number DaaG55-98-10017. The authors are thankful for the encouragement by Dr. Gary Anderson, the Program Director. Thanks are also extended to Dr. Q. Chen and Mr. W. H. Li of Nanyang Technological University, Singapore, for the test results on the MR fluid sample.

REFERENCES

Chilton, R. A., and Stainsby, R., 1998, "Pressure loss equations for laminar and turbulent Non-Newtonian pipe flow," *Journal of Hydraulic Engineering*, Vol. 124, No. 5, pp. 522–529.

Gavin, H. P., Hanson, R. D., and Filisko, F. E., 1996, "Electrorheological dampers, part I: analysis and design," *Journal of Applied Mechanics*, Vol. 63, pp. 669–675.

Ginder, J. M., 1998, "Behavior of Magnetorheological Fluids," *MRS Bulletin*, 26–29.

Goodwin, J. W., Markham, G. M., and Vincent, B., 1997, "Studies on model electrorheological fluids," *Journal of Physical Chemistry B*, Vol.101, pp. 1961–1967.

Gordaninejad, F. and Breese, D. G., 1998, "Magnetorheological Fluid Dampers," U.S. patent no. 6,019,201,2000.

Li, W. H., Chen, G. and Yeo, S. H. 1999, "Viscoelastic Properties of MR Fluids," *Smart Matls. Struct.*, Vol. 8, pp. 460–468.

Marksmeier, T. M., Wang, E., Gordaninejad, F., and Stipanovic, A. 1998, "Theoretical and experimental studies of an electrorheological grease shock absorber," *Journal of Intelligent Materials, Systems and Structures*, Vol. 9, pp. 693–703.

Mokeev, A. A., Korobko, E. V., Vedernikova, L. G. 1992, "Structural viscosity of electrorheological fluids," *Journal of Non-Newtonian Fluid Mechanics*, Vol. 42, pp. 213–230.

Phillips, R. W. 1969, "Engineering applications of fluids with a variable yield stress," Ph.D. Dissertation, University of California.

Shulman, Z. P., and Korobko, E. V. 1978, "Convective heat transfer of dielectric suspensions in coaxial cylindrical channels," *International Journal of Heat and Mass Transfer*, Vol. 21, No. 5, pp. 543–548.

Stanway, R., Sproston, J. L. and Firoozian, R. 1989, "Identification of the damping law of an electro-rheological fluid: A sequential filtering approach," *Journal of Dynamic Systems, Measurement, and Control*, Vol. 111, pp. 91–95.

Stanway, R., Sproston, J. L., and El-Wahed, A. K. 1996, "Application of electrorheological fluids in vibration control: A survey," *Smart Mater. Struct.*, Vol. 5, pp. 464–482.

APPENDIX C

Ericksen, E. O., and Gordaninejad, F., "A Magneto-Rheological Fluid Shock Absorbers for the Rear Suspension of an Off-Road Motorcycle: A Theoretical Study," *Industrial and Commercial Applications of Smart Structures Technologies, Proceedings of SPIE Conference on Smart Materials and Structures,* Ed. by Jack H. Jacobs, Vol. 3991, pp. 273-282, 2000.

Ericksen, E. O., and Gordaninejad, F., "A Magneto-Rheological Fluid Shock Absorbers for an Off-Road Motorcycle," *Proceedings of Asia-Pacific Vibration Conference'99*, Ed. By O. J. Huat and L. K. Meow, Vol. 2, pp. 267-271, 1999.

A magneto-rheological fluid shock absorber for suspension of an off-road motorcycle: a theoretical study

Everet O. Ericksen[a], Faramarz Gordaninejad[1b]

[a] Tenneco-Automotive, Monroe, MI 48161, USA

[b] Composite and Intelligent Materials Laboratory
Department of Mechanical Engineering
University of Nevada, Reno, NV 89557, USA

ABSTRACT

This work presents a theoretical model for the damping force of a magneto-rheological fluid (MRF) shock absorber of an off-road motorcycle. The Bingham plastic model and a three-dimensional electromagnetic finite-element analysis are employed to develop a theoretical model to estimate the damping force of a MRF shock absorber. The model is based on the physical parameters of the device as well as the properties of the fluid, making it a valuable tool in shock absorber design for a particular application. By comparing the theoretical and experimental results, it is demonstrated that the model accurately predicts the damping force.

Keywords: Magneto-rheological fluids, semi-active, field-controllable, damper, off-road motorcycle, suspension

1. INTRODUCTION

As a component of a semi-active suspension system, the role of the controllable shock absorber is to have the capacity to produce variable damping proportionally reactive to the input motion, which is often a random excitation. Semi-active, controllable dampers are being increasingly investigated for various applications[1,2]. One class of controllable, semi-active dampers utilizes a magneto-rheological fluid (MRF) as the working fluid. MRFs are controllable fluids that typically consist of a silicone-based carrier fluid with small iron-based particles in random suspension[3]. The application of a magnetic field to the MRF causes the particles to align themselves as chains along the lines of magnetic flux. The formation of these chains causes a resistance to fluid flow due to a higher fluid shear stress developed at the wall. The higher fluid shear stress due to the application of the magnetic field is referred to as a "MRF valve"[4,5]. The MRF valve can be controlled by varying the input electric current to the device's built-in electromagnet.

[1]correspondence: Email: faramarz@unr.edu, Url: http://Web.me.unr.edu/ciml, Telephone: 775-784-6990, Fax: 775-784-1701

In *Smart Structures and Materials 2000: Industrial and Commercial Applications of Smart Structures Technologies*, Jack H. Jacobs, Editor, Proceedings of SPIE Vol. 3991 (2000) • 0277-786X/00/$15.00

The objective of this research is to develop a theoretical model for a proof-of-concept effort. A fluid mechanics model has been developed based on the materials and geometric properties of the device in order to predict damping characteristics. The experimental component of this study aids in the validation and effectiveness of the developed theoretical model. This paper focuses on the theoretical aspect of this research.

The theoretical model is based on the Bingham plastic theory to develop the pressure drop across the piston for the case where the MRF is in flow mode. In order to determine the effect of the magnetic field on the MRF, a three-dimensional finite element analysis (FEA) is employed. The FEA results provide a function that describes the magnetic saturation of the fluid as a function of input electric current. Integrating the electromagnetic analysis with the fluid mechanics analysis yields a theoretical model based on the physical parameters of the individual device, the properties of the fluid, and the input electric current. Furthermore, the fluid mechanics model accounts for the external accumulator and piston by-pass valving on the compression stroke. A full-scale MRF shock absorber for the rear suspension of a motorcycle is designed, manufactured, and tested based on a University of Nevada, Reno's MRF damper design[6,7]. This damper serves as the testbed for the development of the fluid mechanics model.

2. THEORETICAL MODELING

The pressure drop across the piston can be determined using Bernoulli's equation with an added term to account for the fluid acceleration[8,9]:

$$P_1 + \frac{1}{2}\rho V_1^2 + gZ_1 = P_2 + \frac{1}{2}\rho V_2^2 + gZ_2 + \rho HeadLosses + \rho\int_0^L \frac{dV}{dt}dX \tag{1}$$

Referring to Figure 1, states 1 and 2 have the same fluid velocity, and the change in gravity between the two points can be neglected, so the pressure drop across the piston can be simplified as:

$$\Delta P = \rho(HeadLosses + \int_0^L \frac{dV}{dt}dX) \tag{2}$$

Since either side of the piston has different areas, the damping force is determined by taking the difference between the products of the pressure and area on the front and back sides of the piston.

The flow channels in the MRF motorcycle damper are relatively complex. Because it is sometimes difficult to determine the overall pressure drop developed across the piston, it may be helpful to examine the electric circuit analogue, where ΔP is voltage, volumetric flow rate is the electric current, and the head losses are resistors. The procedure is as follows:

1. Determine each head loss.
2. Factor out a local volumetric flow rate term [$Q_{local}=(V_{local})(Area)=Current$], where the coefficients of each Q_{local} are the resistors.
3. Combine the parallel and series resistors to form a R_{eq} (equivalent circuit with only one resistor and one volumetric flow rate).
4. Determine the pressure drop, $\Delta P=(\rho)(R_{eq})(Q_{total})$, where Q_{total} = overall conserved volumetric flow rate.

A graphical representation of this scheme is presented in Figure 2.

The theoretical model presented is developed to predict the behavior of a new prototype MRF damper (MRF-MC1) for the rear suspension of a motorcycle. A cross-sectional view of the MRF motorcycle damper is shown in Figure 1. The fluid flow path through the piston as well as the critical parametric variables used in the theoretical formulation are demonstrated in the Figure. Referring to Figure 1, the MRF-MC1 damper has an external

accumulator with a pressure-filled bag that deforms to absorb the added volume to the system due to the rod. Also, the damper has piston by-pass valving on the compression stroke. These two features must be addressed in the development of the model. The first step in the derivation of the model is to find the pressure drop across the piston. Then, the effects of the accumulator are integrated into the model to find the overall force of the damper.

Due to the effects of by-pass valving on the compression stroke, the pressure drops across the piston are different on the compression and rebound strokes. As the wave washer on the piston opens (corresponding to large pressure gradients), the diameter of each by-pass valve changes from 0 to D_3. This change is proportional to the velocity which means that when the velocity is very high, the wave washer may be fully open. A function is selected to describe the behavior of the wave washers under a sinousoidal input motion.

$$\beta = \beta_o \cos(\omega t) \tag{3}$$

β_o describes how open each by-pass valve is, β ranges from 0 to β_o. When β=0, the valve is fully closed. This would correspond to the rebound stroke. When $\beta=\beta_o$, the valve opening is a maximum at β_o (ie.: compression stroke). The by-pass valve diameter is equal to βD_3.

There are six resistances to flow through the piston of the MRF-MC1 damper on the compression stroke[8,9]. These resistances are due to frictional effects, inertial effects, and fluid bifurcation effects. The piston resistance network is shown graphically in Figure 3. Combining the series and parallel a single equivalent resistance (R_{eq}) is obtained. Multiplying the equivalent resistance by the overall conserved volumetric flow rate yields the pressure drop across the piston as:

$$\Delta P_{piston} = \frac{32\mu_o L_3 \left(D_p^{\,2} - D_s^{\,2}\right) V_p}{\zeta(\beta D_3)^4} - \frac{32N\mu_o L_3 D_1^{\,2} V_1}{\zeta(\beta D_3)^4} \tag{4}$$

where V_1 is the local fluid velocity through the center of the piston, and given as[10]:

$$V_1 = \frac{\dfrac{32\mu_o L_3 \left(D_p^{\,2} - D_s^{\,2}\right) V_p}{\zeta(\beta D_3)^4} - \dfrac{32 L_{mrf} C_o (C_1 I^2 + C_2 I) sign(V_p)}{D_1}}{\dfrac{64 L_1 \mu_o}{D_1^{\,2}} + 64\dfrac{L_e}{D}\dfrac{\mu_o D_1^{\,2}}{D_2^{\,3}} + \dfrac{32N\mu_o L_2 D_1^{\,2}}{D_2^{\,4}} + \dfrac{32N\mu_o L_3 D_1^{\,2}}{\zeta(\beta D_3)^4}} \tag{5}$$

Some of the parametric variables shown in Equations (4) and (5) are defined in Figure 1. In these Equations, μ_o is the zero-field fluid viscosity, ζ is the number of by-pass valve ports, and N is the number of MRF channel flow ports. Referring to the second term in the numerator of Equation (5), C_o is a material constant. It represents the slope of the line describing the shear stress in the fluid as a function of magnetic field saturation. The term $(C_1I^2+C_2I)$ represents the magentic behavior of the MRF due to input electric current.

The pressure backed accumulator bag acts similar to a spring, where the force on the bag is proportional to its deformation. Therefore, it is necessary to relate the deformation of the accumulator bag to the known main piston displacement. Volumetric flow conservation allows this relation to be developed.

Because of the accumulator, there are two different volumetric flow rates that are conserved in the damper. The first is the flow that is conserved through the piston. The second is a flow generated by the increased volume to the system due to the piston rod, and is given as:

$$Q_2 = \frac{\pi}{4} Ds^2 Xp \tag{6}$$

The flow due to the increase in shaft volume is sent to the accumulator. Equation (6) shows that the amount of fluid sent to the accumulator is a function of the main piston displacement.

The accumulator can be approximated as an isentropic process, meaning that due to minimal friction, the system is internally reversible and that the system is nearly adiabatic[11]. Equation (7) presents the pressure in the accumulator as a function of main piston displacement (X_p):

$$P_a(t) = P_{charge}\left(\frac{V_{charge}}{V_{charge} + \frac{\pi}{4} D_s^2 \left(X_p - X\right)}\right)^{1.4} \tag{7}$$

where P_{charge} and V_{charge} correspond to the initial pressure and and volume of the accumulator bladder, respectively. It should be noted that the piston is fully extended, and X corresponds to the displacement of the main piston from its fully extended position to its oscilation midpoint.

To determine the force on the piston, the actual pressures on the front and back of the piston must be multiplied by the corresponding cross-sectional areas. This gives a force on the front and a force on the back of the piston. The actual force on the piston is the difference of the two. In other words:

$$F_{piston} = P_1 A_{p1} - P_2 A_{p2} \tag{8}$$

where:

$$A_{p1} = \frac{\pi}{4}\left[D_p^2 - D_s^2\right] \tag{9}$$

$$A_{p2} = \frac{\pi}{4} D_p^2 \tag{10}$$

Equation (9) can be expanded as:

$$F_{piston} = \Delta P_{piston}\left[\frac{\pi}{4}\left[D_p^2 - D_s^2\right]\right] - \left[P_a + \Delta P_a\right]\left(\frac{\pi}{4} D_s^2\right) \tag{11}$$

In expanded form, the force on the piston is:

$$F_{piston} = \left[\frac{\pi}{4}\rho\left(D_p{}^2 - D_s{}^2\right)V_p\right]\left[\frac{64L_1\mu_o V_1}{D_1{}^2} + \frac{32L_{mrf}C_o(C_1I^2 + C_2I)sign(V_p)}{D_1}\right]$$
$$+\left[\frac{\pi}{4}\left(D_p{}^2 - D_s{}^2 - \zeta(\beta D_3)^2\right)\right]\left[64\frac{L_e}{D}\frac{\mu_o D_1{}^2 V_1}{D_2{}^3} + \frac{32N\mu_o L_2 D_1{}^2 V_1}{D_2{}^4}\right]$$
$$-P_{charge}\left(\frac{\pi}{4}D_s{}^2\right)\left(\frac{V_{charge}}{V_{charge} + \frac{\pi}{4}D_s{}^2\left(X_p - X\right)}\right)^{1.4} \qquad (12)$$
$$+\left(\frac{32\mu_o L_4 D_s{}^2 V_p}{D_4{}^4} + \left(K_9 + K_{11}\right)\frac{1}{2}\rho\left(\frac{D_s}{D_4}\right)^4 V_p{}^2 sign(V_p)\right)\left(\frac{\pi}{4}D_s{}^2\right)$$

where K_9 and K_{11} represent dimensionless entrance and discharge loss coefficients of the port connecting the main cylinder to the accumulator, respectively.

3. RESULTS

The proposed theoretical model is experimentally verified using a MRF motorcycle damper (MRF-MC1) designed, built, and tested by the authors at UNR. Figure 4 shows the dimensions of the MRF-MC1 damper, and Figure 5 shows the damper mounted on the shock testing dynamometer during testing. The experimental damper underwent many tests to explore the effects of input stroke length, input frequency, and input current to the electromagnet on the force generated by the unit. The results of the tests are force-displacement curves, which represents the work done by the damper. Figures 6 and 7 show the comparison between the theoretical and experimental force-displacement loops as a function of input current at an input stroke of 0.508 cm and input frequencies of 1 and 1.5 Hz, respectively. The properties used to obtain results presented in Figures 6 and 7 are:

D_p = 1.7 in. (0.0432 m), D_s = 0.55 in. (0.0140 m), D_1 = 0.125 in. (0.00318 m), D_2 = 0.1718 in. (0.00436 m), D_3 = 0.0625 in. (0.00159 m), D_4 = 0.156 in. (0.00397 m), L_1 = 0.10 in. (0.00254 m), L_2 = 1.5 in. (0.0381 m), L_3 = 0.1 in. (0.00254 m), L_4 = 0.65 in. (0.0165 m), L_{mrf} = 0.10 in. (0.00254 m), V_{charge}=4.26 in^3 (6.98E-5 m^3), P_{charge}=125 psi (861.8 kPa), ρ = 3004 kg/(m^3), L_e/D = 60.0, K_3 = 0.5, K_4 = 1.0, K_9 = 1.0, K_{11} = 1.0, C_o = 37 Pa/Oersted, C_1 = 32.7 Oersted/amp^2, C_2 = 97.7 Oersted/amp, N = 4, ζ= 6.

Both Figures 6 and 7 show excellent agreement between the theoretical and experimental results. The minor differences between the theoretical and experimental results at the maximum stroke lengths are due to small amounts of air in the damper.

4. CONCLUSIONS

A theoretical model is developed to predict the damping force of a MRF shock absorber for the rear suspension of an off-road motorcycle. The model is based on the Bingham plastic theory. An electromagnetic finite element analysis was performed to incorporate the magnetic effects of MRF valve into the theoretical model. The damping force is estimated for the dimensions of the rear shock absorber of an off-road motor cycle. The validity of the proposed model is checked by a comparison between the theoretical and experimental results, which demonstrated excellent agreement.

ACKNOWLEDGEMENTS

This study is funded by the U. S. Army Research Office. The authors are thankful for the encouragement of Dr. Gary Anderson, the Program Director.

REFERENCES

1. Carlson, J.D. and Weiss, K.D., "A Growing Attraction to Magnetic Fluids." Machine Design, August 8, 1994.

2. 2.Carlson, J. D. and St. Clair, K. A., "Commercial Magneto-Rheological Fluid Devices." *Proceedings of the 5th International Conference on Electro-Rheological Fluids, Magneto-Rheological Suspensions, and Associated Technology,* Sheffield, UK, pp. 20-28, 1995.

3. Rabinow, J. "Magnetorheological Fluid." U.S. Patent Number 2,575,360, 1951.

4. Lampe, D., "2. Basic Properties and Description of ERF and MRF." *Actuator '98,* From Materials Database on Commercially Available Electro- and Magnetorheological Fluids (ERF and MRF), 1998.

5. Lampe, D., "MRF-Overview." *Actuator '98,* From Materials Database on Commercially Available Electro- and Magnetorheological Fluids (ERF and MRF), 1998.

6. Gordaninejad, F. and Breese, D. G., "Magneto-Rheological Fluid Damper," United States Patent, No. 6,019,201, 2000.

7. Ericksen, E. O., and Gordaninejad, F., "A Magneto-Rheological Fluid Shock Absorbers for an Off-Road Motorcycle," *Proceedings of Asia-Pacific Vibration Conference'99*, Ed. By O. J. Huat and L. K. Meow, Vol. 2, pp. 267-271, 1999

8. White, F. M., 1994, "Fluid Mechanics." 3rd edition, *McGraw-Hill Publishing Company,* ISBN 0-07-911695-7, 1994.

9. Yeaple, F., "Fluid Power Design Handbook." 3rd edition, *Marcel Dekker, Inc.,* New York City, New York, 1995.

10. Ericksen, E.O., "Study of Magnetorheological Fluid (MRF) Dampers and Development of a MRF Shock Absorber for a Motorcycle." Master's Thesis, University of Nevada Reno, Department of Mechanical Engineering, 1999.

11. Cengel, Y., and Boles, M. A., "Thermodynamics, An Engineering Approach." 2nd edition, *McGraw-Hill Publishing Company,* ISBN 0-07-911651-5, 1994.

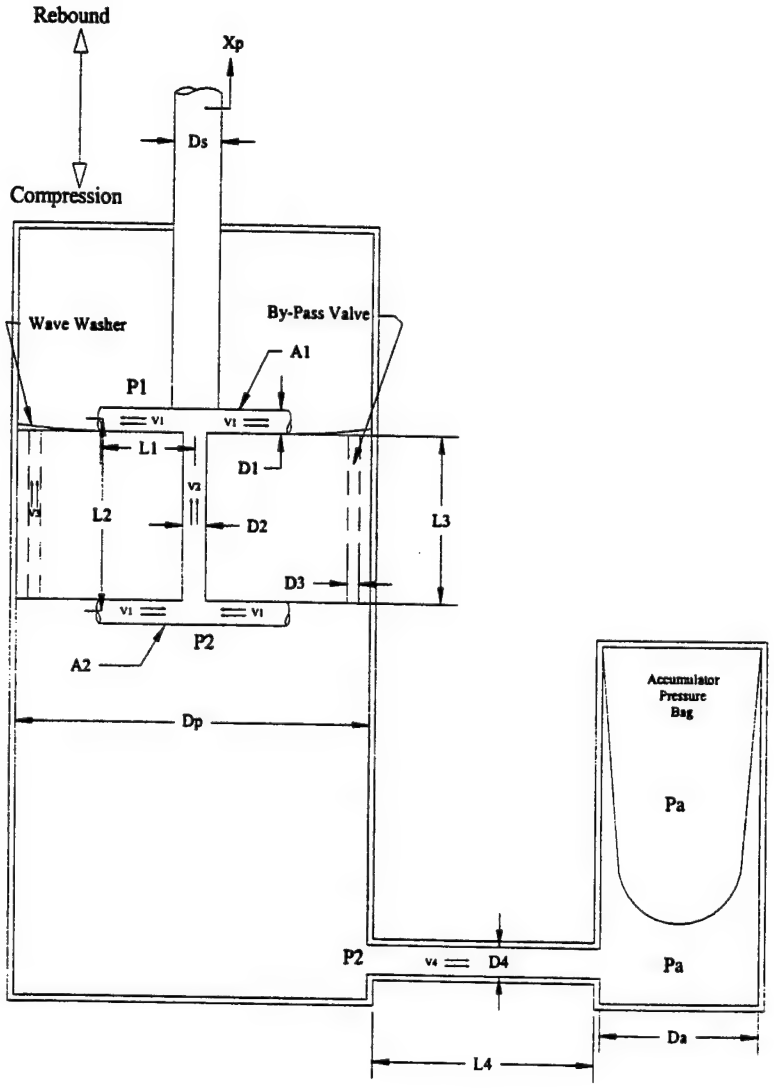

Figure 1. Schematic of flow path for MRF-MC1 damper with by-pass valving.

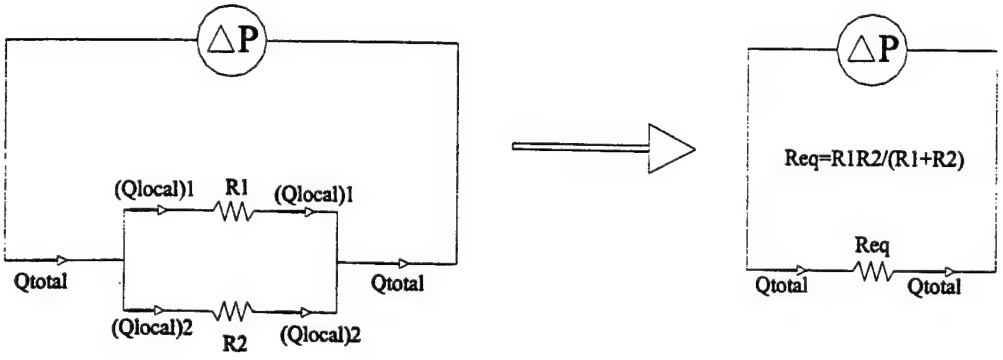

Figure 2. Graphical representation of the electric circuit analogue procedure.

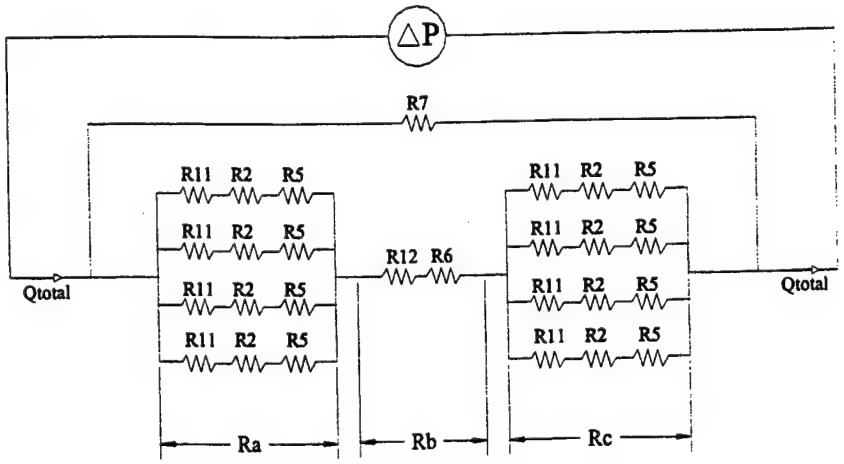

Figure 3. Graphical representation of the compression stroke resistance network.

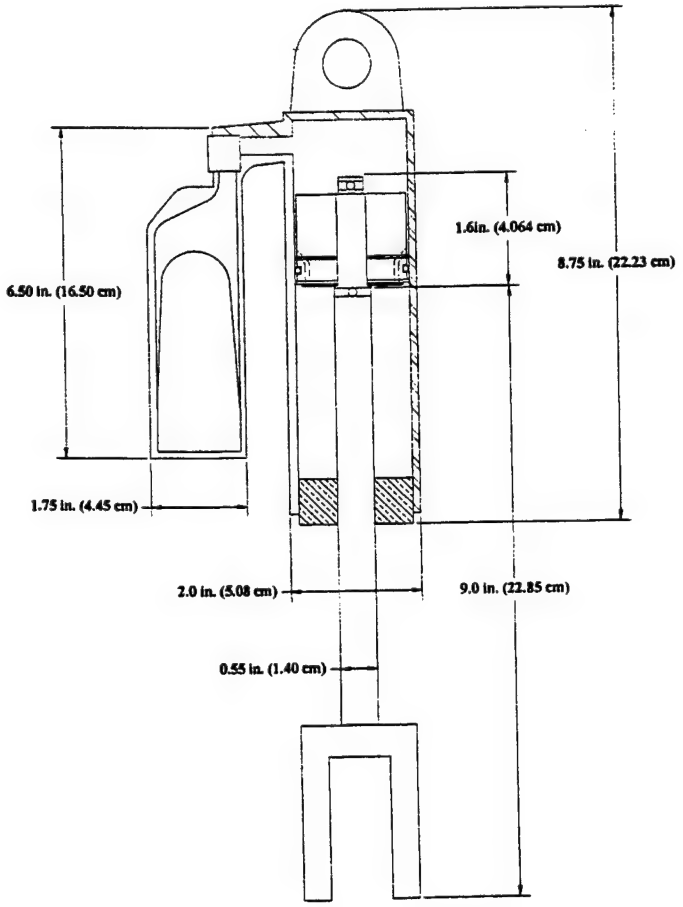

Figure 4. Basic design and dimensions of MRF-MC1 damper.

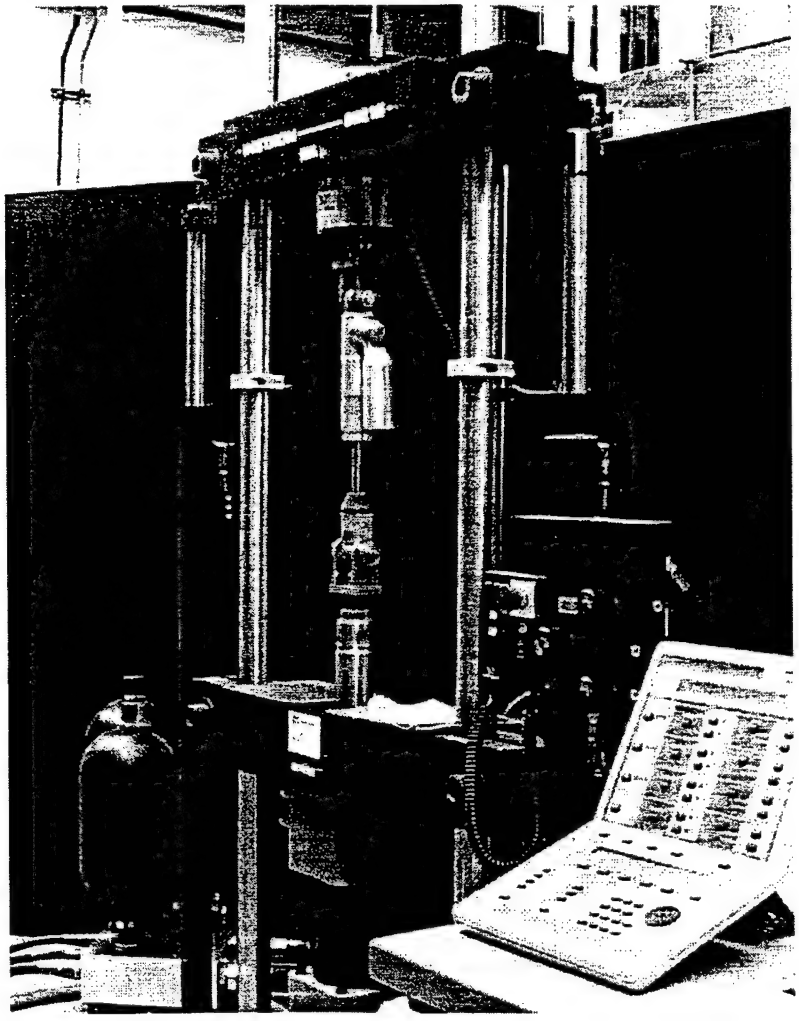

Figure 5. MRF-MC1 shock absorber mounted on Instron shock dynamometer.

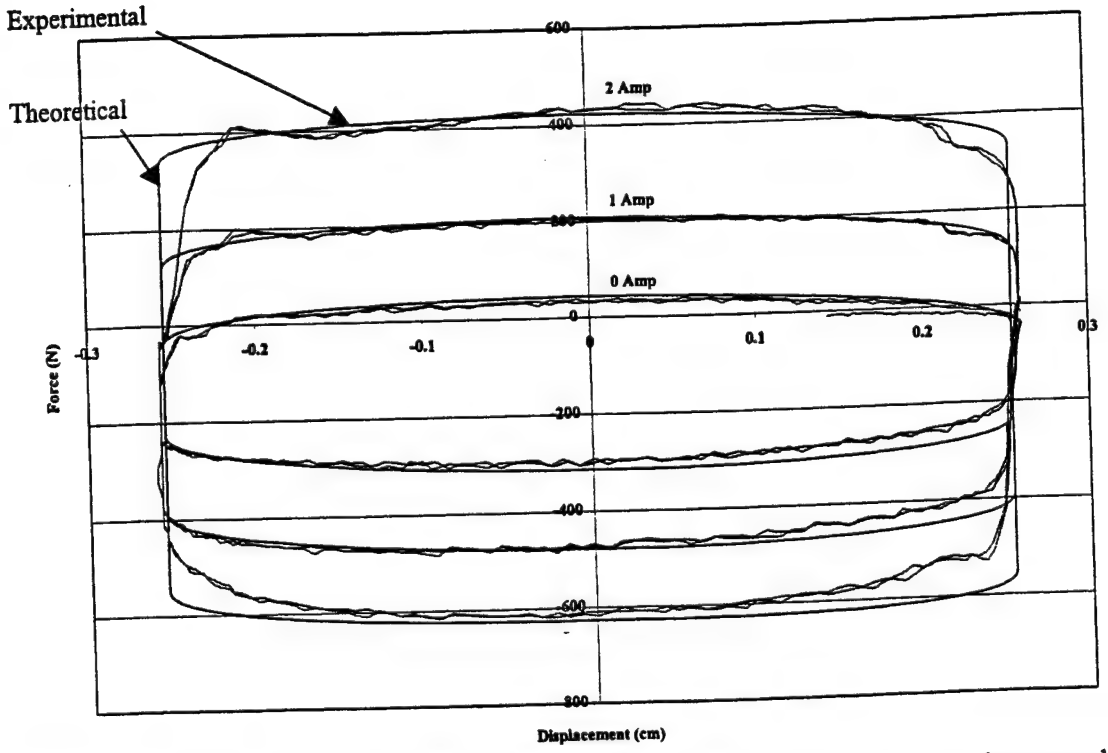

Figure 6. Comparisons between theoretical and experimental results of the MRF-MC1 damper under a sinusoidal motion with 1.5 Hz frequency, and 0.508 cm amplitude input for different electric current input.

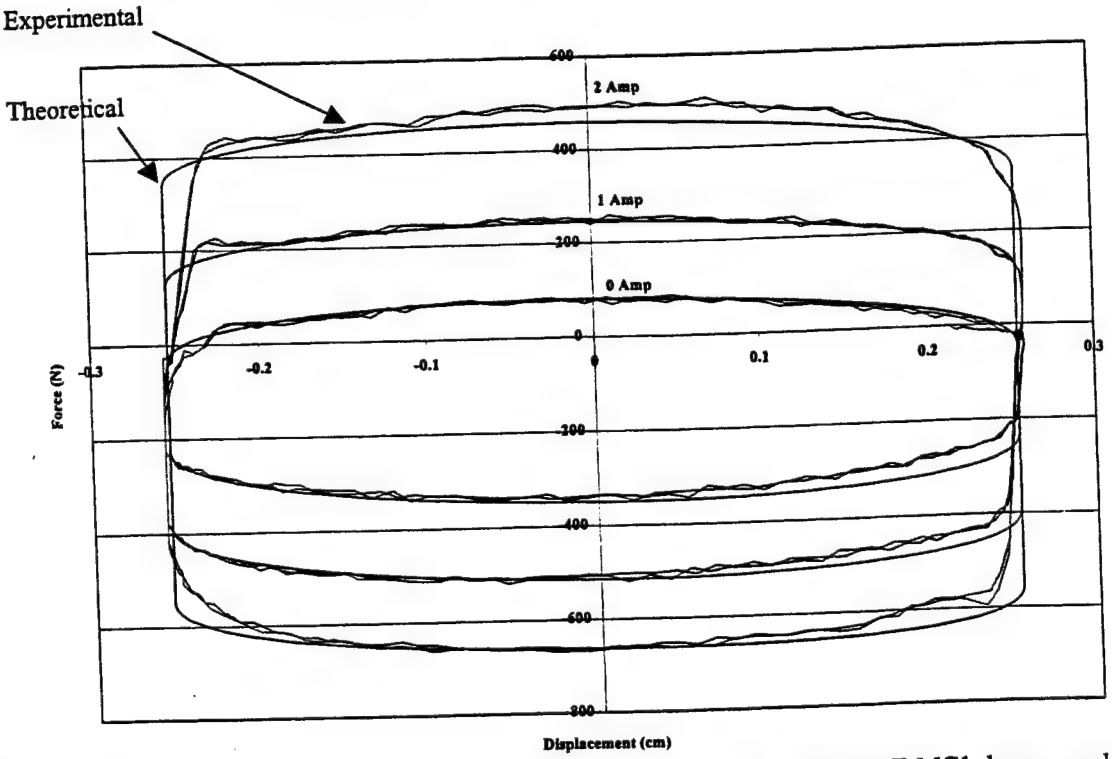

Figure 7. Comparisons between theoretical and experimental results of the MRF-MC1 damper under a sinusoidal motion with 1.5Hz frequency, and 0.508 cm amplitude input for different electric current input.

A Magneto-Rheological Fluid Shock Absorber for an Off-Road Motorcycle

Everet O. Ericksen and Faramarz Gordaninejad
Department of Mechanical Engineering, University of Nevada, Reno, NV 89557, USA
E-mail: faramarz@unr.edu, Fax: 775-784-1701

Abstract

This experimental study presents the development and evaluation of a controllable, semi-active magneto-rheological fluid (MRF) shock absorber for a rear suspension of an off-road motorcycle. The MRF device is designed and constructed at the University of Nevada, Reno (UNR). An experimental study is conducted to examine the performance of the proposed retrofit MRF damper. The experimental results show that the MRF damper can provide wide range damping forces.

INTRODUCTION

As a component of a semi-active suspension system, the role of the controllable shock absorber is to have the capacity to produce variable damping force proportionally reactive to an input excitation. Semi-active, controllable dampers are being investigated increasingly for various applications. One class of controllable, semi-active dampers is MRF shock absorbers. Magneto-rheological fluids typically consist of a silicone-based carrier fluid with small iron-based particles in random suspension [1]. The application of a magnetic field to the MRF causes the particles to align as chains along the lines of magnetic flux. The formation of these chains causes a resistance to fluid flow due to the development of higher fluid shear stresses. By changing the magnetic field, the shear yield stress of the fluid changes; thus producing a controllable force for the MRF damper. In other words, it is possible to control the damping forces of a device utilizing MRF, by varying the input electric current to the device's built-in electromagnet.

The ability to vary damping for a wide range of inputs is the main feature of semi-active suspension systems. Other features include control of vehicle pitch during braking and acceleration and accommodation for a variable vehicle mass (i.e., light or heavy riders). In comparison to typical, passive suspension systems, semi-active shock absorbers allow for softer damping when needed, in addition to harder damping for situations that demand it. The main benefits of the MR technology for off-road motorcycles are: improved operator ride comfort, an increased level of vehicle control due to a lower disturbance input, and faster operational speeds over similar terrain.

Semi-active vibration control devices are receiving significant attention because they can offer combined advantages of both passive and active systems. Examples of such devices include variable orifice dampers, variable stiffness devices, and friction controllable isolators and braces. A class of semi-active controllable devices utilizing MRF has been established. There have been numerous studies on MR fluids and devices in recent years due to the realization that there are many potential applications [1-8].

A new generation of MRF dampers has been designed and developed at UNR that provide robust, cost-effective, vibration damping solutions. Several innovative prototype MRF dampers have been developed and examined at the UNR's Composite and Intelligent Materials Laboratory for different applications, such as mountain bikes, motorcycles, off-road vehicles, and bridges [5-8].

This study focuses on a proof-of-concept experimental study to demonstrate the capabilities of UNR MRF retrofit damper for an off-road motorcycle. A full-scale MRF retrofit shock absorber for the rear suspension of a motorcycle is designed, manufactured, and examined.

EXPERIMENTAL STUDY

a) DESIGN METHODOLOGY: In this study, a specific design methodology is followed in the development of the MRF retrofit damper. This design methodology is based on the fail-safe characteristic of the MRF devices. MRF dampers are fail-safe in their operation, meaning that in zero-field (off-state), passive mode operation (i.e., no electric current supply to the damper) the MRF shock absorber performs similar to the original equipment manufacture (OEM) shock absorber. Therefore, the steps in designing a MRF retrofit shock absorber for the rear suspension of an off-road motorcycle are:

1. Benchmark test the existing OEM shock absorber.
2. Design MRF damper to give similar performance at zero-field as the OEM unit.

3. Apply power to the MRF damper to generate an "envelope" of increased performance, with the OEM performance near the bottom of the envelope.

An OEM rear suspension shock absorber of an off-road motorcycle is characterized in order to determine the base performance of the unit as a function of input amplitude of the motion and frequency. After fully characterizing the OEM damper, it is disassembled and carefully studied. The OEM piston unit is removed from the OEM shock absorber body and a MRF retrofit piston is assembled in its place. Replacing the hydraulic fluid with MR fluid completes the retrofit of the OEM damper. The result is a shock absorber that has the same dimensions as the OEM damper with a MRF piston retrofit. Figure 1 shows the components of the OEM shock absorber, and Figure 2 shows the components of the MRF retrofit damper.

b) MRF SHOCK ABSORBER DESIGN: The design of the MRF shock absorber involves utilizing a parametric non-Newtonian fluid mechanics model and extensive electro-magnetic modeling by means of a three-dimensional magnetic finite element analysis (FEA). For simplicity in manufacturing, and also to demonstrate the feasibility of retrofitting an OEM shock absorber with a MRF piston, the OEM shock absorber, accumulator bag, seal pack, and chrome-plated rod are used in the construction of the UNR MRF retrofit damper. It is important to preserve the 3-inch stroke of the damper, which means that the MRF piston must be, at most, the same size as the OEM piston. The following are the physical design constraints for the MRF piston:

1. Maximum length = 4.064 cm (1.6 inches)
2. Maximum diameter = 4.318 cm (1.7 inches)
3. Piston ring grove width = 0.8128 cm (0.32 inches)

Furthermore, the MRF piston retrofit must have compression by-pass valving to protect the damper from harmful impulse loads on the compression stroke. With the necessary physical constraints of the piston clearly defined as shown above, the next step in the design is to determine the dimension of the fluid flow ports to give damping forces that are similar to the OEM shock absorber. A theoretical non-Newtonian fluid mechanics model, developed by the authors, is employed to estimate the size of the flow channels [7]. The model predicts the damping force based on the physical parameters of the fluid and the device. Using this model, the dimensions of the fluid flow channels in the MRF piston can be determined so that the MRF retrofit shock absorber produces similar damping forces as the OEM damper at zero-field state.

With the physical parameters of the MRF shock absorber specified, the final step in the design is to use FEA to design and characterize the piston's built-in electromagnet. In particular, the effects of material properties on the magnetic flux lines and magnetic saturation of the MRF is investigated by FEA. In addition, by varying the electric input current in the FEA model, a function is generated describing the shear yiels stress of the MRF as a function of input electric current. This provides a controllable, current-dependent term in the fluid mechanics model which accurately predicts the current dependent variability of the MRF damper. Upon completion of the fininte element analysis, the most appropriate material configuration for the construction of the MRF damper, is determined.

By both, non-Newtonian fluid mechanics modeling and electro-magnetic finite element analysis, a MRF retrofit piston is designed. The design preserves the OEM stroke length and performance and incorporates compression stroke by-pass valving to protect the device from harmful impulse loading. Next, a prototype MRF piston is manufactured and characterized.

c) MRF DAMPER CHARACTERIZATION: Figure 3 shows a photo of the experimental set up with UNR MRF retrofit shock absorber mounted on the table. The shock absorbers for this study are tested on an Instron 8821 S hydraulic shock testing dynamometer. The Instron has a maximum stroke of 15.24 cm (6.0 inches), and it is equipped with a 22 KN (5,000 lbf) load cell that measures the damping forces of the shock absorber and a displacement/velocity transducer measures the displacement and velocity of the actuator. Experimental data is collected at a sampling rate of 200 Hz.

Using the Instron shock dynamometer, each of the shock absorbers evaluated in this work is undergone various performance tests. A performance test consists of a frequency sweep held at constant displacement input. Each specific amplitude and frequency represents a run of the performance test. The results of a performance test are a force-displacement and force-velocity response curves. These curves represent the work done and the energy absorbed by the damper, respectively.

RESULTS AND DISCUSSION

The performance of the UNR MRF retrofit damper for rear suspension of an off-road motorcycle is evaluated by conducting numerous tests. The experiments are mainly performed to assess the effects of input amplitude, input frequency, and input electric current to the electromagnet, on the damping force generated by the MRF damper. The results of these tests are a force-displacement performance curve that represents the work done by the damper.

In each of the force-displacement loops presented in this work, the positive force and displacement values correspond to the rebound stroke whereas the negative force and displacement values correspond to the

compression stroke. The compression stroke force values do not increase in value with increasing frequency as much as the rebound force values. This is one effect of by-pass valving on the compression stroke. As the input frequency increases (corresponding to large piston velocities and pressure drops), by-pass valves open to reduce the pressure. The by-pass valves on the rebound stroke are not as dominant, so force grows much higher with increasing frequency.

Figure 4 shows the force-displacement loops for the MRF retrofit shock absorber as a function of input electric current. This plot demonstrates that the maximum rebound damping force changes from about 30 N to 430 N, between 0 and 2 Amp input electric current. In other words, the "performance envelope" is represented by a 400 N window of controllability.

Figure 5 shows the force-displacement comparison between the OEM damper, the UNR MRF retrofit damper at zero-field, and the MRF damper with 2 amps current input at amplitude of 2.5 mm (0.2 in.) and 1 Hz input frequency. Note the performance envelope created around the OEM shock absorber performance. Again, this envelope represents the controllability of the MRF damper. The zero-field (off-state) force is slightly lower than OEM force and the force generated by the 2 Amp electric current input is higher than the OEM force.

Finally, Figure 6 shows the peak rebound force comparison between the OEM and the MRF damper at zero-field, and the MRF damper with 2 Amps electric current input as a function of excitation frequency. The input amplitude for these results is 2.5 mm (0.2 in.). Again, note that the 0 amp and 2 amp curves form an envelope around the OEM damper curve. These results demonstrate the design methodology discussed previously. The OEM damper is characterized as a function of input frequency. Using the fluid mechanics model, the MRF retrofit damper is designed to produce zero-field force values that are slightly less than the OEM damper independent of input frequency. With the application of 2 Amps input electric current to the damper's built-in electromagnet, the MRF damping levels increase by 400 N, creating a significant dynamic force range for the MRF retrofit damper.

CONCLUSIONS

A UNR MRF retrofit damper is designed, constructed and evaluated for an off-road motorcycle. The MRF shock absorber has similar performance to that of an OEM damper at zero-field. With the application of electric current to the damper's built-in electromagnet, a wide controllable range of damping force above the OEM performance is produced. The feasibility of implementing compact, MRF technology onto an off-road motorcycle while maintaining the OEM stroke length performance, and compression by-pass valving characteristics, is successfully demonstrated.

ACKNOWLEDGEMENTS

This study is sponsored by the U.S. Army Research Office and the U.S. National Science Foundation. The authors are thankful for the encouragement of each of the Program Directors. In addition, valuable comments by Mr. Gregory Hitchcock is appreciated.

REFERENCES

(1) J. D. Carlson, D. M. Catanzarite, and K. A.St. Clair. "Commercial Magneto-Rheological Fluid Devices." Proceedings of the 5th International Conference on ER Fluids, MR Fluids and Associated Technology, U. Sheffield, UK, pp. 20-28, 1995.

(2) J.D. Carlson, and M.J. Chrzan. "Magnetorheological Fluid Dampers." U.S. Patent #5,277,281, 1994.

(3) J.D. Carlson, M.J. Chrzan, and F.O. James. "Magnetorheological Fluid Devices." U.S. Patent #5,398,917, 1995.

(4) W.I. Kordonsky. "Elements and Devices Based on Magnetorheological Effect." Journal of Intelligent Material Systems and Structures, Vol. 4, No. 1, p.65, 1993.

(5) Y. Liu, F. Gordaninejad, C. A. Evrensel, and X. Wang. "Semi-active Control of a Bridge Using Controllable Magneto-Rheological Dampers." Proceedings of SPIE Conference on Smart Materials and Structures, Newport Beach, California, March 2000.

(6) D. G. Breese, and F. Gordaninejad. "Semi-Active Controllable Magneto-Rheological Fluid Dampers for A Mountain Bicycle." Proceedings of SPIE Conference on Smart Materials and Structures, Newport Beach, California, March 2000.

(7) F. Gordaninejad, and E. O. Ericksen. "A Magneto-Rheological Fluid Shock Absorbers for the Rear Suspension of an Off-Road Motorcycle: A Theoretical Study." Proceedings of SPIE Conference on Smart Materials and Structures, Newport Beach, California, March 2000.

(8) S. P. Kelso, and F. Gordaninejad. "Magneto-Rheological Fluid Shock Absorbers for Off-Highway, High-Payload Vehicles." Proceedings of the 1999 SPIE Conference on Smart Materials and Structures, Newport Beach, California, March 1999.

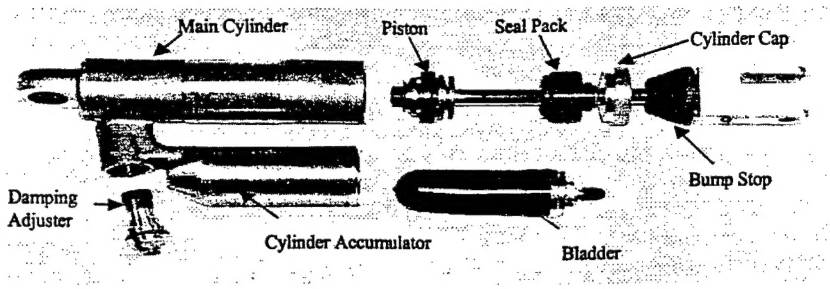

Figure 1. Components of the OEM shock absorber.

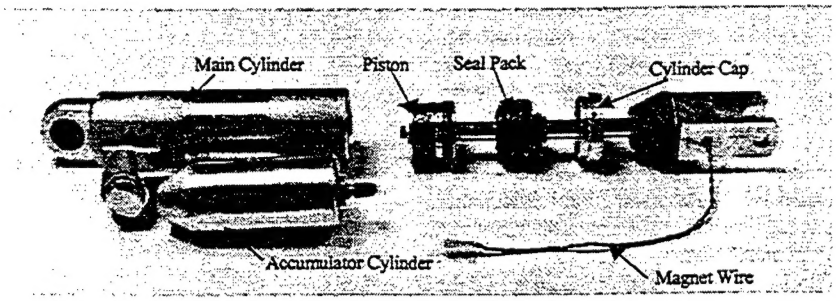

Figure 2. Components of the UNR MRF retrofit damper.

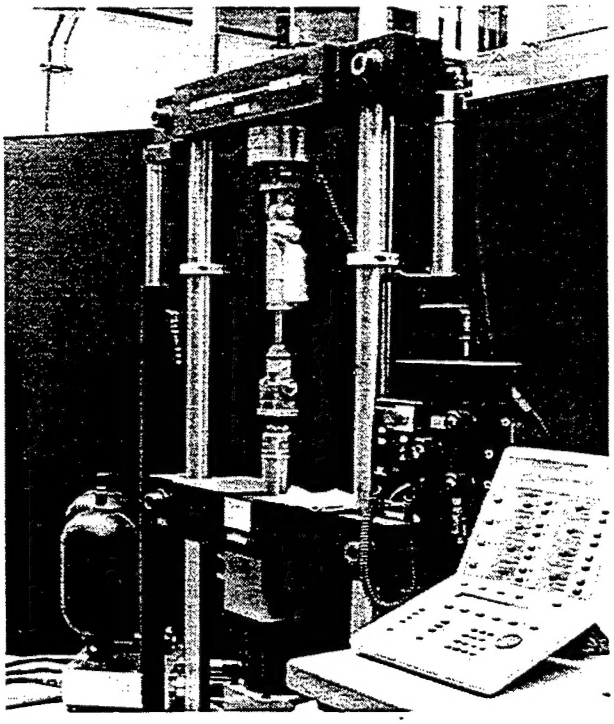

Figure 3. Picture of the experimental set up.

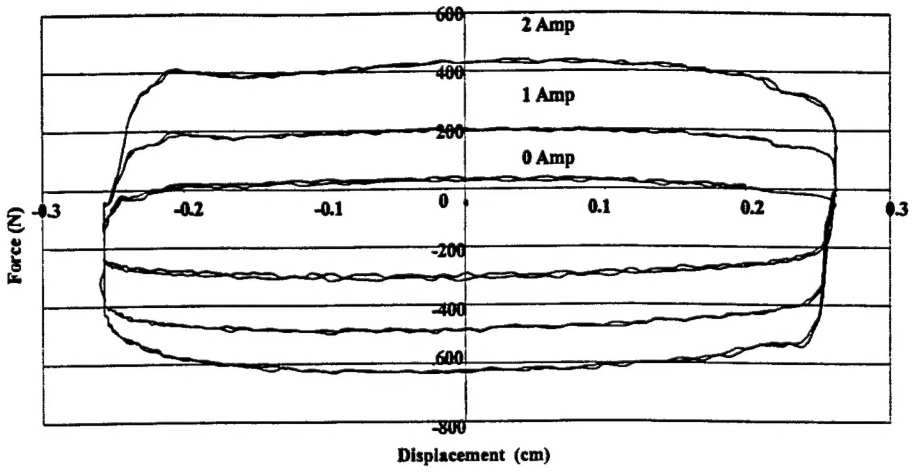

Figure 4. The MRF retrofit damper performance test, 1.0 Hz frequency, 2.5 mm amplitude.

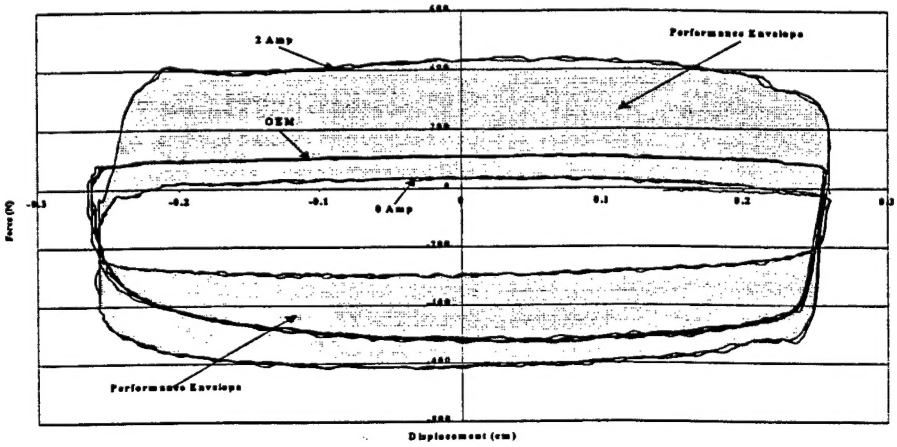

igure 5. Force-Displacement loops for the OEM and the MRF Damper at 1.0 Hz frequency and 2.5 mm amplitude.

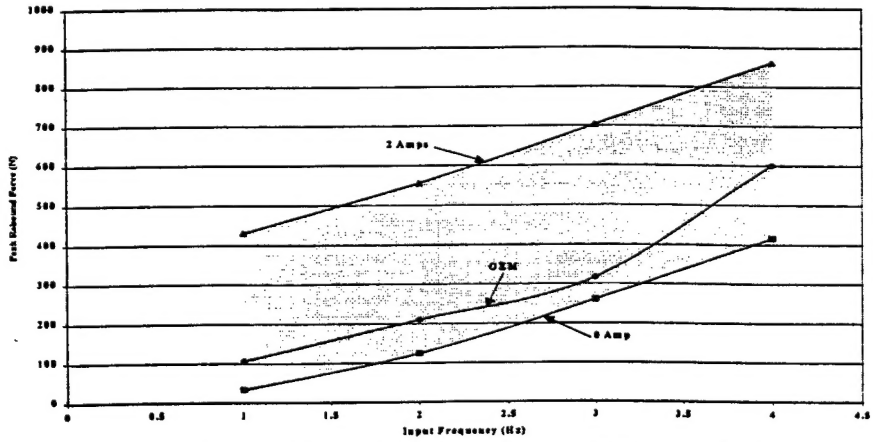

Figure 6. Dynamic force range of the MRF damper at 2.5 mm amplitude.